A study of a tub crane with an unconventional quadruple hook arrangement

A structural feasibility and workability assessment

S.R.L. (Bastijn) van Daalen

Delft University of Technology

A study of a tub crane with an unconventional quadruple hook arrangement

A structural feasibility and workability assessment

by

S.R.L. (Bastijn) van Daalen

In partial fulfillment of the requirements for the degree of

Master of Science

in Offshore & Dredging Engineering
Bottom Founded Structures at the Delft University of Technology,

to be defended publicly on July 26, 2016, 13:00

Student number:	1528572	
Project duration:	September 1, 2015 – July 26, 2015	
Thesis committee:	Prof. dr. A.V. Metrikine,	TU Delft, chairman
	Dr. ir. K.N. van Dalen,	TU Delft, committee member
	Dr. ir. J.M. de Oliveira Barbosa,	TU Delft, supervisor
	Ing. C. Benard,	Heerema Marine Contractors
	Ir. D. Klaasen,	Heerema Marine Contractors

Abstract

In the world of offshore oil and gas production, facilities and structures are constantly increasing in weight and size. The installation of these structures evidently demands more lifting capacity and increasing workability of the contractors. Heerema Marine Contractors (HMC) is exploring the possibilities of meeting these demands with a new crane vessel. A promising concept is an asymmetric semi-submersible with a single crane placed amidships on port side. A new type of crane is introduced with an unconventional rectangular quadruple hook arrangement with the ability to lift and slew 24,000t.

The unconventional crane design raises several questions on the feasibility of the concept and the potential workability. This study addresses three topics: the configuration optimization, the static structural integrity and the dynamics of the crane's daily operations. Additionally a comparison is made between an unconventional and a conventional semi-submersible crane vessel (SSCV). The aim of this thesis is to determine the critical structural elements of the crane and to potentially increase the vessel's workability.

Based on the initial design of the crane, an optimization of the configuration has been performed. A beam model in MATLAB has been constructed to represent the crane structure above the tub. Based on typical transit-, survival- and operational conditions, a set of load cases has been created. The optimum configuration has been derived by solving the system for the lowest overturning moment on the tub. The optimization shows an overall height reduction of the crane, a change in the tub connection legs and a lower center of gravity. The most promising configuration is used to continue this research.

The obtained configuration and beam profiles have been subjected to a detailed static analysis using the finite element software Abaqus. Nine typical heavy lift cases including dynamic amplification have been defined and applied on the crane model. The tub, crane house and bearing have been added to the model to analyze the structural integrity of the complete crane. The optimized configuration looks promising for the defined operational profile. Furthermore the crane weight is reduced in comparison to the original estimations.

A time domain analysis has been performed in Abaqus to include the dynamic effect on the structural integrity of the crane. After determining the favorable orientation for the crane during a storm, the crane has been submitted to typical 3hr survival conditions. Although several brace members exceeded the allowable stress for the survival conditions, the exceedance is not identified as a show stopper. The operational dynamic analysis has been performed for the worst wave heading and peak period. A calm sea state introduced unexpected exceedance of the allowable stress levels, indicating large excitations of the lifted object. Further research shows resonance behavior of the lifted object indicating Eigen frequency excitation. A combination of the short pendulum length of the unconventional hook arrangement and the vessel motions in specific wave heading and period are the root cause for this resonance behavior.

A comparison with a conventional SSCV confirms the reduced workability for certain wave headings and peak periods due to the pendulum resonance. A combination of the roll response of the vessel and excitation around the Eigen period of the system causes these reductions.

Future research is required to determine the possibilities of increasing the Eigen periods of the pendulum object. Furthermore adding a damping mechanism to the lift system could be beneficial for the cranes integrity. Nevertheless the ability to lift from its own deck could lead to a significant increase of the workability compared to conventional SSCVs.

Preface

Dear reader,

First of all, I would like to thank you for taking the time to read my Thesis research. This graduation project is the final step of the Master of Science Degree in Offshore & Dredging Engineering at the Delft University of Technology.

First of all, I would like to thank all members of my graduation committee. Without them this thesis would not have been possible. The daily guidance from Cor Benard and Diederick Klaasen at Heerema Marine Contractors has been invaluable, their support and comments throughout the research are much appreciated. Furthermore, the experience and analytical view of my daily supervisor João Barbosa is greatly valued. Finally, I would like to thank Prof. Andrei Metrikine as the chairman of my committee for his endless support, patiences and sharp comments during our meetings.

Of course I would like to thank my parents Loek and Monique, my brother Maxens and my girlfriend Virpi for their moral support and encouragement during my thesis, but also in my student years prior to graduation. Another special thanks goes out to my fellow students and colleagues for sharing their experiences and the occasional coffee breaks.

Bastijn van Daalen
Leiden, July 19, 2016

Contents

List of Figures

List of Tables

Glossary

List of Acronyms

3mE	Mechanical, Maritime and Materials Engineering
AWL	Area Water Line
CoG	Centre of Gravity
CAPEX	Capital Expenditures
DAF	Dynamic Amplification Factor
DCV	Deepwater Construction Vessel
DNV	Det Norske Veritas
DP	Dynamic Positioning
E.o.M	Equation of Motion
FEA	Finite Element Analysis
FEM	Finite Element Method
HL	Hookload
HLV24k	Heavy Lift Vessel 24,000t
HMC	Heerema Marine Contractors
HFG	Heerema Fabrication Group
JONSWAP	JOint North Sea WAve Project
KMT	Transverse Metacentric height
KML	Longitudinal Metacentric height
LCB	Longitudinal Center of Buoyancy
LCF	Longitudinal Center of Flotation
LCG	Longitudinal Center of Gravity
M2 180	HLV24k configuration, Crane to the stern (180deg), 19m draft
M2 270	HLV24k configuration, Crane to the starboard (270deg), 19m draft
M3 90	HLV24k configuration, Crane to the port side (90deg), 27m draft
M3 180	HLV24k configuration, Crane to the stern (180deg), 27m draft
M3 270	HLV24k configuration, Crane to the starboard (270deg), 27m draft
MPC	Multi-point constraint
MPM	Most Probable Maximum
OPEX	Operating Expenditures

PS	Port Side
RAO	Response Amplitude Operator
SB	Starboard
SDA	Significant Double Amplitude
SSCV	Semi Submersible Crane Vessel
SWL	Safe Working Load
TCB	Transverse Center of Buoyancy
TCG	Transverse Center of Gravity
TU Delft	Delft University of Technology
UTS	Ultimate Tensile Strength
VCB	Vertical Center of Buoyancy
VCG	Vertical Center of Gravity

List of Symbols

Greek Symbols

β	Azimuth angle, XY-plane	[−]
Γ	Gamma function	[−]
γ	Elevation angle, XZ-plane	[−]
γ	Peak enhancement factor	[−]
ω	Wave frequency	[rad/s]
ω_p	Wave peak frequency	[rad/s]
ϕ	Vessel roll/heel	[deg]
ψ	Vessel yaw	[deg]
ρ	Material density	[kg/m^3]
σ	Stress	[N/m^2]
σ_{all}	Allowable stress	[N/m^2]
σ_{eq}	Equivalent stress	[N/m^2]
σ_y	Yield strength	[N/m^2]
τ	Shear stress	[N/m^2]
θ	Rotation	[deg]
θ	Vessel pitch/trim	[deg]
θ	Angle	[deg]
θ_w	Wave direction/heading	[deg]
ζ_a	Wave elevation	[m]
ζ_t	Wave elevation time signal	[m]

Latin Symbols

A	Cross section area	[m^2]
D	Diameter	[m]
d	Center line offset	[−]
E	Elasticity modulus	[N/m^2]
$f(x)$	Optimization goal function	[−]
F_x	Force in x-direction (longitudinal)	[N]

F_y	Force in y-direction (transverse)	[N]
F_z	Force in z-direction (vertical)	[N]
F_{bolt}	Bolt load	[N/mm^2]
$F_{p,bolt}$	Bolt peak load	[N/mm^2]
F_P	Peak load	[N/mm^2]
G	Shear modulus	[N/m^2]
HL	Hookload	[t]
HL_{des}	Design hookload	[t]
I	Area moment of inertia of cross section	[m^4]
J	Torsional moment of inertia	[m^4]
K	Stiffness	[N/m]
k_r	Rotational stiffness	[N/m]
k_s	Shear stiffness	[N/m]
L	Length	[m]
L_{eff}	Effective length	[m]
m	Mass	[kg]
$M_{(axis)}$	Overturning moment around axis	[Nm]
MF_{max}	Most Probable Maximum multiplication factor	[−]
N	Number of cycles	[−]
N	Number of degrees of freedom	[−]
n	Wave spread exponent	[−]
$n_{(part)}$	Number / amount of the part	[−]
OL	Offlead	[deg]
R	Radius	[m]
R_{eff}	Effective radius	[m]
S	Spectral density function	[m^2/s]
S_{JW}	JONSWAP Spectrum	[m^2/s]
SF	Safety Factor	[−]
SL	Sidelead	[deg]
T	Draft	[m]
T	Tensile force	[N]
T	Torsion	[Nm]
t	Wall thickness	[m]
t	Time	[s]
T_p	Wave peak period	[s]
T_{rot}	Euler transformation matrix	[−]
u	Displacement	[m]
V	Shear Force	[N]
W_{des}	Design weight	[t]
W_{rig}	Rigging weight	[t]

1 Introduction

1.1 General introduction

In offshore oil and gas production big heavy facilities and structures are used to provide the world of energy and other resources. A large amount of these structures are bottom founded. During the lifetime of such a structure, it has to be installed and eventually decommissioned. To reduce the risks and costs of these operations, different construction method have been developed.

One of the options is to float the structure making use of its own buoyancy. The structure is towed to location and by means of ballasting lowered to the seabed. This method is only applicable to gravity based structures with the ability to float without ballast. The installation is very dependent on the environmental conditions and the distance from shore.

Topsides do not have the ability to float and can therefore be transported on a barge. The barge is towed to the location and the topside can be floated over the base structures and lowered in place. This method is restricted by the design of the base structure.

Besides float over of a topside, it can also be lifted off the barge and installed on the base structure. Lifting the topside from a barge with different motion behavior characteristic than the crane vessel is highly dependent on the environmental conditions.

Jackets can also be placed on a barge. Again the barge is towed to the location and the jacket is launched from the barge into the sea. The jacket has buoyancy modules attached to its legs and has to be upended by means of ballasting or a crane vessel.

Instead of launching the jackets from the barge, the structure can be lifted of and upended with an offshore crane. Lifting of a barge is restricted by the weather and the motion behavior of the two individual vessels.

In theory all these methods can be reversed for decommissioning of the facility, in practice the first option of re-floating an gravity based structure has never been done before.

In most of the installation and decommissioning operations a crane vessel is required to complete the tasks. Most of these are heavy lifts (>5000t) all performed by semi-submersible crane vessels (SSCV).

1.2 Heerema Marine Contractors

Heerema Marine Contractors (HMC) is a contractor active in the offshore heavy lifting and subsea construction industry. For its clients Heerema offers a variety of services, ranging from installation to decommissioning. All these services are provided by HMC's own fleet. HMC owns and operates three of the world's largest SSCVs, the Thialf, the (DCV) Balder and the Hermod. All outfitted with two independent 360 deg revolving tub cranes. At some point in time the Hermod is likely to be replaced by the SSCV Sleipnir, which is currently under construction, due for delivery end 2018. Besides heavy lift vessels, the fleet includes the DCV Aegir and

a variety of tugs and barges.
Heerema Marine Contractor is part of the Heerema Group together with Heerema Fabrication Group (HFG).

1.3 Relevance

Heerema, as one of the biggest contractors for the oil and gas industry, faces several challenges for the future, in particular the replacement of their aging semi-submersibles. Conditions for a replacement include the oil and gas industry shifting more to remote area's, harsher conditions and deeper water. Adding to the environmental conditions is the fact that loads are getting bigger in size and weight. To remain profitable in these conditions it is essential to sustain and increase the workability and lifting capacity of the replacement vessel. The new concept vessel in this thesis has several features which could be beneficial for the workability and capacity. One of those features is the 24,000t tub crane, providing an increase in capacity compared to the current fleet, with the ability to lift the full capacity from its own deck, leaving out the weather sensitive barge lift operations.
Figure 1.1 provides an overview of the lifting capacity of the current and new Heerema fleet.

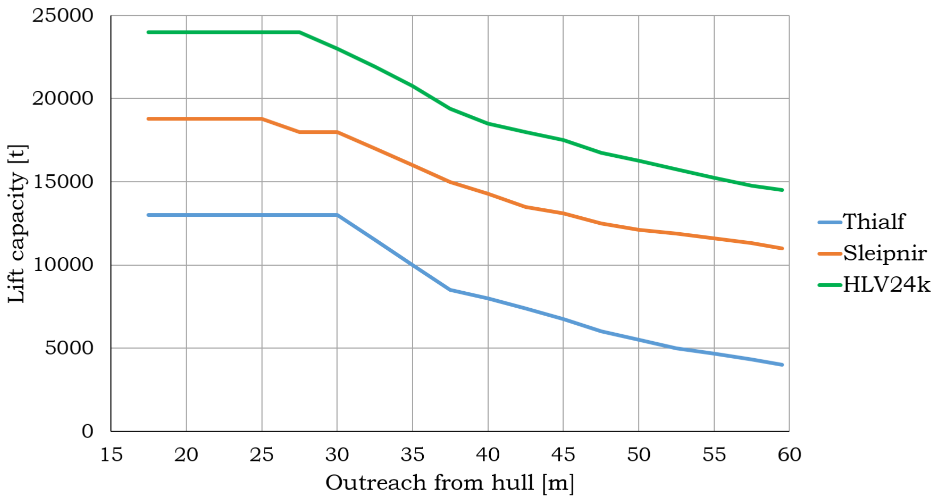

Figure 1.1: Capacity comparison HMC vessels [12]

1.4 Problem definition

The full lifting capacity of the current semi-submersible crane vessels can only be utilized with a dual crane operation. Slewing this load is limited by the configuration, therefore lifting a load from or onto own deck is restricted to the capacity of a single crane. Not being able to slew a heavy load has two main disadvantages:

- The load has to be lifted from a barge; a weather restricted operation
- The slewing of the load has to be performed with the vessel itself, shifting the limitations to the mooring or dynamic positioning (DP) system

Construction and pre-commissioning of offshore structures is typically performed as much as possible onshore. Work done onshore results in less risks and costs of construction. Offshore installation and decommissioning loads become heavier and bigger. Besides the growing base structures and topsides, the projects shift to more remote locations. Efficient transit to location can be a big cost reduction. Innovation of the semi-submersible crane vessel is required.

A possible answer is a asymmetric semi-submersible vessel with a single crane. One fully revolving tub crane with the ability to lift 24,000mT from or onto its own deck. Such a new design makes it possible to lift heavier objects, while being less dependent on the weather influences, increasing the workability.

The innovation faces challenges for the crane design itself, doubling the current highest lift capacity and a configuration that has the potential to lift drilling rigs with a high derrick. Another challenge is the design of the hull, having only a single crane placed on deck.

The conventional option would be a semi-submersible design with the single crane placed on the stern of the vessel. Two, equal in size, pontoons provide symmetry over the length of the vessel. This configuration has the disadvantage of the stern being designed both for maximum buoyancy as well as sailing capabilities, two contrary shapes requirements.

To take full advantage of the single crane semi-submersible arrangement, the crane will be positioned on the port side pontoon, midships, providing the most buoyancy directly underneath the tub. The starboard pontoon will only provide stability and counter ballast during the lift operation, allowing a more slender design. By placing the crane midships, the bow and stern of the pontoons can be optimized for transit and the thrusters can be mounted above the keel line, eliminating the need for retractable thrusters. It also provides the ability to enter into shallower waters.

The new crane has four hooks, each 6,000mT, in a rectangular arrangement. This arrangement creates opportunities for simplifying lift rigging, reduction of lift object modifications and up-righting procedures. Besides the hook arrangement, also the boom configuration will change. The intention is to keep the boom in the upright position during its whole service life, eliminating the boom rest obstacle on the main deck. The luffing mechanism, conventional done with cables, will be replaced with a rigid structure to cope with the compressive loads.

The innovation of this vessel, being still in a conceptual phase, raises several relevant topics considering the design. One of the main topics is the feasibility of designing and engineering a crane of this size.

1.5 Thesis objectives

The judgment of the concept is in this stage based on the lifting capacity and workability. The main objective of this thesis is to investigate the structural feasibility of this crane design and the workability of this vessel, including identification of show stoppers and consequences of the configuration.

Thereby is the hull study, performed by HMC, used as a set boundary conditions.

The research objective for this is formulated as follows:

"Feasibility and effectiveness study of a tub crane with an unconventional rectangular quadruple hook arrangement, capable of lifting and slewing 24,000t from and onto its own deck."

This research objective can be further specified:

- Configuration optimization on the conceptual crane design
- Structural integrity research for governing static load cases
- Dynamic study to determine the crane integrity during operational and survival loading conditions
- Research on the critical factors of the crane design.
- Research on the possibilities of increasing the workability.

1.6 Research approach

The research is performed in the following order.

1. Analysis of the concept: An analysis will be performed on the conceptual study done by Heerema Marine Contractors.
2. General dimensioning of the Crane: The configuration of the crane will be determined using a tool developed in MATLAB. An optimization will be performed on the coordinates of the characteristic points of the crane. The most promising configuration will be used to continue the research. As input for the optimization a rigid beam Liftdyn model will be used to determine the load cases.
3. Static analysis of the crane: The obtained crane configuration will be analyzed using the finite element software Abaqus. Several static load cases will be applied on the structure. This research will provide more insight on the design of the tub, bearing, crane house and the beams of the top structure.

4. Dynamic analysis of the crane: A new Liftdyn model will be made with the optimized configuration and beam bending included in the system. Motion and force time signals will be obtained from the Liftdyn analyses and a wave spectrum. The time signal of the motions of the crane origin and the four hook forces will be input for the finite element model. Furthermore the workability of the vessel will be assessed.

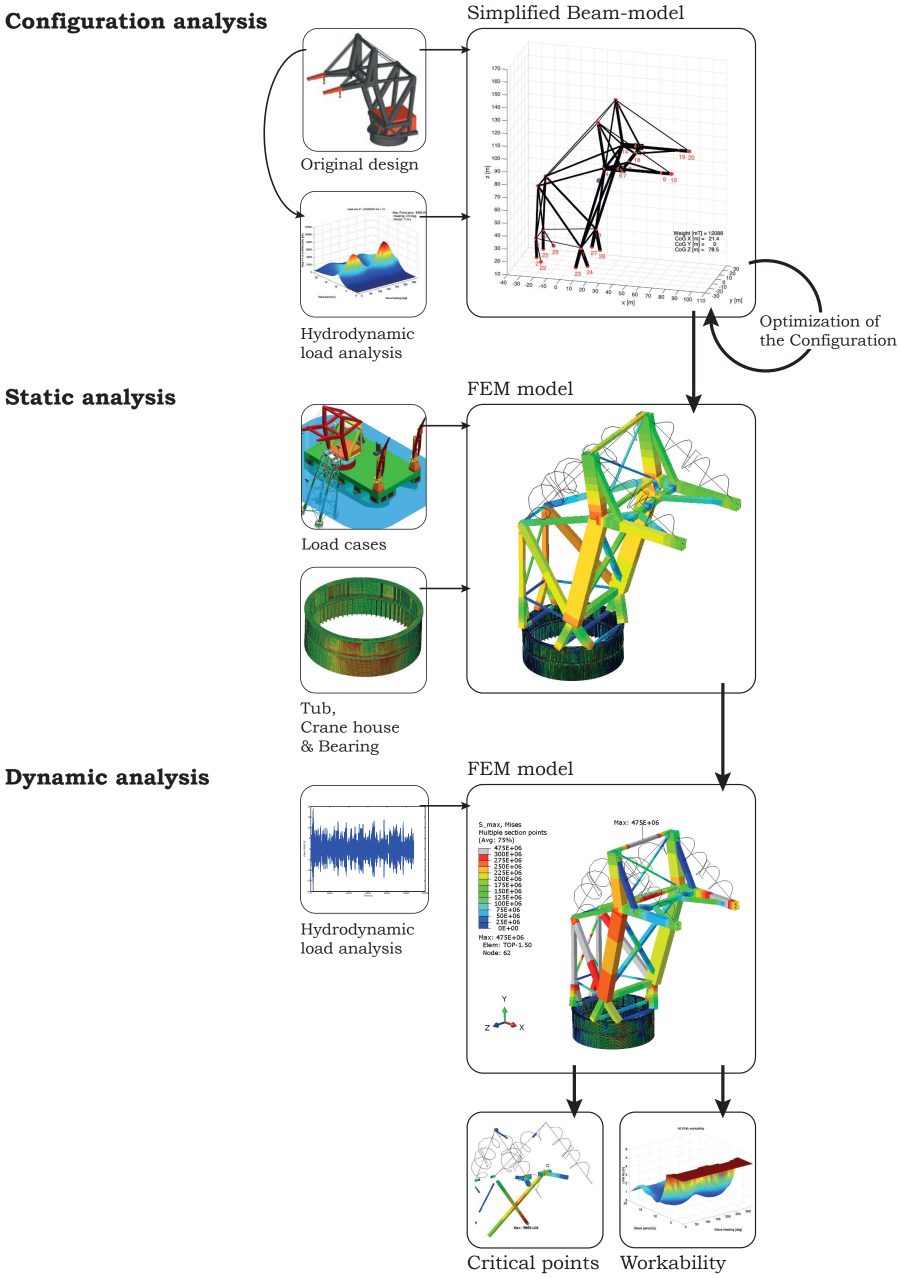

Figure 1.2: Research approach

1.7 Thesis structure

The thesis report is structured in four parts:

- Part I: Configuration analysis
- Part II: Static analysis
- Part III: Dynamic analysis
- Part IV: Evaluation

Throughout the parts of the thesis a general structure is maintained. Firstly the analysis methodology and approach is discussed. Secondly the used models are described and finally the results will be presented and evaluated.

1.8 Statement of Originality

The Author of this Thesis declares to have written this thesis all by himself. He takes full responsibility for the contents of this report. All the work, text, models included in this document are original. The sources used to creating these have been mentioned and referenced.

All the models are built by the author of this thesis excluding the following models:

- HLV24k hull MultiSurf model (author: Heerema Marine Contractors)
- Base function, implemented in the MATLAB optimization [5].
- HLV24k concept Rhino model (author: Heerema Marine Contractors)

2

HLV24k concept

Today HMC owns three of the worlds largest heavy lift vessels. All dating back from the eighties, they sooner or later require replacement. To find an adequate response to this event Heerema, more specific the Innovation department, performs concept studies researching the possibility of new designs. The search for more lifting capacity, increased workability and low cost yielded the HLV24k concept. An ultra Heavy Lift Vessel capable of lifting 24,000t objects onto its own deck, exceeding the capacity of all the existing vessels today. A vessel with an effective deck working space allowing this vessel to be versatile and efficient during offshore operations. Inspired by the Polynesian proa, Figure 2.1, well known for their slender but stable hull, the HLV24k is outfitted with two pontoons differing in size. The vessel is outfitted with a single revolving tub crane with a lifting capacity of 24,000t. The choice for a single crane gives the ability, compared to a dual crane vessel, to lift and slew with the full capacity from its own deck. This can provide an advantage in workability of the vessel, because the limiting barge lifts can be performed in calm waters, like a fjord, instead of offshore at the installation location. The concept study of the Heavy Lift Vessel 24,000t (HLV24k) formed the basis for this research [12].

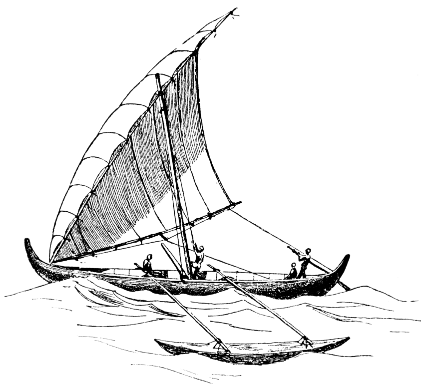

Figure 2.1: A typical Polynesian proa [27]

The use of single crane allows for a vessel design with the crane placed at port side of the vessel mid ships. This placement comes with additional advantages for the hull design. The most buoyancy is required underneath the crane tub, translating into a large pontoon and column size. The most buoyancy is available at mid length of the vessel, also allowing the bow and stern of the hull to be designed more slender. A more slender design allows for improved transit speeds, due to less resistance and a more optimal flow towards the stern thrusters. Next to that the thrusters can be mounted above the keel line of the vessel, allowing the Dynamic Positions System to be used at shallow water and eliminating the need for retractable thrusters. The smaller starboard side pontoon acts here as a counter ballast for the lifting operations, simultaneously providing the stability of the vessel. Figure 2.2 gives an first impression of the concept studied.

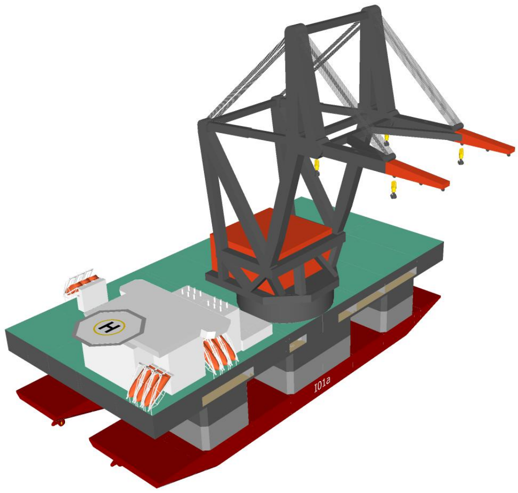

Figure 2.2: HLV24k Concept

Comparing the concept with the current biggest lift vessel, the Thialf, and the one currently being built, the Sleipnir, gives an indication of the relative size of the hull compared to the capacity of the vessel. The width of the vessel should not exceed 124m and the minimal draft should be less than 10m, because of limitations in dry docking. The design effort has been to seek for the minimal length of the pontoons, without any compromises in motion behavior. Besides the CAPEX penalty, also a negative correlation with the OPEX is associated with the length, as the required DP power increases with an increasing length. In a business where vessel size is compared with lift capacity, HLV24k's advantages in design and layout become even more clear, Table 2.1.

Table 2.1: Vessel comparison

Vessel	Lift Capacity $[t]$	LUW $[t]$	Length $[m]$	Width $[m]$	Height $[m]$
HLV24k	24,000	132,928	220	110	49.5
Thialf	14,200	136,709	201.6	88.4	49.5
Sleipnir	20,000	124,000	214	97.5	49.5

As stated earlier a preliminary concept study has been performed, therefore not all details concerning the hull and crane are known. The concept study did include a parametric hull study resulting in one hull design which gave the most promising motion behaviors [13]. This hull is therefore assumed and used in this research. The crane, Figure 2.2, has been investigate on a lower detail level. HMC expertise and engineering judgment led to the basic configuration of the crane. The crane has been configured such that the most ideal lift clearance is obtained. This clearance under the structural crane elements is required for the lift of the base case load, defined as a box of 60x60x100m weighing close to 24,000t. This thesis continues the investigation of the HLV24k crane, analyzing the geometry, structural integrity and workability. The judgment to proceeding with this concept will be, among other things, based on the outcome of this research.

2.1 Crane

The HLV24k crane is a crane in the category 'tub crane', a crane with all it's components placed on a bearing, allowing for full rotation over 360deg. The crane has four main hoists suspended from two adjustable jibs which are, together with the other beam elements, mounted on a rotating basis. The design is primarily configured to lift large object with the four hooks, however the configuration allows for lifting with a reduced number of hoists. During the concept phase the crane is configured such that it is suitable for the main Heerema activities:

- Installation of small and large topsides on floating and fixed support structures
- Upending and installation of jackets

- Upending and installation of foundation piles
- Upending, lowering and installation of suction piles
- Installation of flare booms
- Removals of topsides and jackets
- Personnel transfers
- Supply lifts, containers

The initial design of the crane is visualized in Figure 2.3, showing the clearance under the hooks.

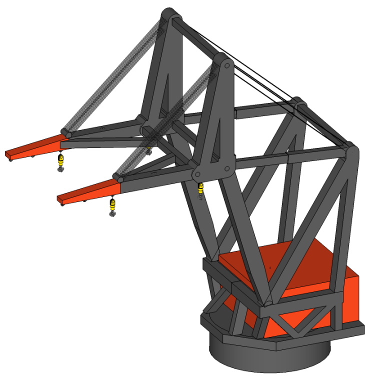

(a) Jibs in horizontal position

(b) Jibs in upright position

Figure 2.3: HLV24k crane Concept

2.1.1 Part

The Crane design is built up from several distinctive parts depicted in Table 2.2 and Figure 2.4.

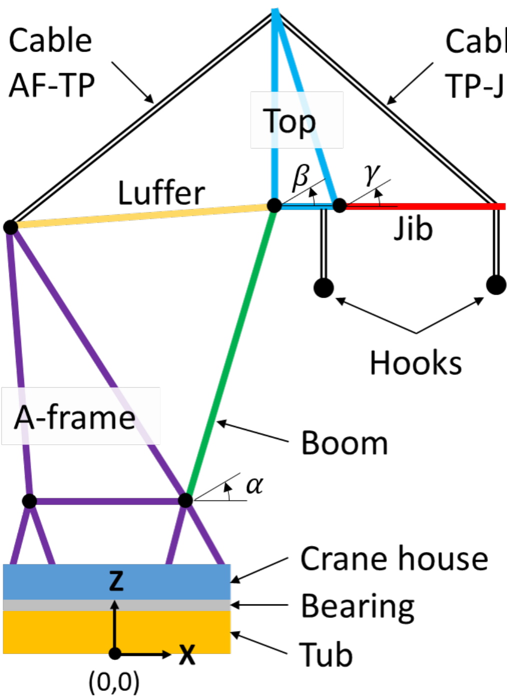

Figure 2.4: Crane parts (side view)

Table 2.2: The general overview of the crane parts

Part	ID	Amount	Description
Tub	TB	1	The cylindrical structure connecting the crane to the vessel
Bearing	-	1	The revolving connection between the tub and crane house
Crane House	CH	1	The cylindrical structure supporting the A-frame, boom and equipment
Winches	-	1	Spool with all the required wires
Heel point	HP	2	Connection point of the boom to the crane house
A-frame	AF	1	The structure on top of the crane house
Boom	BM	1	Support structure for the top frame
Luffer	LF	2	Beam fixing the boom at an certain position
Top frame	TP	1	Structure support two hooks and two jibs
Jib	JB	2	Boom at the top frame supporting the outer hoists
Hook	HK	4	Hook including the main block

2.1.2 Dimensioning

In the pre-study performed by HMC, the main configuration of the crane has been determined. This configuration was used as the starting point for the further optimization and feasibility study. Table 2.3 shows the coordinates and center of gravity (CoG) of the parts and equipment taken into account.

Table 2.3: Main crane part particulars

Part	Length X $[m]$	Width Y $[m]$	Height Z $[m]$	Mass m $[t]$	CoG [X,Y,Z] $[m]$
Tub	50	50	9.288	1711	(0,0,4.64)
Crane house	50	50	7.2	13215	(-3,0,24.4)
A-frame	38.097	50	76.511	2922	(-9.5,0,55.5)
Boom	68.254	50	7	2034	(35.31,0,0)
Luffer	56.32	2	3	678	(28.16,0,0)
Top	13.34	50	46.286	1212	(3.4,0,14.262)
Jib	37.034	5	7	1589	(18.16,0,-0.86)

The four hooks are placed in a rectangular arrangement of 40x50m. These dimensions are based on the average topside connection point spacing and situated in such a way, that the need for additional rigging is reduced. This hook arrangement is set as a boundary condition for the crane configuration. The outreach is measured from the edge of the vessel and the lifting height from deck level.

Table 2.4: Main hook capacity data

Hook	Load $[t]$	Outreach $[m]$	Max. lift height $[m]$
11	6,000	18.2	101.7
12	6,000	58.2	145.5
21	6,000	18.2	101.7
22	6,000	58.2	145.5

The use of hinge points and cable luffing mechanism allows for a range in crane positions. These positions can be adjusted to be suited for the job. In this thesis the default settings are used, which are optimized for the lift of the specified base case. The default crane settings are defined as follows:

Table 2.5: The default crane settings

Setting	Symbol	Value $[deg]$	Positive direction
Slew angle	ψ	0, 90, 180, 270	Rotation from bow to port side
Boom angle	α	73.5	Upward from the horizontal plane
Top angle	β	0	Upward from the horizontal plane
Jib angle	γ	0	Upward from the horizontal plane

2.1.3 Tub diameter

The tub and slewing ring will be much larger than those of existing cranes. The crane tubs of the Thialf measure 28m in diameter, those of the Sleipnir are 30m. A 50m diameter tub is suggested based on scaling with the current Heerema cranes. The tub diameter is checked on the criteria of overturning moment resistance. From experience within Heerema the normative tub diameter is determined by the amount and size of the bolts that can be fitted in the circumferential [6]. Furthermore the Lloyds Register design codes unity checks are performed [18]:

- Total occurring moment / Total resisting moment ≤ 1
- Bolt peak load / Bolt Safe Working Load (SWL) ≤ 1

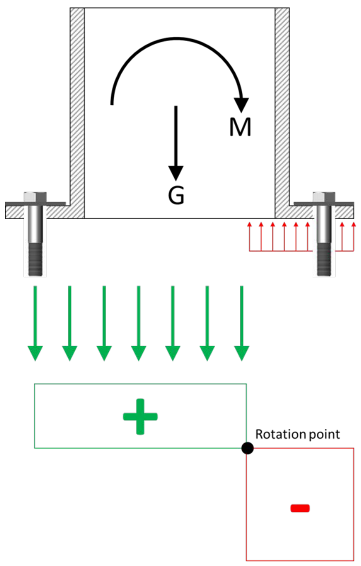

Figure 2.5: Tub overturning moment principle (cross section)

The M80 bolts used in the Sleipnir crane tub are assumed for the unit checks, Table 2.6. The critical point in the tub design is found at the interface with the vessel deck where the occurring axial loads and overturning moment are the highest. The main particulars of the interface connection are depicted in Table 2.7.

Table 2.6: Bolt M80 S900 particulars

Parameter	Symbol	Unit	Value
Min. spacing	-	$[mm]$	182
Effective radius	R_{eff}	$[mm]$	37
Safety factor	SF	$[mm]$	0.4
Ultimate tensile strength	UTS	$[N/mm^2]$	900
Safe working load	SWL	$[N/mm^2]$	360

Table 2.7: Tub vessel deck connection parameters

Parameter	Symbol	Unit	Value
Number of bolts	n	[-]	863
Tub diameter	R	$[m]$	50
Center line offset	d	[-]	0.32
Vertical design load	F_z	$[N]$	$4.7 \cdot 10^8$
Moment design load	$M_{y,occ}$	$[Nmm]$	$1.86 \cdot 10^{13}$
Ultimate tensile strength	UTS	$[N/mm^2]$	900
Safe working load	SWL	$[N/mm^2]$	360

Overturning moment unity check:

$$M_{y,res} = \sum_{\theta=-tan^{-1}(2d)}^{\pi+tan^{-1}(2d)} F_{bolt} \cdot R \cdot ((2d) + sin(\theta)) = 2.07 \cdot 10^{13} \tag{2.1}$$

$$= \sum_{\theta=-0.57}^{3.7} 1.55 \cdot 10^6 \cdot 25000 \cdot ((2 \cdot 0.32) + sin(\theta)) = 2.07 \cdot 10^{13} \tag{2.2}$$

$$\frac{M_{y,occ}}{M_{y,res}} = \frac{1.86 \cdot 10^{13}}{2.07 \cdot 10^{13}} = 0.89 \leq 1 \tag{2.3}$$

Bolt peak load unity check:
The bolt peak load is measured on the outermost bolt, the one subjected to the largest overturning moment.

$$F_{P,bolt} = \left(\frac{4M_{y,occ}}{D_{tub}} - F_z \right) / n_{bolt} \tag{2.4}$$

$$= \left(\frac{4 \cdot 1.86 \cdot 10^{13}}{50000} - 4.7 \cdot 10^8 \right) / 863 = 1.18 \cdot 10^6 N \tag{2.5}$$

$$\sigma_{p,bolt} = \frac{F_{P,bolt}}{\pi \cdot R_{eff}^2} = \frac{1.18 \cdot 10^6}{4300} = 275 N/mm^2 \tag{2.6}$$

$$\frac{\sigma_{p,bolt}}{SWL_{bolt}} = \frac{275}{360} = 0.76 \leq 1 \tag{2.7}$$

The bolt peak load does not exceed the safe work load limit.
Both unity checks show results which are within the set limits. Therefore is concluded that the tub diameter is sufficient for this crane design.

2.2 Report definitions

In this report the following agreements have been used to avoid confusion. The agreements relate to the coordinate system, terminology and elements ID's.

2.2.1 Coordinates system

In this report, if not specified otherwise, the following coordinate system is used, also referred as the right-handed ship fixed system. Figure 2.6 gives an overview of the origin of the axis system, as well as the positive directions.

Table 2.8: Right-handed ship co-ordinate fixed system

Direction	Symbol	Axis	Positive when
Longitudinal	X	X-axis	Forward
Transverse	Y	Y-axis	Towards Port side
Vertical	Z	Z-axis	Upwards
Roll	ϕ	Rotation around X-axis	Port side up
pitch	θ	Rotation around Y-axis	Bow down
Yaw	ψ	Rotation around Z-axis	Rotation bow to port side

Table 2.9: Ship origin (SO)

Position	Axis	Location
Longitudinal	X_s	Stern pontoon
Transverse	Y_s	Mid of the width
Vertical	Z_s	Keel

Table 2.10: Feature origins

Origin	Symbol	X_s $[m]$	Y_s $[m]$	Z_s $[m]$
Ship	SO	0.0	0.0	0.0
Crane	CO	110	30	49.5
WAMIT	WO	110	2.27	draft

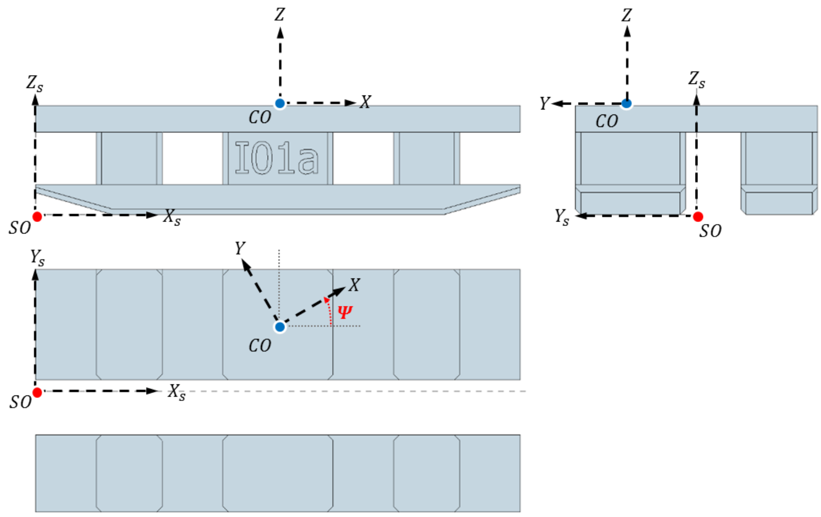

Figure 2.6: Origin of the ship and crane

2.2.2 Terminology

The following definitions are used in this report (see also the references [14], [15]):

Allowable stress $[\sigma_{all}]$ ultimate tensile strength devided by the safety factor

$$\sigma_{all} = \frac{\sigma_y}{SF}$$

Lift object $[-]$ the structure, facility or topside which is to be lifted

Design weight $[W_{des}]$ the dry weight of a lift object increased with a weight contingency

Rigging weight $[W_{rig}]$ the total weight of all the detachable tools required to connect the lift object to the crane hooks, the main ones being slings, grommets, shackles and spreaderbars

Dynamic Amplification Factor $[DAF]$ the factor by which the weight is multiplied to account for vertical dynamic loads resulting from the lift operation

Table 2.11: Dynamic Amplification Factors

Lift operation	Design weight lift object	
	< 100t	≥ 100t
Inshore areas	1.1	1.05
Offshore lift at vessel deck	1.1	1.05
General offshore	1.2	**1.1**
Offshore submerged	≥ 1.5	≥ 1.2

Hookload	$[HL]$	the weight of the lift object and rigging suspended from the crane hook $$\mathrm{HL} = W_{des} + W_{rig}$$
Design hookload	$[HL_{des}]$	the weight suspended from the crane hook including dynamic contingencies $$\mathrm{HL_{des}} = \left(W_{des} + W_{rig}\right) \cdot \mathrm{DAF}$$
Safe working load	$[SWL]$	the maximum hookload of the crane given the conditions
Crane Lift Capacity	$[-]$	Number of hooks times the maximum hookload for the crane configuration
Top block	$[-]$	the pack of sheaves placed in the crane boom/jib from which the load is suspended
Hook	$[-]$	the main hook including the pack of sheaves
Offlead	$[OL]$	a horizontal load at the crane tip (top block) caused by a radial displacement of the hook
Sidelead	$[SL]$	a horizontal load at the crane tip (top block) caused by a transverse displacement of the hook
Heel	$[\phi]$	Initial tilt of the vessel around X-axis
Trim	$[\theta]$	Initial tilt of the vessel around Y-axis
Lift clearance	$[-]$	Minimum clearance between the heavy lift vessel (including cranes and appurtenances) and the lift object

2.2.3 Hydrodynamics

The wave heading directions are defined in Figure 2.7, with heading zero in the positive X-direction (from stern to bow), rotating anti-clockwise.

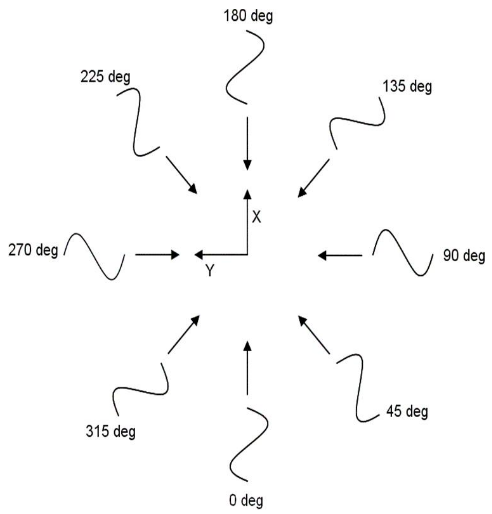

Figure 2.7: Wave heading

2.2.4 Hooks

The four hooks used in this concept design are defined as follows:

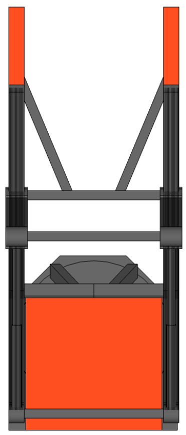

(a) Crane render (top view)

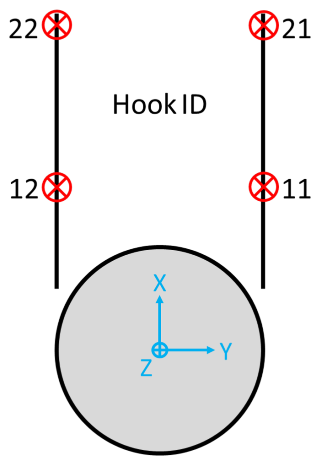

(b) Schematization of the crane (top view)

Figure 2.8: Hook IDs as seen from the top

I
Configuration analysis

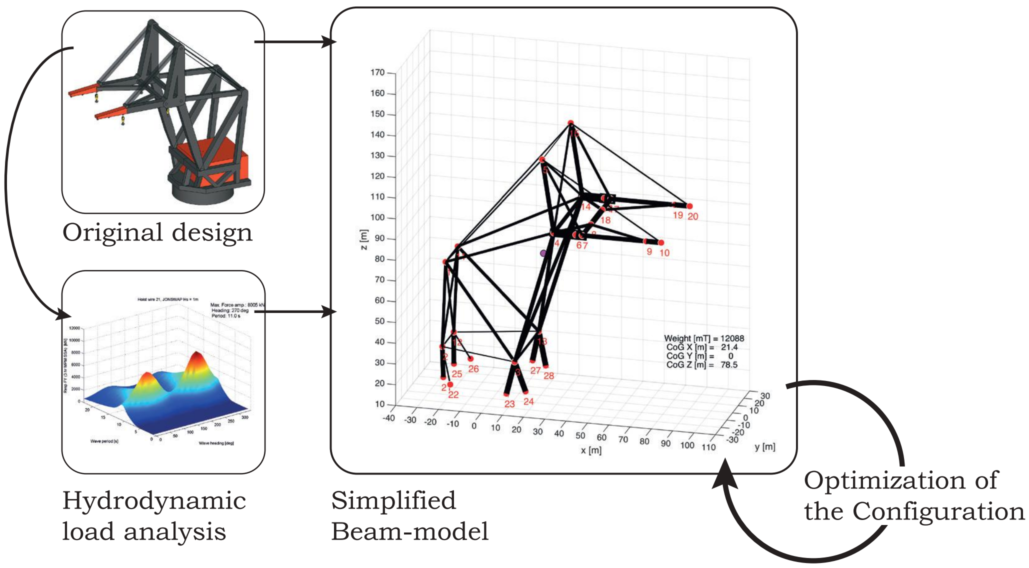

3
Analytical beam model

In the pre-study done by HMC, the main configuration of the crane has been determined. In order to check and optimize this configuration a simplified beam model is made. The crane's upper structure, excluding the tub, bearing and crane house, was modeled with beam elements in MATLAB [19]. The basic model principle used is stated in the book "MATLAB Codes for Finite Element Analysis" [5]. The crane parts are simplified to beam members, assigning the member with a cross-section and the material properties result in a stiffness matrix.

3.1 Beam members

A beam element is an object spanning the gap between two points, which is generally slender. For a structural analysis a beam is represented as an element with a node at each end. When the element is loaded the nodes are horizontally (u) and vertically (v, w) displaced and rotated (θ_x,θ_y,θ_z). Both the nodes are therefore subjected to axial forces, shear forces and moments. In total the element has six degrees of freedom (DoF) at each node, summing up to twelve DoF [24], [17], [23].

The initial beam configuration is based on the original crane configuration. All the beams are represented by two nodes connected with an element. This element is given the appropriate properties. Figure 3.1 shows the representation of the crane in MATLAB.

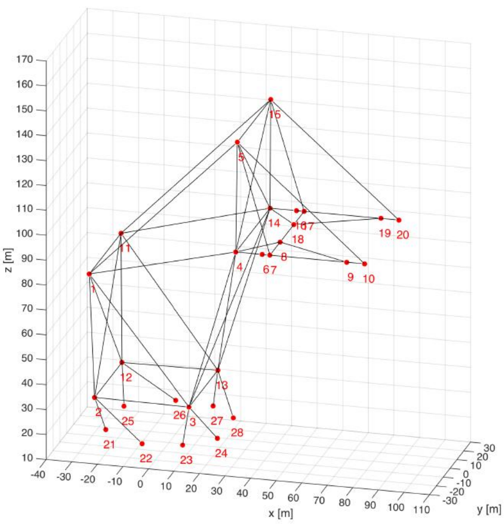

Figure 3.1: MATLAB beam model initial crane configuration

3.2 Stiffness matrix

The elements in the model are assigned a stiffness matrix, Equation 3.1. This matrix represents a spacious beam with six DoF at the two nodes. The stiffness matrix represents a beam behaving according to the Euler-Bernoulli beam equations. The beams are considered slender structures therefore the approximation with the Euler-Bernoulli equations is sufficient. The Timoshenko shear correction may be omitted if beam slenderness is the case [1].

$$[K] = \begin{bmatrix} k1 & 0 & 0 & 0 & 0 & 0 & -k1 & 0 & 0 & 0 & 0 & 0 \\ 0 & k2 & 0 & 0 & 0 & k3 & 0 & -k2 & 0 & 0 & 0 & k3 \\ 0 & 0 & k6 & 0 & -k7 & 0 & 0 & 0 & -k6 & 0 & -k7 & 0 \\ 0 & 0 & 0 & k10 & 0 & 0 & 0 & 0 & 0 & -k10 & 0 & 0 \\ 0 & 0 & k7 & 0 & k8 & 0 & 0 & 0 & k7 & 0 & k9 & 0 \\ 0 & k3 & 0 & 0 & 0 & k4 & 0 & -k3 & 0 & 0 & 0 & k5 \\ -k1 & 0 & 0 & 0 & 0 & 0 & k1 & 0 & 0 & 0 & 0 & 0 \\ 0 & -k2 & 0 & 0 & 0 & -k3 & 0 & k2 & 0 & 0 & 0 & -k3 \\ 0 & 0 & -k6 & 0 & k7 & 0 & 0 & 0 & k6 & 0 & k7 & 0 \\ 0 & 0 & 0 & -k10 & 0 & 0 & 0 & 0 & 0 & k10 & 0 & 0 \\ 0 & 0 & -k7 & 0 & k9 & 0 & 0 & 0 & k7 & 0 & k8 & 0 \\ 0 & k3 & 0 & 0 & 0 & k5 & 0 & -k3 & 0 & 0 & 0 & k4 \end{bmatrix} \tag{3.1}$$

with:

$$\begin{aligned} k1 &= \frac{E \cdot A}{L} & k5 &= \frac{2 \cdot E \cdot I_Z}{L} & k8 &= \frac{4 \cdot E \cdot I_Y}{L} \\ k2 &= \frac{12 \cdot E \cdot I_Z}{L^3} & k6 &= \frac{12 \cdot E \cdot I_Y}{L^3} & k9 &= \frac{2 \cdot E \cdot I_Y}{L} \\ k3 &= \frac{6 \cdot E \cdot I_Z}{L^2} & k7 &= \frac{6 \cdot E \cdot I_Y}{L^2} & k10 &= \frac{G \cdot J}{L} \\ k4 &= \frac{4 \cdot E \cdot I_Z}{L} \end{aligned} \tag{3.2}$$

For each member the cross-section properties are derived by basic material mechanics.

3.2.1 Interface conditions

Some of the parts are connected via hinges, for instance the boom connection to the crane house. These hinges are modeled by modifying the rotational degree of freedom in the stiffness matrix. Equation 3.3 shows the modification in the stiffness matrix for the boom-member, which hinges around the Z axis, at both nodes [2].

$$\begin{aligned} [K], \text{row } 2 &= \begin{bmatrix} 0 & k2 & 0 & 0 & 0 & k3 \Rightarrow 0 & 0 & -k2 & 0 & 0 & 0 & k3 \Rightarrow 0 \end{bmatrix} \\ [K], \text{row } 6 &= \begin{bmatrix} 0 & k3 \Rightarrow 0 & 0 & 0 & 0 & k4 \Rightarrow 0 & 0 & -k3 \Rightarrow 0 & 0 & 0 & 0 & k5 \Rightarrow 0 \end{bmatrix} \\ [K], \text{row } 8 &= \begin{bmatrix} 0 & -k2 & 0 & 0 & 0 & -k3 \Rightarrow 0 & 0 & k2 & 0 & 0 & 0 & -k3 \Rightarrow 0 \end{bmatrix} \\ [K], \text{row } 12 &= \begin{bmatrix} 0 & k3 \Rightarrow 0 & 0 & 0 & 0 & k5 \Rightarrow 0 & 0 & -k3 \Rightarrow 0 & 0 & 0 & 0 & k4 \Rightarrow 0 \end{bmatrix} \end{aligned} \tag{3.3}$$

3.3 Mass matrix

The continuous mass matrix, Equation 3.4, is used to represent the mass distribution over the beam member [1] .

$$[M] = \begin{bmatrix} m1 & 0 & 0 & 0 & 0 & 0 & m2 & 0 & 0 & 0 & 0 & 0 \\ 0 & m3 & 0 & 0 & 0 & m4 & 0 & m5 & 0 & 0 & 0 & -m6 \\ 0 & 0 & m3 & 0 & -m4 & 0 & 0 & 0 & m5 & 0 & m6 & 0 \\ 0 & 0 & 0 & m7 & 0 & 0 & 0 & 0 & 0 & -m8 & 0 & 0 \\ 0 & 0 & -m4 & 0 & m9 & 0 & 0 & 0 & -m6 & 0 & -m10 & 0 \\ 0 & m4 & 0 & 0 & 0 & m9 & 0 & m6 & 0 & 0 & 0 & -m10 \\ m2 & 0 & 0 & 0 & 0 & 0 & m1 & 0 & 0 & 0 & 0 & 0 \\ 0 & m5 & 0 & 0 & 0 & m6 & 0 & m3 & 0 & 0 & 0 & -m4 \\ 0 & 0 & m5 & 0 & -m6 & 0 & 0 & 0 & m3 & 0 & m4 & 0 \\ 0 & 0 & 0 & -m8 & 0 & 0 & 0 & 0 & 0 & m7 & 0 & 0 \\ 0 & 0 & m6 & 0 & -m10 & 0 & 0 & 0 & m4 & 0 & m9 & 0 \\ 0 & -m6 & 0 & 0 & 0 & -m10 & 0 & -m4 & 0 & 0 & 0 & m9 \end{bmatrix} \tag{3.4}$$

with:

$$m1 = \frac{A \cdot L \cdot \rho}{3} \quad m5 = \frac{9 \cdot A \cdot L \cdot \rho}{70} \quad m8 = \frac{J \cdot L \cdot \rho}{6}$$
$$m2 = \frac{A \cdot L \cdot \rho}{6} \quad m6 = \frac{13 \cdot A \cdot L^2 \cdot \rho}{420} \quad m9 = \frac{A \cdot L^3 \cdot \rho}{105}$$
$$m3 = \frac{13 \cdot A \cdot L \cdot \rho}{35} \quad m7 = \frac{J \cdot L \cdot \rho}{3} \quad m10 = \frac{A \cdot L^3 \cdot \rho}{140}$$
$$m4 = \frac{11 \cdot A \cdot L^2 \cdot \rho}{210} \tag{3.5}$$

3.4 Integration point

The beams are represented by a box cross-section to model the typical crane truss sections. The stress levels in the model are calculated using the forces and overturning moments per beam. The combination of these forces and moments result in the following stress:

- Normal stress due to axial force
- Shear stress due to shear force
- Shear stress due to torsion
- Bending stress due to overturning moment

Because the stress distribution over the cross-section is not homogeneous it has to be calculated on several spots. These integration points (●) are shown in Figure 3.2. The points are selected on locations where the maximum stresses are expected to occur. Symmetry is assumed over the diagonal (blue dashed line), because the box is rectangular with a homogeneous wall thickness.

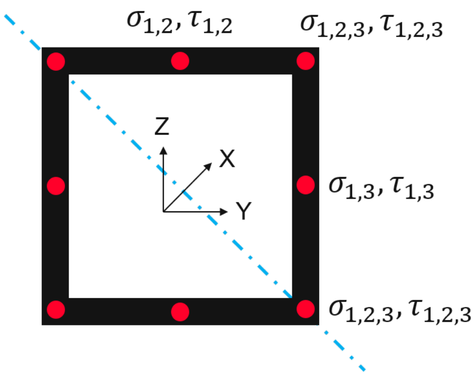

Figure 3.2: Beam cross section integration points

$$\sigma_1 = \frac{F_X}{A} \tag{3.6}$$

$$\sigma_{(2,3)} = \frac{M_{(Y,Z)} \cdot d}{I_{(Y,Z)}} \tag{3.7}$$

$$\tau_1 = \frac{T \cdot c}{J} \tag{3.8}$$

$$\tau_{(2,3)} = \frac{V_{(Y,Z)} \cdot Q}{I_{(Y,Z)}} \tag{3.9}$$

The relation between the cross-section area and the moment of inertia is set. This relation is calculated based on the assumption that the ratio wall thickness:beam size = 1:10, as can be seen in Figure 3.3. This ratio has to be specified in order for the optimization to calculate all forces and moments associated with a cross-section area.

An equivalent stress is calculated for the eight integration points with Equation 3.10.

$$\sigma_{eq} = \sqrt{(\sigma^2 + 3 \cdot \tau^2)} \tag{3.10}$$

The calculation has been performed for both nodes of the beam member. The maximum equivalent stress value is taken form the eight points and assumed over the whole cross-section. This is considered to be a conservative method, because local peak stresses are assumed for the whole element [21], [22], [26], [28].

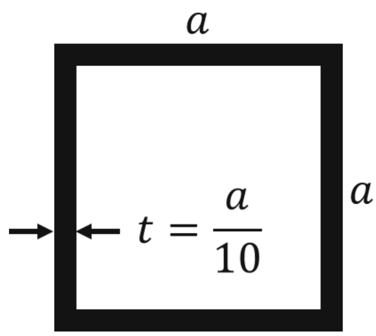

Figure 3.3: Beam ratio assumption

3.5 Model input

The beam model made requires a list of input parameters in order to calculated all the displacements and forces. The input parameters used for the crane model are stated below.
Node coordinates: input for the model are the 28 nodes. To model the beams a list with the node connections has to be provided.

Table 3.1: Node co-ordinates MATLAB model

Input	Parameter	Unit	Source
28 nodes	X, Y, Z	$[mm]$	Original crane model
52 elements	node 1, node 2	[-]	Original crane model

Material properties: two types of material have been used: the beam elements steel and the cable element steel.

Table 3.2: Material properties MATLAB model

Input	Parameter	Unit	Value
Beam element	Steel grade	[-]	S450
	σ_y	$[N/mm^2]$	450
	ρ	$[kg/m^3]$	7850
	E	$[N/mm^2]$	210,000
	G	$[N/mm^2]$	70,000
	SF	[-]	1.5
	σ_{all}	$[N/mm^2]$	300
Cable element	Steel grade	[-]	1960
	ρ	$[N/mm^2]$	9000
	E	$[N/mm^2]$	100,000
	σ_{all}	$[N/mm^2]$	650

Loading: the loading can only be applied on the nodes of the beam model. The loading must be applied in the global coordinate system.

Table 3.3: Loading conditions MATLAB model

Input	Parameter	Unit
Node forces	$F_x, F_y, F_z, M_x, M_y, M_z$	$[N]$

Boundary conditions: the eight points at the tub connections are constraint in all six DoF simulating the welded connection with the tub. This translates into a stiffness matrix where the DoF stiffnesses of the specific node are set to zero.

Table 3.4: Boundary conditions MATLAB model

Point	DoF	Value
21	1-6	fixed
22	1-6	fixed
23	1-6	fixed
24	1-6	fixed
25	1-6	fixed
26	1-6	fixed
27	1-6	fixed
28	1-6	fixed

4
Hydrodynamic analysis

During the operational lifetime of the HLV24k a variety of vessel conditions can be observed. The vessel conditions can be divided in three main categories: transit, operational and survival. The conditions are primarily distinguished by the draft of the vessel and the work limits (maximum significant wave height H_s) as can be seen in Table 4.1. This research will focus on the operational and survival loading conditions, because these are the main indicators for the structural integrity of the crane. The transit case is mainly interesting for the fatigue life of the vessel and crane due to the large number of loading cycles the vessel encounters during transit periods.

Table 4.1: Limit Hs per loading condition

Loading Condition	Draft $[m]$	Max. H_s $[m]$
Transit	12	6
Operational (lift)	27	3
Operational (non-lift)	27	5.5
Survival	19	Figure 4.1

The significant wave height per load conditions is depicted in Table 4.1. For transit and operational conditions the wave height limit is based on Heerema regulations and experience with the current heavy lift vessels. If this wave is exceeded the operations are stopped and safety measures will be taken. The survival loading conditions are limited by physics, which is translated into a maximum wave height Hs-Tp contour, Figure 4.1. This graph indicates the maximum wave height per wave peak period, constructed by a combination of the maximum wave steepness curve and the 50-year North Atlantic statistics [7].

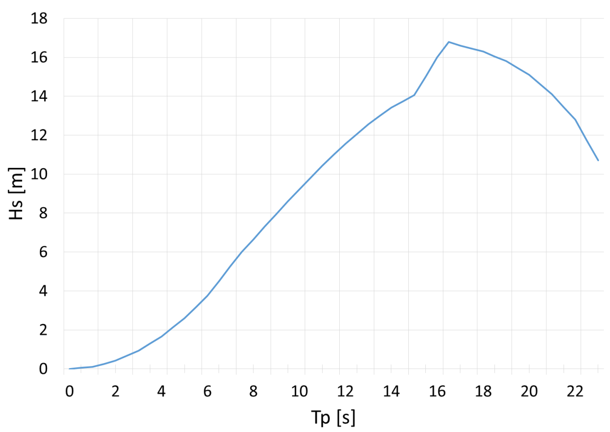

Figure 4.1: Max. wave height - wave peak period contour

4.1 Hull selection

A hull research has been performed by Heerema Marine Contractors, in order to obtain the most optimal hull for workability and the deck layout [13]. Several hull configurations were analyzed and based on predetermined criteria it has been concluded that hull model I01a, Figure 4.2, shows the best characteristic of all the hull analyzed. Therefore this hull will be used for further development of the HLV24k concept, including this thesis. Further detail is defined in Appendix B.

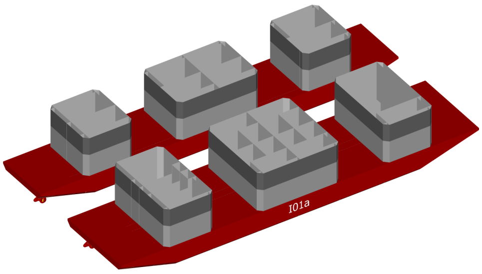

(a) Hull render (ISO view)

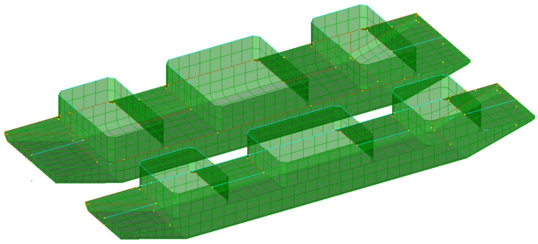

(b) WAMIT input hull 27m draft, cutoff at the waterline (ISO view)

Figure 4.2: Hull I01a (ISO View)

4.2 WAMIT analysis

The first step to obtain the hydrodynamic properties of the vessel is to perform a WAMIT analysis [25]. The WAMIT software uses diffraction theory to create a hydrodynamic database describing the vessel responses to waves for a specific draft. The diffraction analysis is performed for the three drafts used in the research: 12, 19 and 27m. The wave parameters used in the analysis are described in Table 4.2. The details of the WAMIT analysis are found in section B.3.

Table 4.2: WAMIT parameters

Parameter	Unit	Range	Step size
Wave frequency	$[rad/s]$	0.03 - 1.59	0.01
Wave frequency	$[Hz]$	0.005 - 0.25	0.0015
Wave heading	$[deg]$	0 - 345	15

All WAMIT outputs are dimensionless and therefore post-process with HMC conversion script. The Wamit outputs are converged to dimensions and frequency domain and stored in a hydrodynamic database. This database is further used as input for the Liftdyn[10] analysis.

4.3 Liftdyn original model

With the output of the diffraction analysis in WAMIT, a frequency domain analysis has been performed. HMC developed a software package Liftdyn to perform such an analysis [10]. Liftdyn is software that is designed to model and solve general linear hydrodynamic problems in the frequency domain. In Liftdyn a system of rigid bodies is created. The rigid bodies are connected to each other via springs, dampers and joints. Solving the system of bodies and connections results in a frequency depended response or response amplitude operator (RAO). The RAOs can be post processed to a motion, velocity and acceleration of any point relative to an other point. In the connector elements a force is calculated. Using a wave spectrum the responses of these parameters are determined.

In this research Liftdyn is used to model the combination of the hull and the crane. With these models the acceleration of the crane parts has been calculated. These accelerations were the basis for the optimization analysis. All the analyses have been performed for a 1m significant wave height. Because of the linearity the results can be scaled to the required wave height.

The original configuration of HLV24k is the basis for this Liftdyn model. The model consists of the following elements:

Table 4.3: Lifdyn model elements

Part	Element type	Amount	Connection	Particulars
Hull	Rigid body	1	Hydrodynamics	Weight
Tub & crane house	Non-structural body	1	Joint	Weight
A-frame	Non-structural body	1	Fixed to vessel	Weight
Boom	Rigid body	1	Hinges	Weight
Top	Rigid body	1	Hinges	Weight
Jib	Rigid body	2	Hinges	Weight
Luffer	Connector	2	Spring	Weight
Jib brace	Connector	2	Spring	Weight
Cable AF-TP	Connector	2	Spring & dashpot	Pre-tension
Cable TP-JB	Connector	2	Spring & dashpot	Pre-tension
Hoist wires	Connector	4	Spring & dashpot	Pre-tension
Lift object	Rigid body	1	Hoist wires	Weight

The crane elements are visualized in Figure 4.3. The orange tub, crane house and A-frame are non-structural elements, modeled for visual purpose only. The elements are fixed to the vessel and the center of gravity and weight of the elements have been accounted for in the hull body.

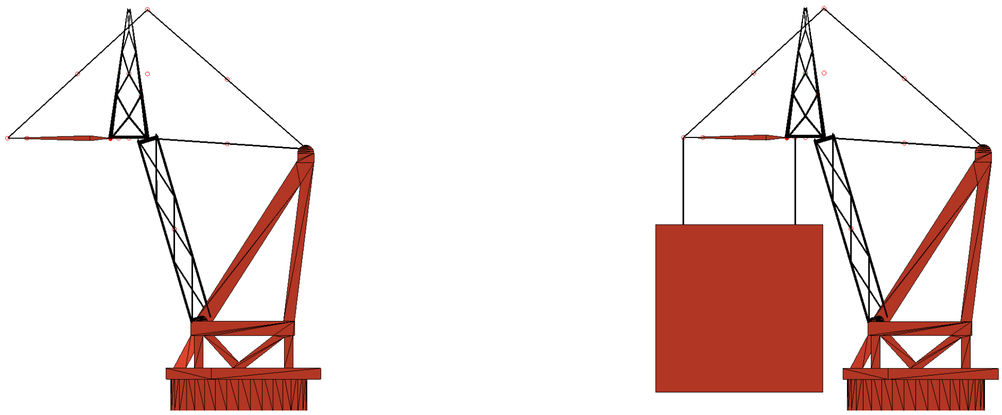

(a) No lift object (side view)

(b) Lift object (side view)

Figure 4.3: Liftdyn rigid crane model

4.3.1 Survival models

To analyze the survival conditions two models have been created. During a storm the crane is positioned above deck, therefore two crane positions have been considered: towards the stern (180deg) and towards starboard (270deg). Which positions is favorable during survival conditions will be determined during the dynamic analysis, chapter 10. The survival models are visualized in Figure 4.4.

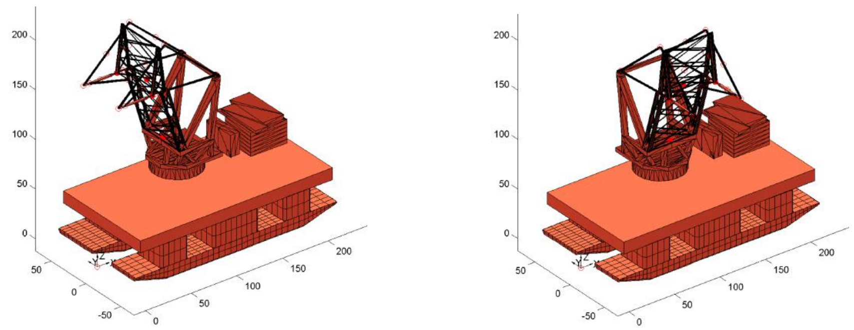

(a) M2 180 (ISO view) (b) M2 270 (ISO view)

Figure 4.4: M2: liftdyn survival model

4.3.2 Operational models

A typical lift operation for the HLV24k is lifting the module of its own deck (crane: 270deg), slewing the crane over the stern (crane: 180deg) to the set down position over port side (crane: 90deg). In reality the slewing is a continuous process, however on average it takes around 30min to slew 180deg. Because it is such a slow process, three snapshots of the operation are used to analyze the accelerations. The 90, 180 and 270deg orientations have been assessed, because the highest crane responses are expected. The crane response are related to the highest roll and pitch responses of the vessel. Three models are shown in Figure 4.5.

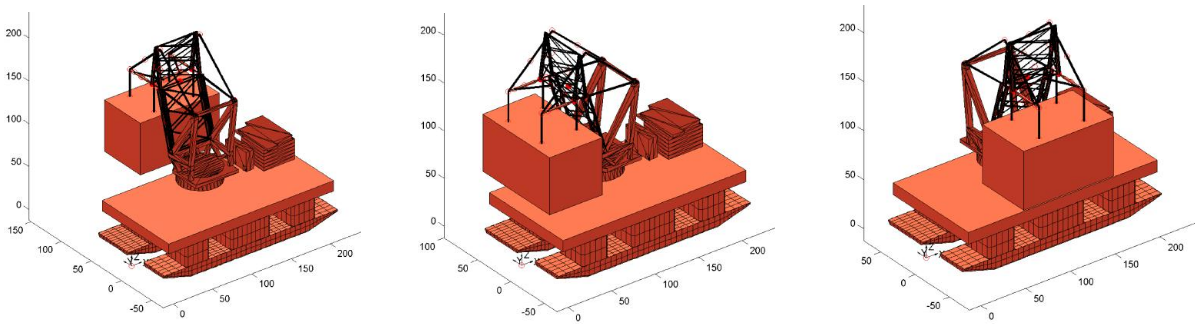

(a) M3 90 (ISO view) (b) M3 180 (ISO view) (c) M3 270 (ISO view)

Figure 4.5: M3: liftdyn operational model

Table 4.4 shows an overview of the five models used to create the input for the optimization.

Table 4.4: Liftdyn models

Model ID	Condition	Draft $[m]$	Crane orientation $[deg]$	Hook load $[t]$
M2 180	Survival	19	180	0
M2 270	Survival	19	270	0
M3 90	Operational	27	90	24,000
M3 180	Operational	27	180	24,000
M3 270	Operational	27	270	24,000

4.3.3 Response Amplitude Operator

In order to calculate the response of the system the RAO must be obtained. A RAO describes the relation between a regular wave amplitude and the vessel parameter response, including the phase lag between them. The RAO is presented over a range of wave frequencies and wave headings [16].

In this research the acceleration RAO's in X, Y and direction have been calculated in Liftdyn. An example of a RAO for the accleration in X-direction of the jib CoG is given in Figure 4.6

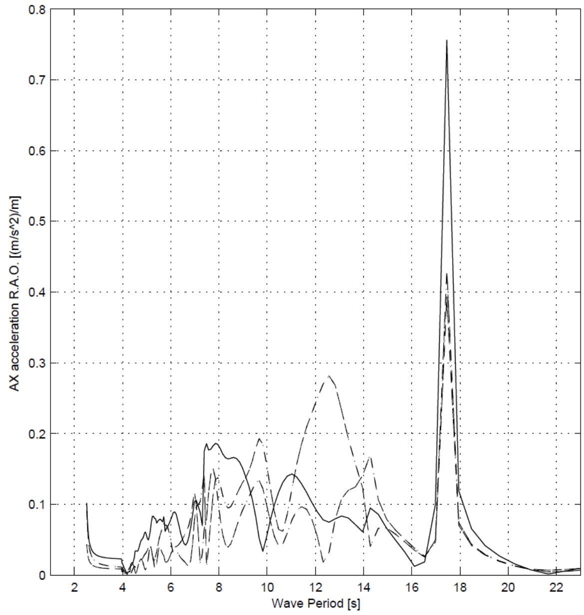

Figure 4.6: M2 270 Jib CoG RAO acceleration in X-direction

4.3.4 Wave energy spectrum

A sea state is described as an irregular wave elevation time signal ζ_t. This signal is decomposed in a large number of regular wave component with an own frequency, amplitude and phase. These waves are time independent and described in the frequency domain. The energy of each of the regular waves (per ω) is described by $\frac{1}{2}\zeta_a^2/\Delta\omega$. All of these regular waves together form the energy density spectrum, also referred to as the wave spectrum. The phases are not included in this spectrum.

$$S_{JW}(\omega) = \frac{320 \cdot H_s^2}{T_p^4} \cdot \omega^{-5} \cdot exp\left(\frac{-1950}{T_p^4} \cdot \omega^{-4}\right) \cdot \gamma^A \tag{4.1}$$

$$A = exp\left\{-\left(\frac{\frac{\omega}{\omega_p} - 1}{\sigma\sqrt{2}}\right)^2\right\} \tag{4.2}$$

$$\sigma = \begin{cases} 0.07 & \text{if } \omega \leq \omega_p \\ 0.09 & \text{if } \omega > \omega_p \end{cases} \tag{4.3}$$

Wave spreading has been used to correct for the directionality of the wind waves, by multiplying the spectrum with the wave spreading function Equation 4.4. The energy is spread over a certain angle contained with the interval $[-0.5\pi, 0.5\pi]$ from the wind direction.

$$f(\theta_w) = \frac{\Gamma(1 + n/2)}{\sqrt{\pi}\Gamma(1/2 + n/2)} \cdot cos^n(\theta_w - \theta_p) \tag{4.4}$$

For the survival conditions an exponent of $n = 10$ is used, a very narrow spreading. Operational conditions are calculated with an exponent of $n = 6$, a wider spreading. The total wave spectrum can formulated as follows:

$$S(\omega, \theta_w) = S(\omega) \cdot f(\theta_w) \tag{4.5}$$

The response of the system is calculated for a particular wave spectrum. For both the survival and operational loading conditions wind seas are assumed. The JONSWAP spectrum describes these wind seas [11].

4.3.5 Response

The responses of the system are calculated based on the RAO and wave spectrum. Because the input parameter for the wave spectrum is the significant wave height, the response is calculated as the Significant Double Amplitude (SDA):

$$SDA = 4 \cdot \sqrt{\int_{-\pi}^{\pi} \int_{0}^{\infty} \{RAO_{\omega,\theta_w}\}^2 \cdot f(\theta_w) \cdot S(\omega,\theta_w) \cdot d\omega \cdot d\theta_w} \tag{4.6}$$

For the optimization the maximum response amplitude for the sea state is of interest. The maximum response occurs at the maximum wave height, which is dependent of the wave steepness limit and the wave statistics. The steepness limit is dependent on the wave peak period. The wave statistics indicate the chance of wave height exceedance. From HMC experience the maximum wave height is determined as the wave height that will be exceeded once every 1000 waves (N). The assumption is made that it will take approximately 3 hours for 1000 waves to pass, including the peak value. The occurrence of the maximum wave height is accounted for by a multiplication factor (MF_{max}).

$$MF_{max} = \sqrt{(0.5 * ln(N))} \tag{4.7}$$

By multiplying the Significant Double Amplitude by 0.5 and the maximum wave height factor the "3hr Most Probable Maximum response amplitude" (MPM) is obtained.

$$\text{MPM} = \frac{SDA}{2} \cdot MF_{max} \tag{4.8}$$

The MATLAB beam model accepts input in the from of forces on the nodes. These input forces are calculated with the acceleration and hoist force responses. The following steps have been performed to obtain the 3hr MPM accelerations responses.

Step 1
The acceleration RAOs at the CoG off all rigid crane bodies have been obtained in X, Y and Z direction. Furthermore the hoist wire force RAOs have been extracted for the same directions.

Step 2
For each loading condition a JONSWAP spectrum has been created with the parameters in the following table:

Table 4.5: Liftdyn wave spectrum parameters

Spectrum	Hs	Peak enhancement factor	Wave spreading exponent	
		γ	Operational	Survival
	$[m]$	[-]	[-]	[-]
JONSWAP	1	3.3	6	10

Step 3
Calculation of the 3hr MPM force responses in X, Y and Z direction for the four hoist wires.

Step 4
Calculation of the 3hr MPM acceleration responses for the crane elements.

4.3.5.1 Response maxima

For the optimization the maximum responses are of interest. By determining the worst wave heading and peak period combinations from step 3 and 4, the peak response has been determined. Figure 4.7 gives an example of the 3hr MPM responses calculated and the corresponding peak values.

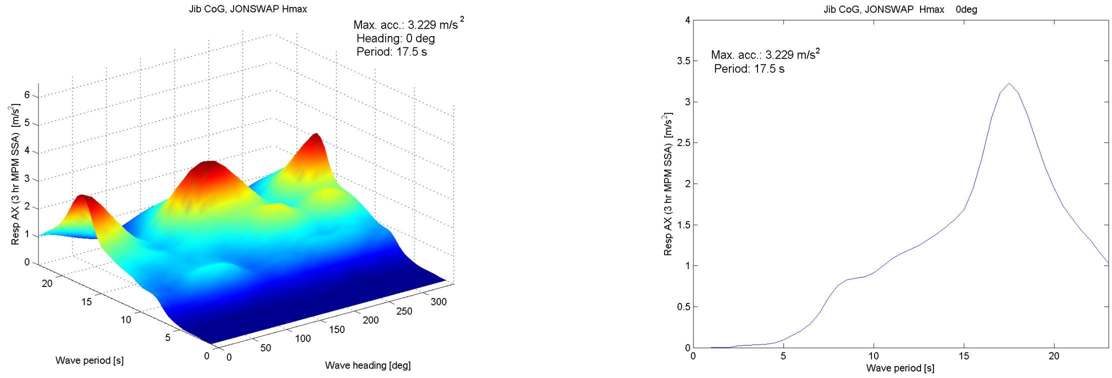

(a) Response for all wave headings and peak periods

(b) Response for the worst heading

Figure 4.7: M2 270 jib CoG 3hr MPM acceleration response in X-direction

4.3.6 Forces

The force responses in the hoist wires are directly outputted by Liftdyn. The force due to inertia effects of the crane parts are derived form the accelerations of those parts. The acceleration responses are calculated at the CoG's of the crane parts, Figure 4.8.

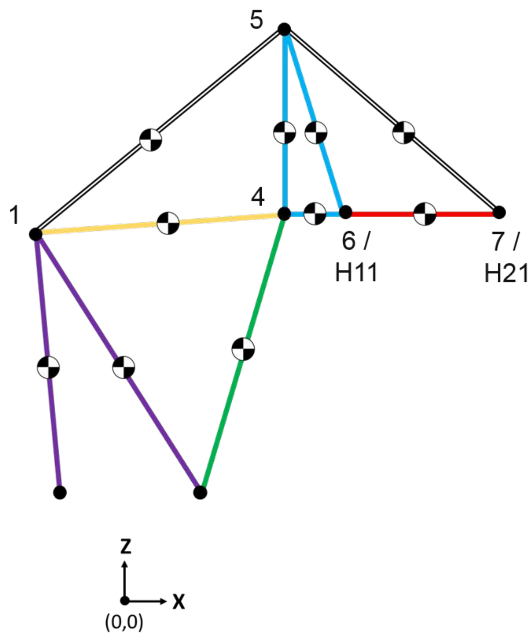

Figure 4.8: Crane model CoG's and nodes

The force on a node is calculated by multiplying the weight of the adjacent elements with their acceleration, Equation 4.9. The weight of the crane parts is taken from the initial crane design. The assumption is made that the weight is spread homogeneous over a beam element, which results in an equal weight per node. Therefore the force in a beam element is split equally over the two nodes. Force summation of all the adjacent beam gives the total force on a node.

$$\text{Node force} = \sum^{n} \text{part}_\text{n}\ \text{mass} \cdot \text{part}_\text{n}\ \text{accelaration} \tag{4.9}$$

The results from all the force calculations are displayed in Table 4.6

Table 4.6: Total node forces for the five loading conditions

Model	H_s $[m]$	θ_w $[deg]$	T_p $[s]$	Force	Node 1 $[m]$	Node 4 $[kN]$	Node 5 $[kN]$	Node 6 $[kN]$	Node 7 $[kN]$	H11 $[kN]$	H21 $[kN]$
M2 180	16.5	0	17.5	F_x	2,859	4,183	2,995	2,859	1,129	-	-
				F_y	2,207	3,379	2,447	2,398	1,009	-	-
				F_z	3,124	3,866	2,330	2,603	1,038	-	-
M2 270	16.8	0	16.5	F_x	2,910	4,341	3,221	3,042	1,324	-	-
				F_y	2,255	3,238	2,581	2,329	1,031	-	-
				F_z	3,074	2,523	1,507	1,470	546	-	-
M3 90	1	270	10.5	F_x	63	111	72	80	39	1,500	1,800
				F_y	327	443	321	303	133	7,933	7,933
				F_z	80	210	130	182	96	10,678	12,740
M3 180	1	270	10.5	F_x	144	178	114	109	35	3,153	3,153
				F_y	338	535	372	387	169	6,633	7,502
				F_z	193	210	120	115	26	16,079	3,980
M3 270	1	270	10.5	F_x	56	98	71	74	35	2,100	2,100
				F_y	357	489	355	335	147	7,838	7,838
				F_z	169	64	48	59	42	11,328	11,957

4.3.7 Optimization load cases

The forces obtained in the previous step are the occurring peaks. The in or out of phase movement of the lift object compared to crane motions make several load cases.

- Crane phase: positive (in) and negative (out) roll/pitch of the vessel
- Hoist phase: motion of the lift object similar (in) and opposite (out) to the crane motion

Because of the linearity in the Liftdyn output, the response can be scaled to other wave heights. By combining the forces and phasing in total 76 load cases have been generated. Table 4.7 gives an overview of the combinations that have been used for the optimization.

Table 4.7: Load case combinations

Case	Model	Load cases $[-]$	Hs $[m]$	Crane phase	Hoist phase F_x	Hoist phase F_y
Survival	M2 180	2	16.5	in - out	-	-
	M2 270	2	16.8	in - out	-	-
Operational	M3 90	24	1, 2, 3	in - out	in - out	in - out
	M3 180	24	1, 2, 3	in - out	in - out	in - out
	M3 270	24	1, 2, 3	in - out	in - out	in - out

5 Configuration optimization

The configuration optimization has been performed with the MATLAB model describe in chapter 3. The load cases have been obtain from Liftdyn section 4.3. The configuration has been minimized to a predefined goal function. The results are compared to the original configuration and the most promising one is used to continue this research.

5.1 MATLAB solver

In order to obtain the most sufficient design based on the static load cases an optimization has been performed in MATLAB. The beam model has been optimized with the help of a build-in solver of MATLAB. For the optimization the minimization function fmincon has been used. The fmincon function is a multidimensional constrained nonlinear minimization tool, which finds the minimum value of the goal function $f(x)$. The solver finds the local minimum of the the following problem statement:

$$\min_{x} f(x) = \begin{cases} A \cdot x \leq b & \text{prescribe condition} \\ Aeq \cdot x \leq beq & \text{prescribe condition} \\ lb \leq x \leq ub & \text{lower and upper boundary of x} \end{cases} \tag{5.1}$$

As stated earlier the function searches for a local minimum, however the global minimum is the one of interest. To overcome this problem the MultiStart MATLAB functionality has been used. This function allows the fmincon to start from a specified number of points, instead of just one. By default the fmincon starts from a single assigned starting point, Figure 5.1a. MultiStart randomly selects a specified number of starting point within the set boundary conditions, Figure 5.1b, finding all the local minima for those points. The use of the MultiStart does not guarantee to find the global minimum, but it does improve the change of finding it significantly.

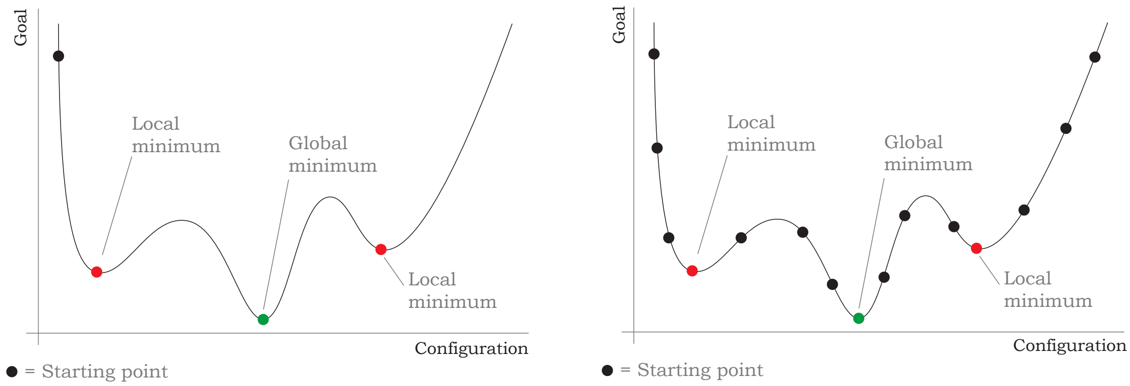

(a) Fmincon solver

(b) Fmincon solver MultiStart

Figure 5.1: Fmincon solver principle

From a convergent study it has been concluded that the sufficient number of starting points for this optimization is 50.

5.1.1 Goal function

The optimization of the crane configuration is governed by two main criteria:
Minimizing weight

- Construction cost are linear dependent on the weight
- Vessel capacity: the heavier the crane, the less can be lifted

Lowering (minimizing) the center of gravity

- A lower CoG improves vessel motion behavior
- A lower CoG has a positive influence on the forces acting on the crane, especially because the crane is always in the upright position.

The goal function is therefore formulated as a combinations of these two criteria: The weight times the distance to the crane origin. In other words the overturning moment at the crane origin Figure 2.4.

$$\begin{aligned} f(x) &= weight \times CoG_{XYZ} \\ CoG_{XYZ} &= \sqrt{(CoG_X)^2 + (CoG_Y)^2 + (CoG_Z)^2} \end{aligned} \tag{5.2}$$

5.2 Constraints

The possible solutions of the minimization are all to be found within the set boundary conditions. For this optimization these boundary conditions are depicted by the required clearance profile under the crane and the tub size. This resulted in the following nodes to have the 'freedom' to choose the best location. The boundary conditions are specified in Table 5.1, stating starting point, lower and upper boundary. The boundary conditions are stated for one side of the crane, because the nodes are mirrored in the XZ-plane, making the crane symmetric in this plane. The color scheme refers nodes in Figure 5.2.

Table 5.1: Boundary conditions optimization nodes

Node			Coordinates		
ID	Color	Direction	Original $[m]$	Lower BC $[m]$	Upper BC $[m]$
1	●	X	-24.560	-25	13.537
1	●	Y	25	0	25
1	●	Z	84.399	32.888	200
2	●	X	-23	-25	13.537
2	●	Y	25	10	25
3	●	Y	25	0	25
4	●	X	30	0	32.899
4	●	Z	98.338	98.338	200
5	●	X	32.899	-25	46.239
5	●	Y	25	0	25
5	●	Z	144.624	110	200
2#	●	X	-	$R \cdot cos(\angle)$	$R \cdot cos(\angle)$
2#	●	Y	-	$R \cdot sin(\angle)$	$R \cdot sin(\angle)$

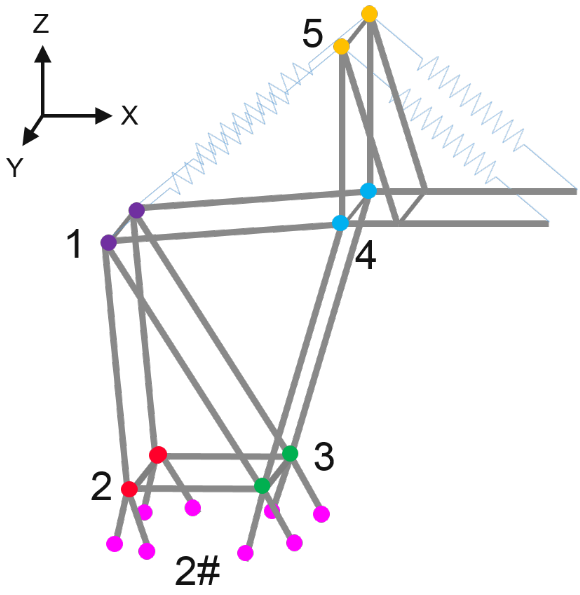

Figure 5.2: Optimization boudary conditions

To ensure that the optimization process yields to configurations that are possible to construct, the following constraints are set:

$$\begin{aligned} \text{Node } 4_X &\geq \text{Node } 5_X \\ \text{Node } 5_Z &\geq \text{Node } 1_Z \\ \text{Node } 5_Z &\geq \text{Node } 4_Z \end{aligned} \tag{5.3}$$

5.3 Optimization sequence

The following optimization sequence has been used to obtain the 76 different optimized configurations:

1. For each load case a geometry optimization, with the goal function, has been performed. The 50 Multi-Start points of the optimization resulted in the co-ordinates of the "free" nodes yielding to an optimized configuration within the boundary conditions. The result is the optimum configuration for the corresponding load case. In total 76 configurations are created.
2. The "free" nodes are fixed at the optimized co-ordinates. In the following steps the nodes have set co-ordinates. Deformation and displacement due to loading are not restrained. This step results in 76 set configurations.
3. Each one of the configurations is submitted to all the 76 load cases.
4. The 76 load cases give 76 loading conditions of all the individual beams of the configuration. For each beam the normative cross-section area is calculated based on the eight integration points, section 3.4 and allowable stress.
5. The weight of each beam is calculated by multiplying the normative areas by the length of the beam.
6. The weight of each configurations is calculated by summation of the weight of all beams.
7. The previous steps results in 76 optimized configurations, including the minimum required beam cross-section areas, profile and the lowest overall weight.

5.4 Optimization results

In total 76 different load cases have been used for the optimization resulting in 76 different configurations. All the results are judged on their weight, overturning moment and physical feasibility. From all these cases the following four optimization results are selected to be the most promising, Table 5.2. Configuration 25 is chosen to be the most suitable for the crane configurations, the main driver being the low overturning moment.

One configurations (17) shows an even lower overturning moment, but based on construction restrictions this configuration is not considered feasible. The space (Y-axis) required to place the sheaves in the top of the A-frame (Node 1) has not been considered in the constrains described above. Comparing the spacing of an existing crane A-frame and the optimization results, it is concluded that configuration 17 is impossible to construct.

Table 5.2: The most promising optimization results

Model	Weight		CoG		Overturning moment
		X	Y	Z	
	$[t]$	$[m]$	$[m]$	$[m]$	$[kNm]$
1	12,072	21.7	0	79.6	$9.77 \cdot 10^6$
17	12,198	21.2	0	76.3	$9.48 \cdot 10^6$
25	**12,088**	**21.1**	**0**	**78.5**	$\mathbf{9.64 \cdot 10^6}$
53	12,312	19.1	0	78.7	$9.78 \cdot 10^6$

Figure 5.3 visualizes the final beam model configuration as they where produced by the MATLAB optimization. Figure 5.3a a shows the element configuration, where Figure 5.3b shows the configuration with lines thicknesses representing the beam profiles calculated.

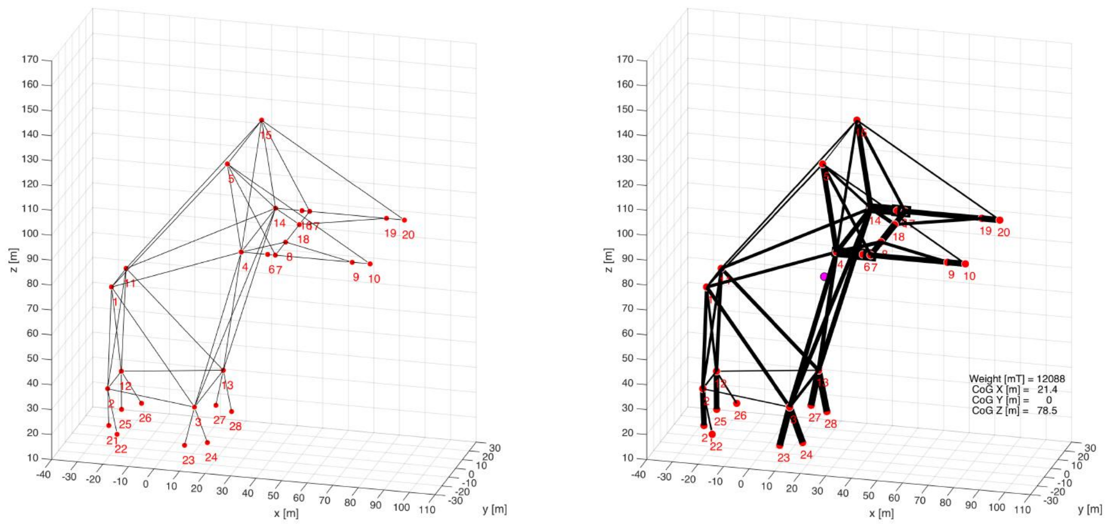

(a) Element configuration

(b) Configuration including beam profiles

Figure 5.3: Final configuration 25

5.5 Final configuration

The final configurations coordinates are compared with the original ones in Table 5.3. The bold numbers indicate the coordinates which have significant changes. The node ID's refer to the nodes in Figure 5.3.

Table 5.3: Node coordinates of the optimized and original configuration

Node ID	Part	Optimized X [m]	Optimized Y [m]	Optimized Z [m]	Original X [m]	Original Y [m]	Original Z [m]
1	A frame	22.618	**-10.650**	**74.106**	-24.560	**-25.000**	**94.399**
2	A frame	22.618	**-10.650**	32.888	-23.000	**-25.000**	32.888
3	Heel point	13.537	-21.018	32.888	13.537	-25.000	32.888
4	Boom	32.899	-25.000	98.338	32.899	-25.000	98.338
5	Top	**27.476**	-25.000	**133.225**	**32.899**	-25.000	**144.624**
6	Top	43.239	-25.000	98.338	43.237	-25.000	98.338
7	Top	46.239	-25.000	98.338	46.239	-25.000	98.338
8	Top	46.239	-10.000	98.338	46.239	-10.000	98.338
9	jib	76.239	-25.000	98.338	76.239	-25.000	98.338
10	Jib	83.273	-25.000	98.338	83.273	-25.000	98.338
11	A frame	22.618	**10.650**	**74.106**	-24.560	**25.000**	**94.399**
12	A frame	22.618	**10.650**	32.888	-23.000	**25.000**	32.888
13	Heel point	13.537	21.018	32.888	13.537	25.000	32.888
14	Boom	32.899	25.000	98.338	32.899	25.000	98.338
15	Top	**27.476**	25.000	**133.225**	**32.899**	25.000	**144.624**
16	Top	43.239	25.000	98.338	43.237	25.000	98.338
17	Top	46.239	25.000	98.338	46.239	25.000	98.338
18	Top	46.239	10.000	98.338	46.239	10.000	98.338
19	jib	76.239	25.000	98.338	76.239	25.000	98.338
20	Jib	83.273	25.000	98.338	83.273	25.000	98.338
21	Back in	-24.400	5.444	17.888	-23.500	-8.529	17.888
22	Back out	-19.750	15.328	17.888	-15.000	-20.000	17.888
23	Front out	7.000	-24.000	17.888	7.000	-24.000	17.888
24	Front in	20.000	-15.000	17.888	20.000	-15.000	17.888
25	Back in	-24.400	5.444	17.888	-23.500	8.529	17.888
26	Back out	-19.750	15.328	17.888	-150.000	20.000	17.888
27	Front out	7.000	24.000	17.888	7.000	24.000	17.888
28	Front in	20.000	15.000	17.888	20.000	15.000	17.888

The new configuration shows the main differences in the A-frame and the top structure compared to the original configuration. These differences are made visible in Figure 5.4, where the gray dashed line represents the original configuration and the solid lines the new outline of the crane.

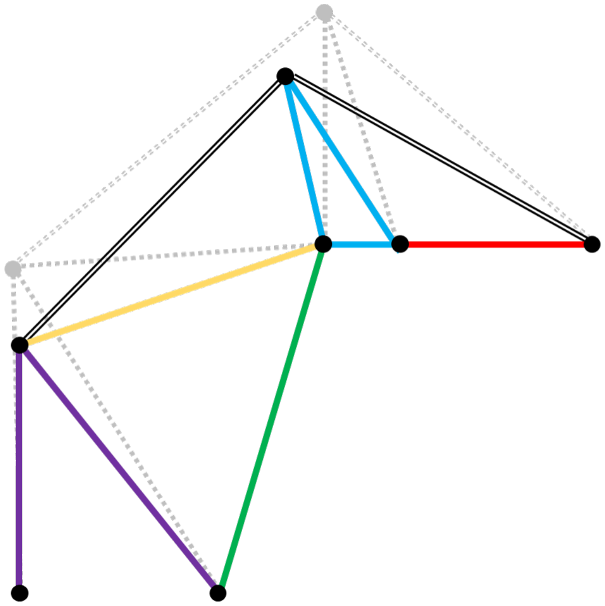

Figure 5.4: Changes in configuration (side view: gray = original, color = optimized)

5.5.1 Tub connections points

The tub connections points are constraint on the perimeter of the crane house. Clearly visible in Figure 5.2 is the adjustment of the nodes connecting the eight A-frame-legs (green dots) with the rest of the A-frame (blue dots) and the boom heelpoint (red dots). The nodes original position (gray dots) lays outside the tub perimeter in-line with the hooks. By repositioning the nodes above the perimeter the shear forces and bending moment in the eight A-frame-legs are reduced, resulting in a smaller cross-section profile requirement.

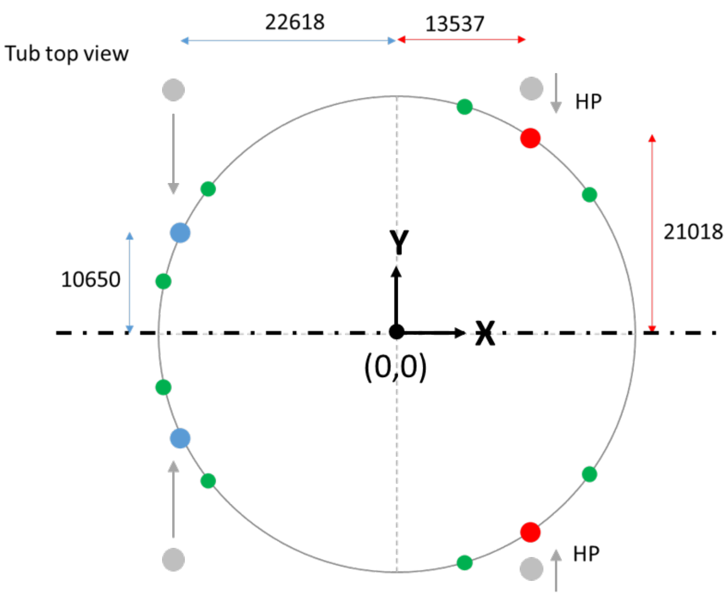

Figure 5.5: Changes in tub connection points [mm]

5.6 Evaluation

Compared to the original crane, the new configuration shows large changes in the height of the top structure, A-frame and the connection with the crane house A-frame-legs. Based on this optimization study the following conclusions can be drawn:

- **CoG:** The center of gravity of the crane is lowered compared to the original design, which is beneficial to the motion behavior of the vessel. A low center of gravity is beneficial for the stability of the vessel.
- **A-frame-legs:** Where in the original design the legs were attached at an angle to the crane house edge, the new configuration set this angle to be in-line with the crane house shell. By using the A-frame-legs as mainly axial compression and tensile members, less shear and bending moment in legs and crane house occur. Reducing the shear stress and bending moment in the beam has a positive effect on the weight of the structure. Shear stress is the governing weight incubator, as the shear strength of the legs is related to a fraction of the axial stress and therefore to the cross-section area. Bending moment in the legs mainly influences the size and profile type of the beam, which do not influence the weight. However the bending moment is of large influence on the crane house structure. The shell structure is less adaptively because of the cylindrical shape required for the bearing. Reducing the bending moment on the cylinder edged, reduces the size of stiffeners, cross beams and other measures, resulting in weight saving.

II
Static analysis

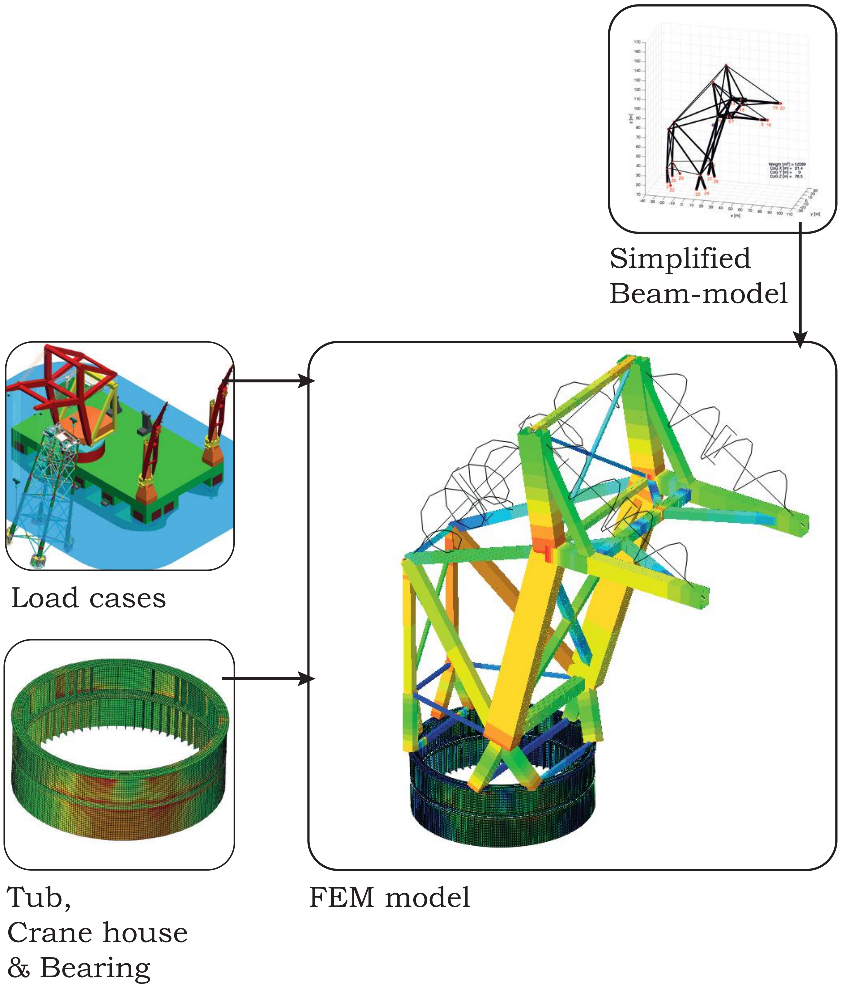

6
Static finite element model

With the dimension requirements determined in the analysis phase, a static model will be made. The structural integrity will be considered for the static load cases. This model will provide the overall dimensions and design of the crane. General information on cross section area, moment of inertia and weight of the several crane beams will be obtained from the optimization study. These properties have been used as the starting point for the static research. This research will be conducted with Finite Element Analysis software FEA.

For this research the Finite Elements software package Abaqus 6.13 is used [3]. The coordinate system in Abaqus differs from the standards set, Figure 2.6. The axis system used in all Abaqus analyses is given in Figure 6.1.

Table 6.1: Abaqus coordinate system

Direction	Symbol
Longitudinal translation	X
Transverse translation	Z
Vertical translation	Y
Rotation around X-axis	ϕ
Rotation around Z-axis	θ
Rotation around Y-axis	ψ

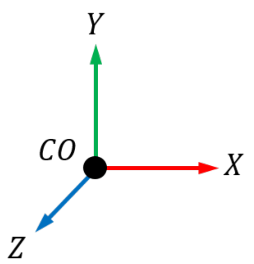

Figure 6.1: Abaqus displacement and rotational degree of freedom

6.1 Material properties

In this FEM model only one grade of steel is used, construction steel S450. The parameters included in this study are found in Table 6.2.

Table 6.2: Steel S450 material properties

Parameter	Unit	Value
Type	[-]	S450
Yield strenght	$[N/m^3]$	$450 \cdot 10^6$
Density	$[kg/m^3]$	7,850
E-modulus	$[N/m^3]$	$210 \cdot 10^9$
G-modulus	$[kg/m^3]$	$70 \cdot 10^9$
Poisson ratio	[-]	0.3

6.2 Beam elements

The upper structure of the crane in modeled in beam elements. The beam member cross-sections are provided in Table 6.3.

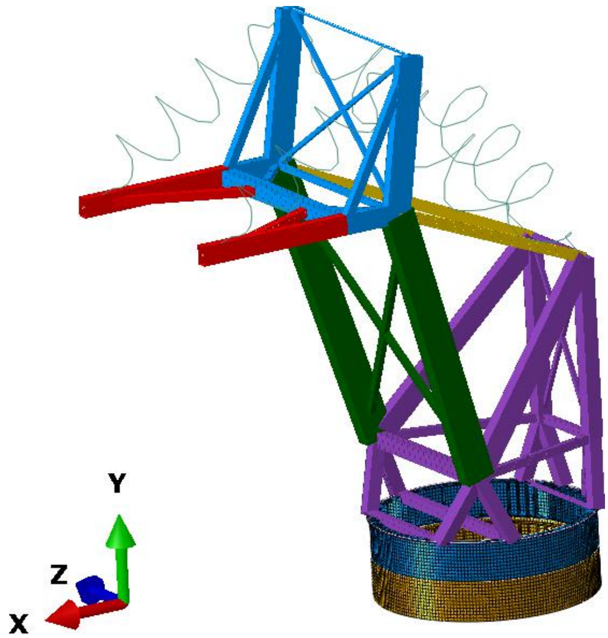

Figure 6.2: Abaqus crane model

Table 6.3: Beam profile

Part	Profile	Width $[m]$	Height $[m]$	Thickness $[mm]$
Boom	MAIN	5	9	50
	DIAG	2.5	2.5	20
A-frame	AF-BACK-CROSS-OUT	1	2	20
	AF-BACK-IN	3	3	50
	AF-BACK-LEG	2.5	2.5	100
	AF-BACK-OUT	3	3	50
	AF-BASE	1	1	20
	AF-BASE-FRONT	3.5	3.5	30
	AF-DIAG	1	1	20
	AF-FRONT-CROSS-IN	1	2	20
	AF-FRONT-CROSS-OUT	1	2	20
	AF-FRONT-IN	4	4	100
	AF-FRONT-LEG	2.5	4.5	50
	AF-FRONT-OUT	4	4	100
	AF-TOP	1.5	2.5	20
JIB	MAIN	4	5	40
	DIAG	2.5	2.5	20
Luffer	LUFFER	2	3	30
Top	BACK-LEG	5	7.5	70
	DIAG-HOR	2	2	20
	DIAG-VER	1	1	20
	FRONT	3	3	30
	FRONT-LEG	3	3	20
	MAIN	5	5	70
	MIDDLE	2	2	20
	TOP	2	2	20

6.3 Shell elements

The tub and crane house are modeled with shell elements. Figure 6.3a gives a small section cut from the whole tub. The color scheme represents different plate thicknesses, clearly visible are the vertical stiffeners (red) and the thick top flange (green). In Figure 6.3b the plate thicknesses are stated in a vertical cross-section of the tub.

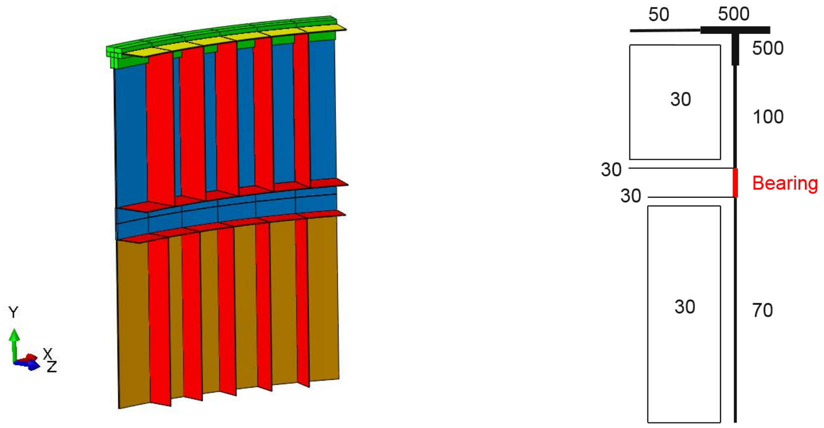

(a) Tub and crane house cut (ISO view) (b) Plate thickness [mm] (cross section)

Figure 6.3: Shell elements used in the tub and crane house

6.4 Constraints

The following table gives an overview of the constraints used in the model.

Table 6.4: Constraint types used

Constraints	DOFs	Master	Slave	Method
Equations	1 2 3 4 5 6	One point	Multiple points	The equation of motion of the nodal variables is equal to zero
Kinematic coupling	1 2 3 4 5 6	Node 1	Node 2	Limit the motion of a group of nodes to the rigid body motion defined by a reference node
MPC		One point	Multiple points	
-Beam	1 2 3 4 5 6	Node 1	Node 2	Rigid beam between two nodes
-Tie	1 2 3 4 5 6	Node 1	Node 2	Make all active degrees of freedom equal for two nodes
-Elbow	1 2 3 4 5	Line 1	Line 2	Hinge of two lines of two parts
Surface-based coupling	1 2 3 4 5 6	Node	Surface nodes	Couples the motion of a collection of nodes on a surface to the motion of a reference node

6.5 Cables

For this research the properties of Bridon Dyfrom 8 cables, used on the Aegir vessel, are assumed. A safety factor of 5 has been taken into account for all the cables, as prescribed in DNV standard, Appendix A. The Crane design makes use of three cable categories, connection between A-Frame-Top, Top-jibs and the four hoist wires arrangements (hook tackle, hook and sling), Table 6.5.

Table 6.5: Crane cable arrangements

Cables	ID	Amount [-]	Length [m]	No. Falls (n) [-]	Mass [t]
Top luffing	AF-TP	2	76	152	293
Jib luffing	TP-JB	2	68	126	200
Hook tackle	HK	4	15	76	278
Sling	Sl	4	7	4	-

All the cranes luffing wires are modeled with an in-line spring-dashpot element. This type of connector only works in the axial vector between the two connections nodes. Change of node location, therefore the axial vector, is adjusted during the analysis. The spring-dashpot properties, Table 6.6, have been calculated with the following equations: Stiffness for the combination of all falls:

$$K = \frac{E_{cable} \cdot A \cdot n}{L} \tag{6.1}$$

Damping: 10% of the critical damping:

$$C = 0.1 \cdot 2 \cdot \sqrt{m \cdot K} \tag{6.2}$$

Pre-tension:

$$F_{pre} = F_x \cdot g \tag{6.3}$$

Table 6.6: Model spring-dashpot particulars

ID	Stiffness [kN/m]	Damping [kNs/m]	Pre-tension [kN]
AF-TP	$5.51 \cdot 10^5$	$5.78 \cdot 10^4$	$1.51 \cdot 10^5$
TP	$5.09 \cdot 10^5$	$4.76 \cdot 10^4$	$1.11 \cdot 10^5$
Hoist*	$5.88 \cdot 10^5$	$3.80 \cdot 10^4$	$5.87 \cdot 10^4$

* The properties of the hoist is the combination of the properties of the hook tackle, hook and sling. The hook, measuring 10m in height, is assumed to be rigid.

6.6 Additional mass

Due to limitation in the Abaqus software and design simplifications several elements have not been modeled. These elements have been considered as non structural masses, and have been compensated for by the placement of mass-points. These mass-points are both taken into account in static and dynamic calculations. The mass-points have been connected on specific nodes and tied with Multiple Point Connector (MPC). This connector type slaves the motion of the specific nodes to the motion of the master point, the mass-point. The following table outlines the masses added in the model:

Table 6.7: Model added inertia points

Part	Amount [-]	Weight [t]	Placement [@]
Crane house	1	4,330	C.o.G
Winches	1	2,160	C.o.G
Top luffing wires	4	146.5	Connection nodes
Jib luffing wires	4	100	Connection nodes
Top block	4	250	Top and jib

6.7 Boundary conditions

The crane is constraint at the tub shell and stiffeners edge at deck level of the vessel (Figure 6.4a red line). All six degrees of freedom are fixed, representing the welded connection with the vessel. In reality the tub structures continues into the hull to make a proper connection with the column of the vessel. For this thesis it has been assumed that the connection at deck level is rigid. A close up view of the boundary conditions is visual in Figure 6.4b: the blue and orange cones.

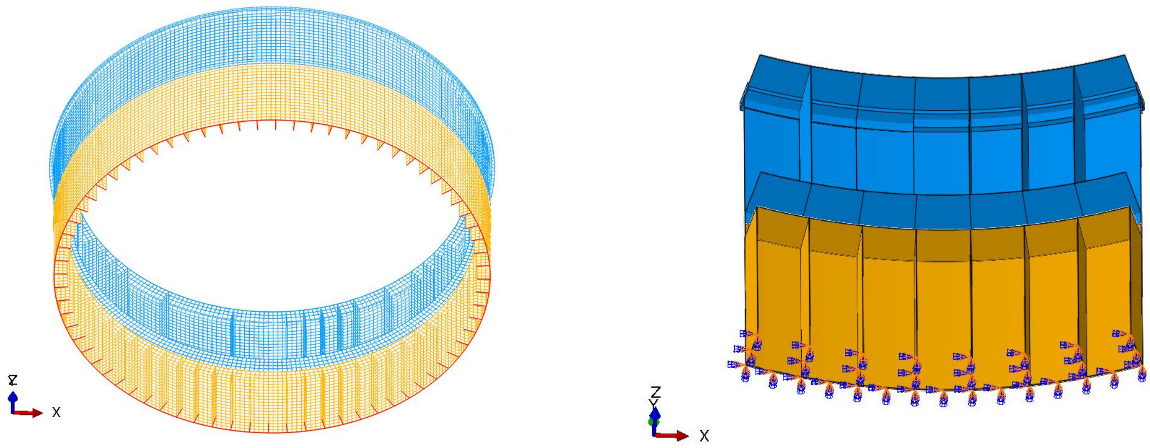

(a) Tub & crane house (transparent bottom view)

(b) Tub & crane house close up (cut ISO View)

Figure 6.4: Boundary conditions vessel-crane interface

6.7.1 Bearing modeling

For the HLV24k the bearing type of the Sleipnir cranes is used. Figure 6.5 shows an schematic cross-section of the bearing. The gray part is rigid connected to the vessel, whereas the blue part is the underside of the crane house and slews. The vertical loads are transmitted by the green rollers, both up- and downwards. The checkered white friction pads transmit the radial loading between the to parts. The motion in the tangential direction of the bearing is free to allow for slewing. The slewing and breaking of the crane is performed by a set of sprockets and a ring gear.

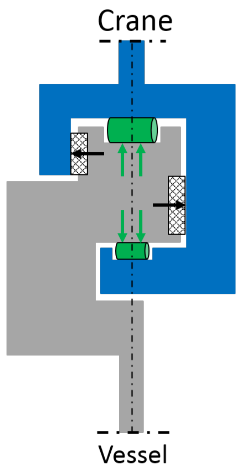

Figure 6.5: Schematic model of the Sleipnir bearing (cross-section)

Modeling of the bearing with rollers and friction pads can only be performed with contact areas. The solvable system becomes very sensitive for convergence by implementing these contacts. Besides the stability issues the use of contacts comes at great computational costs. Therefore the bearing modeling has been done with couplings. All the adjacent nodes of the tub and crane house have been connected by a coupling in a cylindrical coordinate system. The couplings are fixed in the radial (R) and vertical direction (Z). The tangential direction (θ) is free, which means that the stresses in this direction are not transmitted between the tub and crane house. This effect is observed in Figure 6.7, where an arbitrary displacement of the crane house in the X-direction results in a stress development over the circumferential.

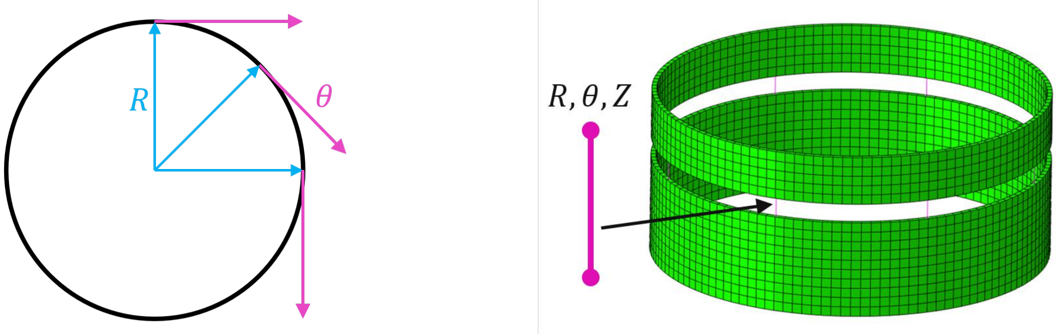

(a) Tangential directions (top view)

(b) Coupling princple (the top cylinders is given an offset for illustrational purposes)

Figure 6.6: Boundary conditions vessel-crane interface

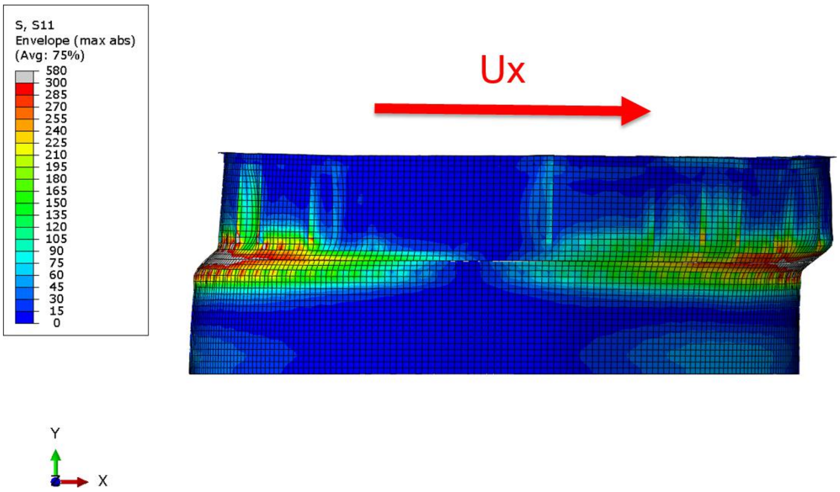

Figure 6.7: Bearing shear stress [N/mm^2] (side View)

However the couplings introduce a restriction for the slewing motion. The tangential direction is calculated for the initial positions of the nodes. Rotating of the crane top structure would result in a radial increase of the crane house. Therefore the used of the coupling bearing is only valid for a rotational displacement of zero. By applying a break on the crane house in the form of a fixed rotation boundary condition, the bearing modeling is valid for the analyses performed.

6.8 Mesh

In order to obtain accurate results from the FEA the mesh has to be sufficient. The size of the mesh influences the accuracy of the results and the computation time of the model. To determine the mesh size, a convergence analysis has been done with a simple model of a beam connected to a shell. A comparison has been made between the mesh size and calculated stresses.

Several runs of the model have been performed, each with a different mesh size. The first run with a coarse mesh, the second run with the mesh size halved and so on. It is assumed that the deviation between two consecutive results of 0.5% or less indicates convergence of the results. This convergence indicates a sufficient accuracy to perform the analyses. The results of the mesh size study can be found in Table 6.8.

Table 6.8: Mesh size study results

Run	Size $[mm]$	Nodes $[-]$	Time $[s]$	Result ratio $[-]$	Diviation [%]
1	10,000	190	27.3	1	-
2	5,000	580	73	0.752	24.76
3	2,500	1,960	208	0.621	17.52
4	1,250	7,120	628	0.590	4.94
5	625	27,040	2,104	0.582	1.31
6	313	105,280	6,903	0.579	0.48
7	156	415,360	22,942	0.578	0.17

The convergence limit was found for a mesh size of 312.5mm. A mesh size of 300mm has been used for both the shell and beam element.

6.9 loading

The static analyses are performed with a "Static General" step. This solving technique uses small increments step at which the system of equilibrium equations is solved. The load cases depicted in section 6.10 are implement on the model at the four hook locations, Figure 6.8.

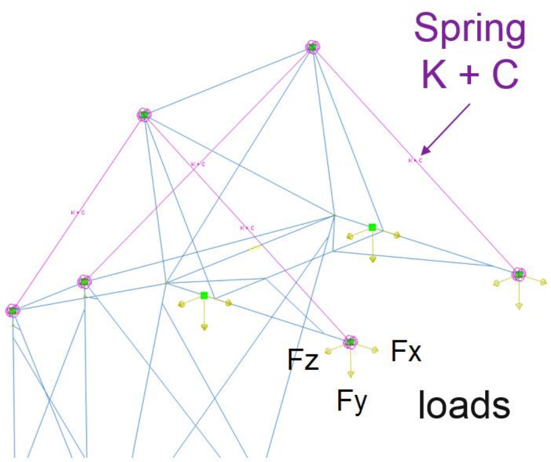

Figure 6.8: Boundary conditions vessel-crane interface

The loading of each hook has been done with three point loads in the global X, Y and Z directions. The loads are built up as follows:

- F_X = Offlead
- F_y = Design hookload + hook mass + hoist wire mass
- F_z = Sidelead

The mass of the hook itself is 278t.
The mass of the hoist wires is 250t.

6.10 Static Load cases

With information obtained in the previous two phases several load cases will be formulated concerning the main activities of the crane. These load cases will be used as a criterion for the structural integrity of the crane. During the conceptual study of HLV24K, several hull shapes were developed and tested on buoyancy, weight and motion responses during operation and transit. This study has led to a hull, which shows a good compromise between the various design objectives. It was concluded that this hull is a good basis for further development of the concept and is therefore used in this research as input for the crane. During the crane's 30 year service life several loading situation occur, non-operational and operational. The following two sections show an indication of those cases.

For the static research a set of nine load cases is drafted representing the variety of operations expected in the operational lifetime, Table 6.9. The loads in the table are stated without the DAF. These values have been multiplied in the finite element analyses loading.

Table 6.9: Static load case overview

LC	Load type	Hookload	Description
1	Even keel	24,000t	The maximum attainable load with even keel conditions
2	Max. vessel Heel/Trim	24,000t	The maximum attainable load with initial heel and trim
3	Load CoG transverse shift	17,160t	Transverse offset of the loads CoG
4	Load CoG longitudinal shift	17,320t	Longitudinal offset of the loads CoG
5	Outer Spread	19,840t	Lifting of a topside with an outside pad eye spread
6	Inner Spread	8,4000t	Lifting of a topside with an inside pad eye spread
7	Jacket	15,000t	Lifting of a jacket structure
8	Diag. hooks	12,000t	A lift with the diagonal opposite hooks
9	Outer hooks	12,000t	A lift at greatest possible outreach

The load cases are visualized in Figure 6.9 to 6.14 to indicate the off- and sidelead introduced on the crane part by the lifting points on the lift object. These lifting points are based on lifts performed by Heerema in the past. The weight of the topside lift objects is calculated with the rule of thumb: topside density = $0.1\,t/m^3$.

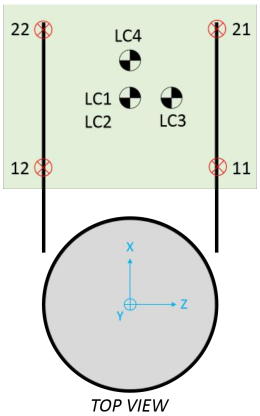

Figure 6.9: Load cases 1, 2, 3, 4

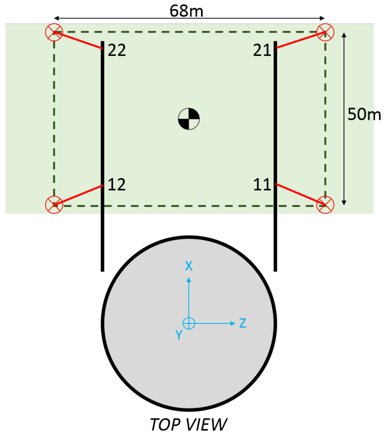

Figure 6.10: Load case 5

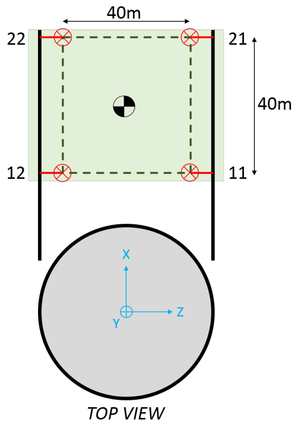

Figure 6.11: Load case 6

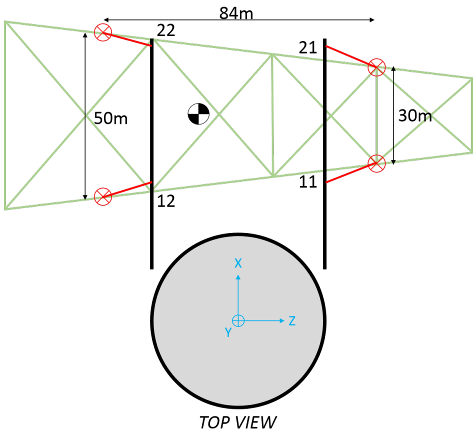

Figure 6.12: Load case 7

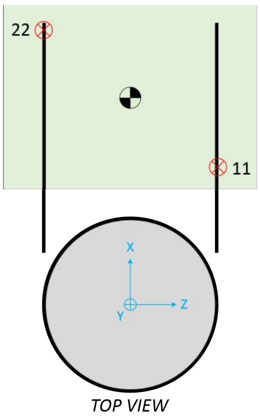

Figure 6.13: Load case 8

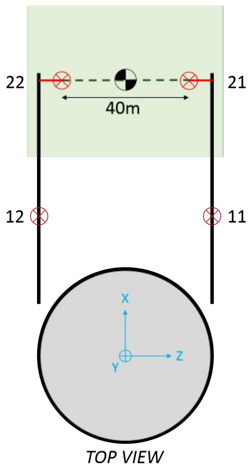

Figure 6.14: Load case 9

6.11 ABAQUS input

The nine load cases are translated in to input parameters for the static analysis in the finite element software, Abaqus.

Table 6.10: Static load case abaqus input

Load case			1	2	3	4	5	6	7	8	9
Vessel	Heel	$[deg]$	0	3	0	0	0	0	0	0	0
	Trim	$[deg]$	0	3	0	0	0	0	0	0	0
Hook 11	HL	$[t]$	6,000	6,000	5,429	3,000	4,909	0	2,857	6,000	0
	HL_{des}	$[t]$	6,600	6,600	5,972	3,300	5,400	0	3,143	6,600	0
	Offlead	$[t]$	0	345	0	0	-484	0	211	0	0
	Sidelead	$[t]$	0	345	0	0	865	0	704	0	0
Hook 21	HL	$[t]$	6,000	6,000	6,000	6,000	6,000	4,620	2,857	0	6,000
	HL_{des}	$[t]$	6,600	6,600	6,600	6,600	6,600	5,082	3,143	0	6,600
	Offlead	$[t]$	0	345	0	0	582	0	-211	0	0
	Sidelead	$[t]$	0	345	0	0	1,040	-458	704	0	0
Hook 12	HL	$[t]$	6,000	6,000	2,714	2,769	4,017	0	4,643	0	0
	HL_{des}	$[t]$	6,600	6,600	2,985	3,046	4,419	0	5107	0	0
	Offlead	$[t]$	0	345	0	0	-404	0	-323	0	0
	Sidelead	$[t]$	0	345	0	0	-722	0	-1081	0	0
Hook 22	HL	$[t]$	6,000	6,000	3,000	5,538	4,909	3,780	4,643	6,000	6,000
	HL_{des}	$[t]$	6,600	6,600	3,300	6,092	5,400	4,158	5,107	6,600	6,600
	Offlead	$[t]$	0	345	0	0	484	0	323	0	0
	Sidelead	$[t]$	0	345	0	0	-865	383	-1,081	0	0

7

Static analysis results

7.1 Criteria

A finite element analyses has been performed for the nine load cases. The results of the analyses are judged on the following two criteria.

Von Mises stress

The stress levels in structural elements are a useful indicator for the structural integrity of the model. Under the assumption of ductile material the prediction of the stresses can be done with the Von Mises failure criteria, 7.1.

$$\sigma = \frac{1}{2}\sqrt{(\sigma_{xx}-\sigma_{yy})^2+(\sigma_{yy}-\sigma_{zz})^2+(\sigma_{zz}-\sigma_{xx})^2+6\sigma_{zy}^2+6\sigma_{xz}^2+6\sigma_{zx}^2} < \sigma_{all} \tag{7.1}$$

The Von Mises criteria uses the distortion energy theory, proposing that the total strain energy can be split in two parts. The volumetric strain energy and the strain energy depended on the change in shape. Yielding of the material occurs when the shape (distortion) strain energy component exceeds the tensile yield strength of the material.
For this research Steel S450 is used, a ductile material with a yield strength of 450N/mm^2. After applying the required safety factor of 1.5, the allowable stress becomes 300N/mm^2 Appendix A.

Displacement

Besides the stress levels in the elements, the design is judged on the displacement of the structure. The displacement is visualized as the magnitude of the combinations of the displacement in X, Y and Z direction, Equation 7.2.

$$U = \sqrt{(U_X)^2+(U_Y)^2+(U_Z)^2} \tag{7.2}$$

Although there are no strict limits defined on displacement in the codes used for the research, the displacement results are judged on the practical limits and HMC experience.

7.2 Weight

To make an indication of the weight of the crane, the main steel parts are summed and the main equipment weight is added. The steel weight is calculated in Abaqus, whereas the equipment and non-structural elements are scaled from the Sleipnir crane. A comparison is made between the original-, optimized HLV24k and the Sleipnir, Table 7.1. As a rule of thumb the weight of a crane is about the same as its lift capacity. The original configuration does not comply with this rule with a 4000t weight exceedance, however the optimized version of the HLV24k does comply with the rule.

Table 7.1: Crane weight comparison

Parameter	Units	Sleipnir	HLV24k Original	HLV24k Optimized
Lift capacity	$[t]$	10,000	24,000	24,000
Tub diameter	$[m]$	30	50	50
Crane House	$[t]$	2,362	13,215	2,942
Equipment	$[t]$	-		3,937
Winches	$[t]$	818		1,963
Hooks	$[t]$	-		1,112
Wires all	$[t]$	837	404	2,118
Tub	$[t]$	-	1,711	1,150
A-frame	$[t]$	-	2,922	2,736
Boom	$[t]$	-	2,034	1,723
Top + blocks	$[t]$	-	1,212	2,286
Luffer L	$[t]$	-	339	395
Luffer R	$[t]$	-	339	395
Jib L + block	$[t]$	-	1,589	510
Jib R + block	$[t]$	-	1,589	510
Contingency factor	[-]	1.1	1.1	1.1
Total weight	$[t]$	8916	27889	23955

7.3 Crane

The Figure 7.1 to 7.6 show the results of the static analysis. In order to judge the crane for all the load cases on the criteria the "envelope" method has been used. The method does the following: For each node in a system the maximum value for a specified parameter is taken over all the analyzed load cases. This provides an overview of the maxima for each node of that parameter.

The Von Mises stress and displacement of the nine load cases have been visualized with the envelope method. The results can be found in Figure 7.1 to 7.6.

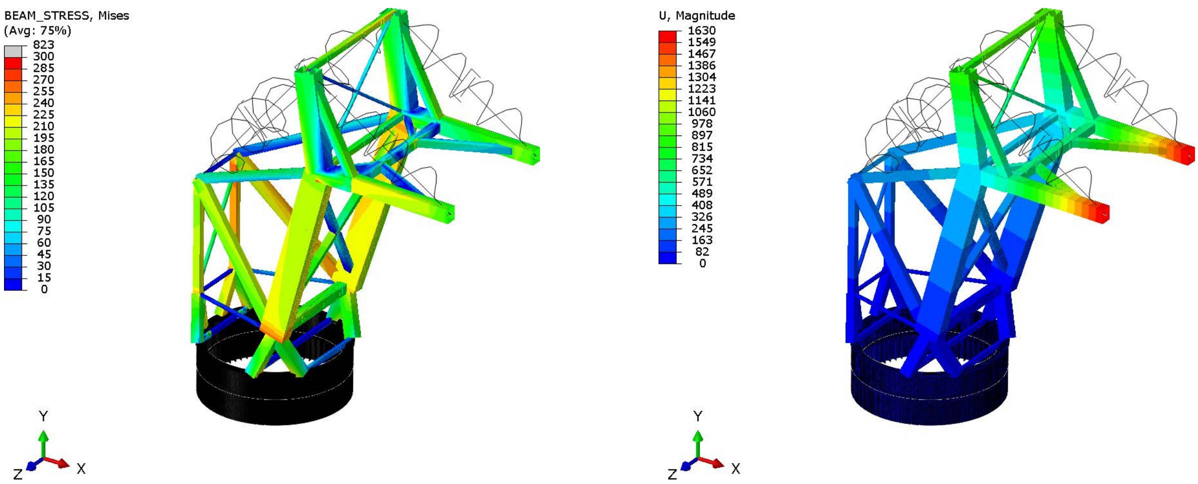

(a) Von mises Stress $[N/mm^2]$

(b) Displacement, combined directions $[mm]$

Figure 7.1: HLV24k Static analysis results (ISO view)

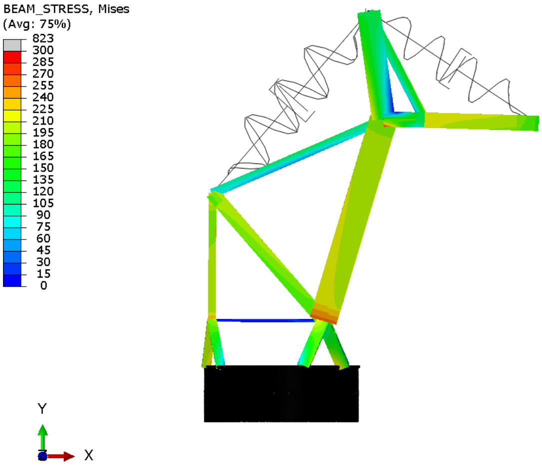

(a) Von mises Stress $[N/mm^2]$

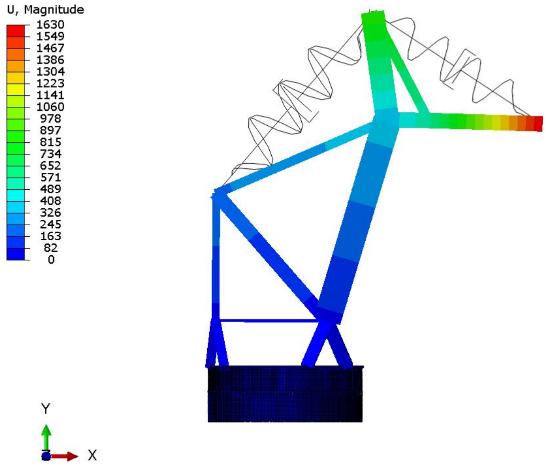

(b) Displacement, combined directions $[mm]$

Figure 7.2: HLV24k Static analysis results (Side view)

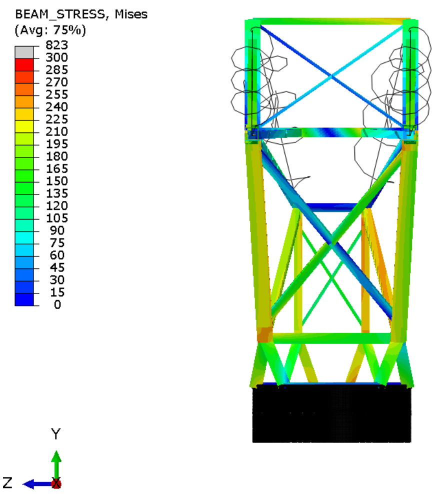

(a) Von mises Stress $[N/mm^2]$

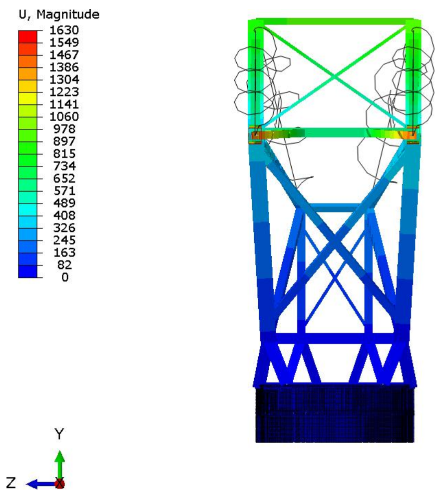

(b) Displacement, combined directions $[mm]$

Figure 7.3: HLV24k Static analysis results (Front view)

7.4 Tub

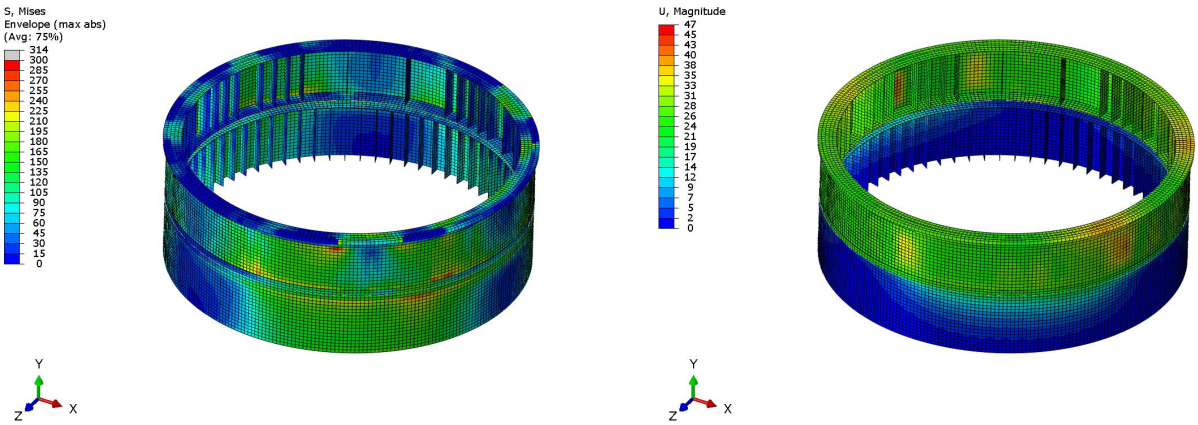

(a) Von mises Stress $[N/mm^2]$

(b) Displacement, combined directions $[mm]$

Figure 7.4: Tub Static analysis results (Front view)

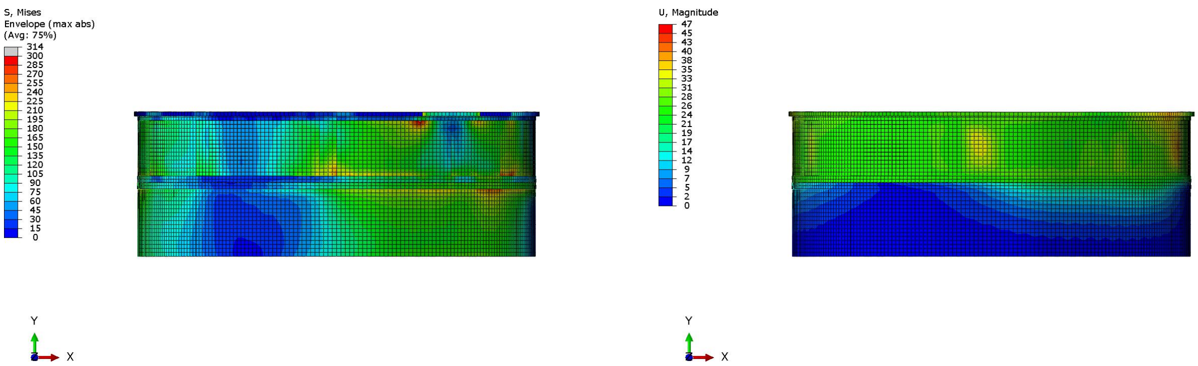

(a) Von mises Stress $[N/mm^2]$

(b) Displacement, combined directions $[mm]$

Figure 7.5: Tub Static analysis results (Front view)

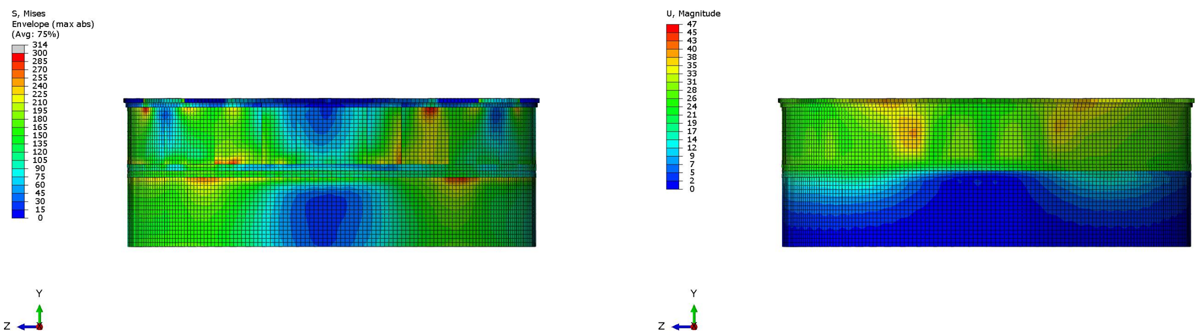

(a) Von mises Stress $[N/mm^2]$

(b) Displacement, combined directions $[mm]$

Figure 7.6: Tub Static analysis results (Front view)

7.5 Evaluation

A finite element analysis has been performed on the optimized crane configuration. Nine governing static load cases have been assessed individually. From which the following conclusions can be drawn:

- **Crane weight:** The crane weight has decreased in comparison with the original design, from 27889t to 23995t. The main weight reductions are seen in the two jibs and the crane house structure. Whereas increases are found at the tub structure and wires.
- **Structural Strength:** The results of the load cases has been evaluated and the crane showed sufficient structural strength during all the cases. The allowable stress of $300N/mm^2$ has only been exceeded locally. The main parts of the crane all showed sufficient material strength.
  The displacement of crane parts were within limits set by HMC experience. A jib-end displacement of 2m at the maximum lift capacity is not considered a rarity in current cranes. Furthermore, in reality the displacement of crane parts is reduced by the crane operator. Deflection of the boom/jib and elongation of the wires are compensated by hoisting in the wires.
- **Beam profiles:** Several beam elements have been updated after a first run of static calculations. The initial square beam profiles were taken from the MATLAB optimization study. Loading conditions during the static research showed direction dependent strength requirements, resulting in beam profile of a rectangular shape, not necessary square.

Based on the results of the static analysis it can be concluded that the new optimized configuration looks promising for the load cases determined. It has to be noted that the beam profiles calculated by the MATLAB sequence are not optimal. The square profile does not suit the loading conditions of several beams. The profile of these beams have therefore been adjusted in the model. The static loading included a dynamic amplification factor (DAF), to cover for the variation in loading due to the effect of inertia, load- and vessel motions. The dynamic analysis will provide inside on these effects and the choice of the DAF.

III
Dynamic analysis

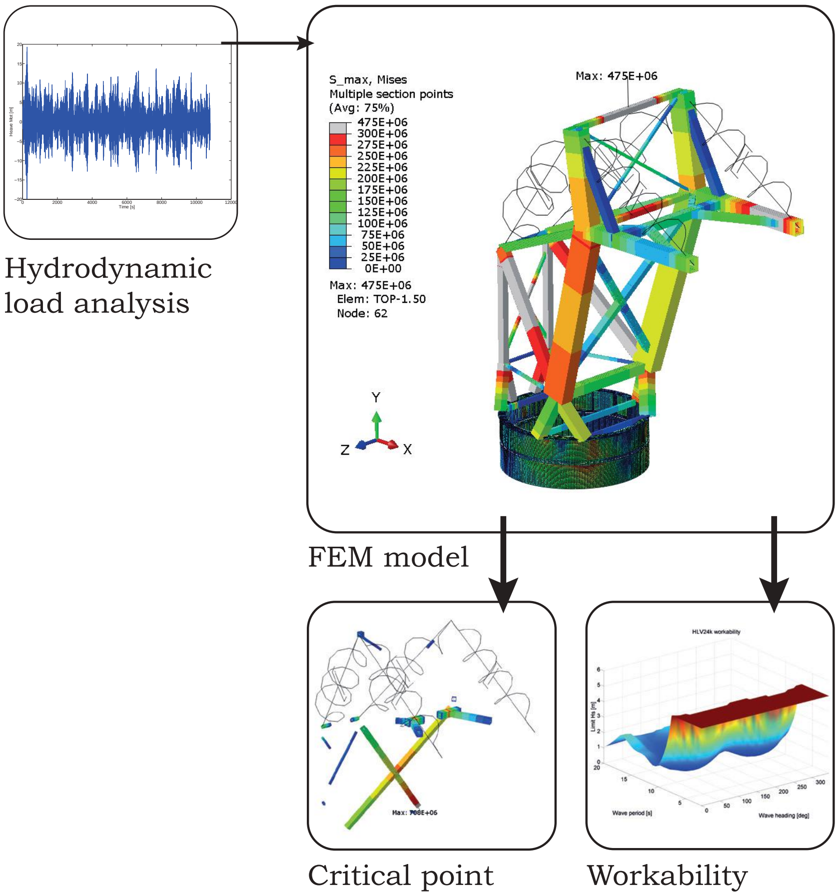

8

Flexible Liftdyn model

Especially the dynamics occurring during the survival and operations are of a major influence on the structural design of the crane. Because of the size and unconventional configuration the dynamics are hard to predict and therefore necessary to analyze.

For the dynamic analyses new Liftdyn models have been created. The hull of the vessel has not been change, so the hydrodynamic properties of the previous Liftdyn model have been used, chapter 4. The crane in this previous model has been configured with the original crane design from the pre-study. The new Liftdyn models have been updated to the new crane geometry. Furthermore the flexibility of the crane structure, as derived form the optimization, has been implemented.

New Liftdyn analyses have been performed, which resulted in the loading and boundary conditions for the finite element analyses.

8.1 Beam bending

The previous Liftdyn analyses have been performed with a model of rigid bodies and connectors. The flexible behavior of the beams has not been taken into account in the results. In order to obtain a more accurate simulation of the dynamics, the flexibility of the beams have been modeled. Because Liftdyn only accepts rigid bodies, each beam has been modeled with four rigid bodies interconnected with a set of springs. The properties of the beam have been translated into spring stiffnesses, describing the bending behavior [20]. Figure 5.4 shows the flexibility beam concept: four rigid bodies connected with a rotation and transverse springs in one plane.

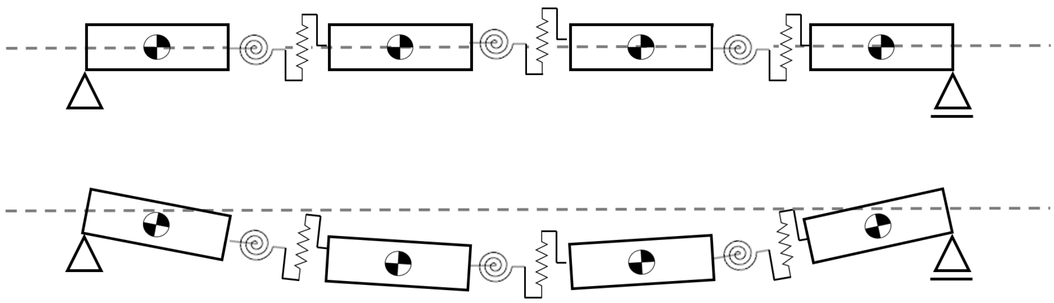

Figure 8.1: Beam bending system principle

8.1.1 Beam bending system

In the crane model the stiffness is required for both the bending directions of the beam's cross-section. All the beams used have a rectangular cross-section. The behavior of the beam in this cross-section is formulated with the same equations for both directions, therefore the equations have been solved for one plane.

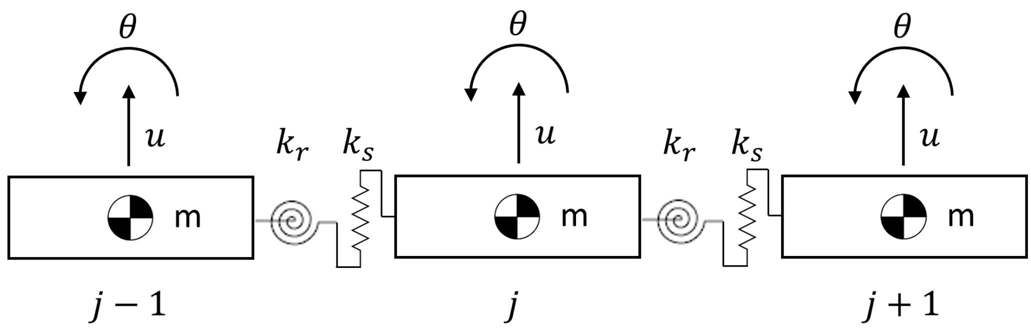

Figure 8.2: 2D beam element system

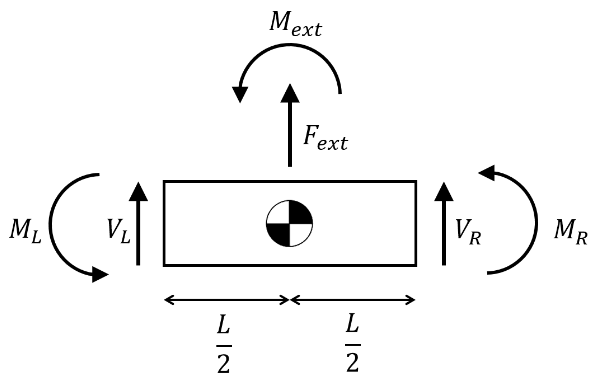

Figure 8.3: Section j of the 2D beam element

Moment at the left side of section j:

$$M_L = k_r \cdot (\theta_{j-1} - \theta_j) \tag{8.1}$$

Moment at the right side of section j:

$$M_R = k_r \cdot (-\theta_j + \theta_{j+1}) \tag{8.2}$$

Shear force at the Left side of section j:

$$V_L = k_s \cdot \left(u_{j-1} - u_j + \theta_{j-1} \cdot \frac{L}{2} + \theta_j \cdot \frac{L}{2}\right) \tag{8.3}$$

Shear force at the right side of section j:

$$V_R = k_s \cdot \left(-u_j + u_{j+1} - \theta_j \cdot \frac{L}{2} - \theta_{j+1} \cdot \frac{L}{2}\right) \tag{8.4}$$

Sum of the forces on the section j:

$$\sum F = m \cdot \ddot{u}_j \tag{8.5}$$

$$k_s \cdot \left(u_{j-1} - 2u_j + u_{j+1} - \theta_{j-1} \cdot \frac{L}{2} + \theta_j \cdot \frac{L}{2} - \theta_j \cdot \frac{L}{2} - \theta_{j+1} \cdot \frac{L}{2}\right) = m \cdot \ddot{u}_j \tag{8.6}$$

Sum of the moments on the section j:

$$\sum M = J \cdot \ddot{\theta}_j \tag{8.7}$$

$$\begin{aligned} k_r \cdot (\theta_{j-1} - 2\theta_j + \theta_{j+1}) - \frac{L}{2} k_s \cdot \left(u_{j-1} - u_j + \theta_{j-1} \cdot \frac{L}{2} + \theta_j \cdot \frac{L}{2}\right) + \cdots \\ \frac{L}{2} k_s \cdot \left(-u_j + u_{j+1} - \theta_j \cdot \frac{L}{2} - \theta_{j+1} \cdot \frac{L}{2}\right) = J \cdot \ddot{\theta}_j \end{aligned} \tag{8.8}$$

Rewriting of the equations for the summed moments and summed shear forces results in the following Equation of Motion of element j.

$$\begin{bmatrix} m_j & 0 \\ 0 & J_j \end{bmatrix} \begin{Bmatrix} \ddot{u}_j \\ \ddot{\theta}_j \end{Bmatrix} + \begin{bmatrix} -k_s & -\frac{L}{2}k_s & 2k_s & 0 & -k_s & \frac{L}{2}k_s \\ \frac{L}{2}k_s & -k_r + \frac{L^2}{4}k_s & 0 & 2k_r + \frac{L^2}{2}k_s & -\frac{L}{2}k_s & -k_r + \frac{L^2}{4}k_s \end{bmatrix} \begin{Bmatrix} u_{j-1} \\ \theta_{j-1} \\ u_j \\ \theta_j \\ u_{j+1} \\ \theta_{j+1} \end{Bmatrix} = \begin{Bmatrix} F_{ext,j} \\ M_{ext,j} \end{Bmatrix} \tag{8.9}$$

8.1.2 Stiffness matrix

A beam is represented as two nodes connected with an element, Figure 8.4

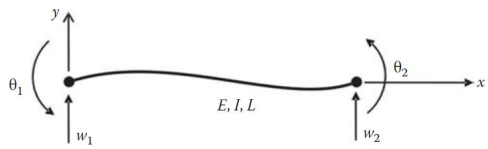

Figure 8.4: 2D beam element system [2]

The force-displacement relation of the end nodes are described in the following stiffness matrix:

$$\begin{Bmatrix} F_{y,1} \\ M_{z,1} \\ F_{y,2} \\ M_{z,2} \end{Bmatrix} = \begin{bmatrix} \frac{12EI}{L^3} & \frac{6EI}{L^2} & -\frac{12EI}{L^3} & \frac{6EI}{L^2} \\ \frac{6EI}{L^2} & \frac{4EI}{L} & -\frac{6EI}{L^2} & \frac{2EI}{L} \\ -\frac{12EI}{L^3} & -\frac{6EI}{L^2} & \frac{12EI}{L^3} & -\frac{6EI}{L^2} \\ \frac{6EI}{L^2} & \frac{2EI}{L} & -\frac{6EI}{L^2} & \frac{4EI}{L} \end{bmatrix} \begin{Bmatrix} w_1 \\ \theta_1 \\ w_2 \\ \theta_2 \end{Bmatrix} \tag{8.10}$$

In case of three beams ($j-1$, j and $j+1$) connected along the axial direction, the individual stiffness matrices 8.10 are combined in the stiffness matrix describing the whole system. The force displacement of all the nodes are formulated in Equation 8.11.

$$\begin{Bmatrix} F_{y,1} \\ M_{z,1} \\ F_{y,2} \\ M_{z,2} \\ F_{y,3} \\ M_{z,3} \\ F_{y,4} \\ M_{z,5} \end{Bmatrix} = \begin{bmatrix} \frac{12EI}{L^3} & \frac{6EI}{L^2} & -\frac{12EI}{L^3} & \frac{6EI}{L^2} & 0 & 0 & 0 & 0 \\ \frac{6EI}{L^2} & \frac{4EI}{L} & -\frac{6EI}{L^2} & \frac{2EI}{L} & 0 & 0 & 0 & 0 \\ -\frac{12EI}{L^3} & -\frac{6EI}{L^2} & \frac{24EI}{L^3} & 0 & -\frac{12EI}{L^3} & \frac{6EI}{L^2} & 0 & 0 \\ \frac{6EI}{L^2} & \frac{2EI}{L} & 0 & \frac{8EI}{L} & -\frac{6EI}{L^2} & \frac{2EI}{L} & 0 & 0 \\ 0 & 0 & -\frac{12EI}{L^3} & -\frac{6EI}{L^2} & \frac{24EI}{L^3} & 0 & -\frac{12EI}{L^3} & \frac{6EI}{L^2} \\ 0 & 0 & \frac{6EI}{L^2} & \frac{2EI}{L} & 0 & \frac{8EI}{L} & -\frac{6EI}{L^2} & \frac{2EI}{L} \\ 0 & 0 & 0 & 0 & -\frac{12EI}{L^3} & -\frac{6EI}{L^2} & \frac{12EI}{L^3} & -\frac{6EI}{L^2} \\ 0 & 0 & 0 & 0 & \frac{6EI}{L^2} & \frac{2EI}{L} & -\frac{6EI}{L^2} & \frac{4EI}{L} \end{bmatrix} \begin{Bmatrix} w_1 \\ \theta_1 \\ w_2 \\ \theta_2 \\ w_3 \\ \theta_3 \\ w_3 \\ \theta_3 \end{Bmatrix} \tag{8.11}$$

The values of k_s and k_r can be determined by solving the equilibrium on one element. The shear force on a single element is calculated as the summation of the shear forces on its two nodes. An examples will explain this method:

Element j

$$F_{y,j} = F_{y,2} + F_{y,3} = \frac{24EI}{L^3} \cdot w_2 - \frac{12EI}{L^3} \cdot w_3 - \frac{12EI}{L^3} \cdot w_2 + \frac{24EI}{L^3} \cdot w_3 = \frac{24EI}{L^3} \cdot u_j \tag{8.12}$$

$$F_{y,j} = 2k_s \cdot u_j \tag{8.13}$$

$$2k_s = \frac{24EI}{L^3} \Longrightarrow k_s = \frac{12EI}{L^3} \tag{8.14}$$

This same method has been used to solve the k_r.

$$\begin{gathered}-k_r+\frac{L^2}{4}k_s=\frac{2EI}{L}\\ -k_r+\frac{L^2}{4}\frac{12EI}{L^3}=\frac{2EI}{L}\Longrightarrow k_r=\frac{EI}{L}\end{gathered} \tag{8.15}$$

By filling in k_s and k_r in 8.9 the following Equation of Motion is obtained.

$$\begin{bmatrix} m_j & 0 \\ 0 & J_j \end{bmatrix}\begin{Bmatrix}\ddot{u}_j\\ \ddot{\theta}_j\end{Bmatrix}+\begin{bmatrix}-\frac{12EI}{L^3} & -\frac{6EI}{L^2} & \frac{24EI}{L^3} & 0 & -\frac{12EI}{L^3} & \frac{6EI}{L^2}\\ \frac{6EI}{L^2} & \frac{2EI}{L} & 0 & \frac{8EI}{L} & -\frac{6EI}{L^2} & \frac{2EI}{L}\end{bmatrix}\begin{Bmatrix}u_{j-1}\\ \theta_{j-1}\\ u_j\\ \theta_j\\ u_{j+1}\\ \theta_{j+1}\end{Bmatrix}=\begin{Bmatrix}F_{ext,j}\\ M_{ext,j}\end{Bmatrix} \tag{8.16}$$

The stiffness matrix in equation 8.16 matched the first six columns of rows three and four and the last six columns of rows five and six in the composed stiffness matrix 8.11.

8.2 Liftdyn spring implementation

In the Liftdyn model, rigid beam elements can be connected via joints or connectors. In the case a spring and/or damping is required between two elements the connector can be used. The properties of the six DoF connectors are formulated in the matrix 8.17. This matrix is defined in the elements local coordinates system.

$$K_{connector}=\begin{bmatrix}0&0&0&0&0&0\\0&k_s&0&0&0&0\\0&0&k_s&0&0&0\\0&0&0&0&0&0\\0&0&0&0&k_r&0\\0&0&0&0&0&k_r\end{bmatrix}=\begin{bmatrix}0&0&0&0&0&0\\0&\frac{12EI}{L^3}&0&0&0&0\\0&0&\frac{12EI}{L^3}&0&0&0\\0&0&0&0&0&0\\0&0&0&0&\frac{EI}{L}&0\\0&0&0&0&0&\frac{EI}{L}\end{bmatrix} \tag{8.17}$$

The connectors specified in Liftdyn are defined in the global coordinate system. To obtain the correct direction of the connectors, the local matrix has to be rotated to align with the global directions. The rotations, Equation 8.18, have been performed with the Euler angle transformations combined in a rotation matrix (T_{rot}) [9].

$$[K_{global}]=[K_{local}]\cdot[T_{rot}] \tag{8.18}$$

8.2.1 Implementation

Due to limitation in Liftdyn, solving the system with all the beams modeled individual was not possible. Therefore the main crane parts are modeled as bending beams. The crane part that are mainly loaded in the axial direction are modeled with in-line connectors. In case of the A-frame and Top, the structure is split in multiple parts. Table 8.1 gives an overview of the parts that are updated from the previous Liftdyn model. The Hull, tub and crane house have not been changed.

Table 8.1: Liftdyn updated elements

Part	Element type
A-frame back	in-line connector
A-frame front	Bending beam
Boom	Bending beam
Luffer	in-line connector
Top front	in-line connector
Top back	Bending beam
Top main	Bending beam
Jib	Bending beam
Jib brace	in-line Connector
All wires	in-line Connector

Figure 8.5 shows the updated crane model. The hollow red dot indicate the CoG of a rigid body, the solid red dot represents a spring matrix. In-line connectors are visualized by the solid black lines. The black truss- and orange box are the rigid body elements.

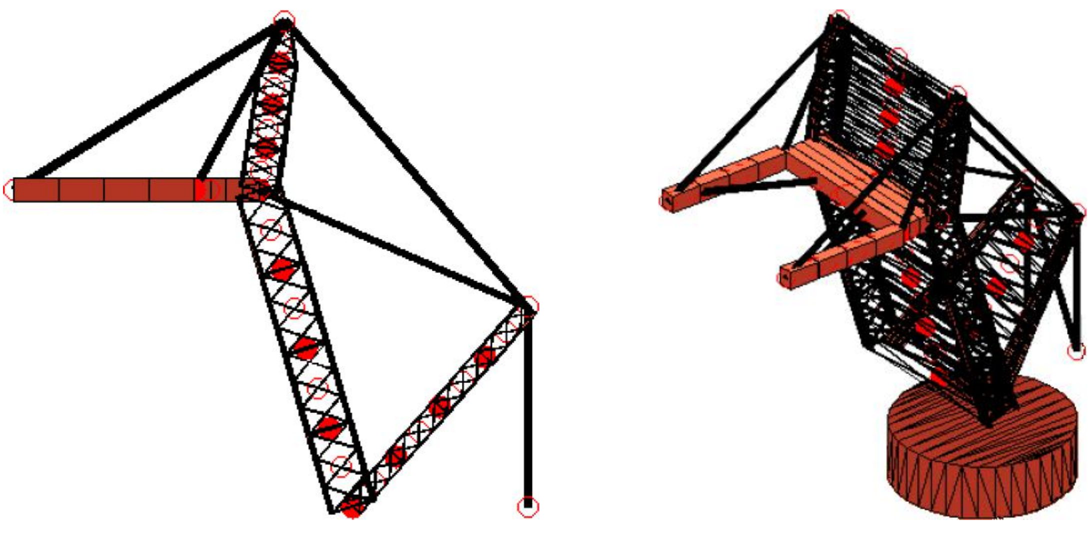

(a) Crane (side view)

(b) Crane (ISO view)

Figure 8.5: Updated liftdyn crane model

The load cases have been re-analyzed with this new crane model, see Figure 4.4 and 4.5 for the original models.

8.2.2 Comparison

Liftdyn analyses for existing vessel with conventional crane are performed with rigid bodies. The flexibility of the crane is calibrated to the real situation by tweaking the stiffness, damping and pre-tension of the luffing en hoist wires.

The response of a conceptual unconventional crane can not be validated with a real life model, therefore the flexibility of the beams is modeled. A comparison between the "flexible" model and a "rigid" model of the HLV24k concept has been performed. First the Eigen frequencies have been evaluated. The main deviations are found for modes depicted by the sideways bending of the crane. This motion is restricted in the fixed model, hence the differences.

The X, Y and Z motion response of hook 22 for a significant wave height of 1m have been evaluated per wave heading. The response envelope of the three motions are visual in Figure 8.6 to 8.8.

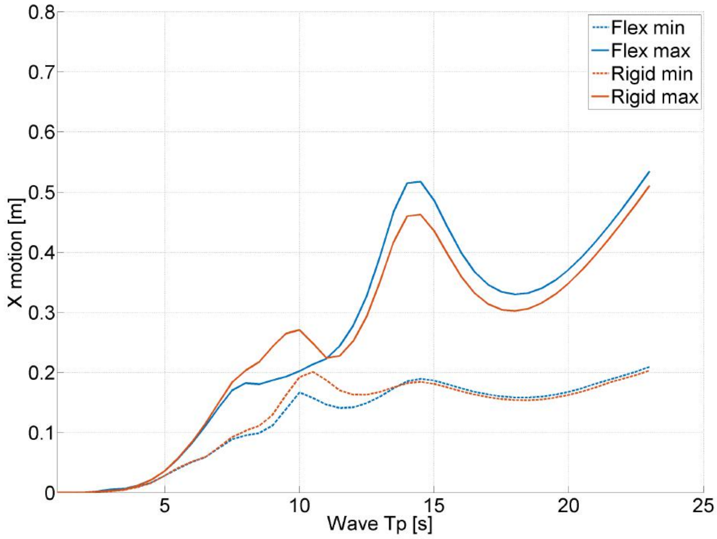

Figure 8.6: Response hook 22 X motion, flexible and rigid beams

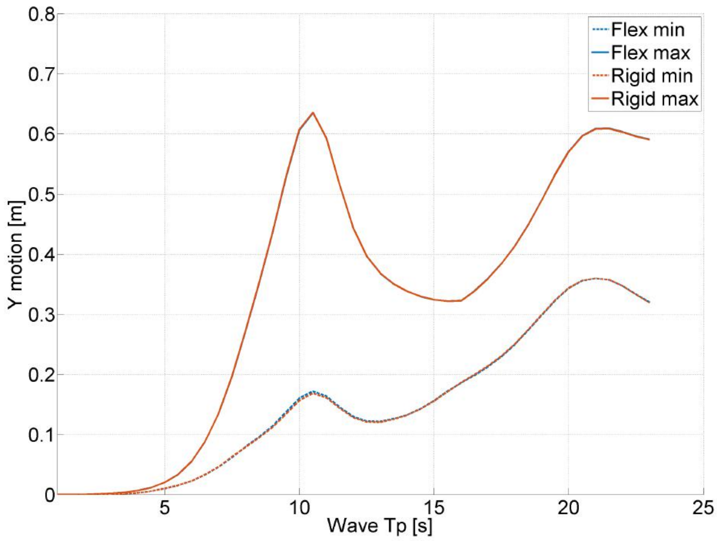

Figure 8.7: Response hook 22 Y motion, flexible and rigid beams

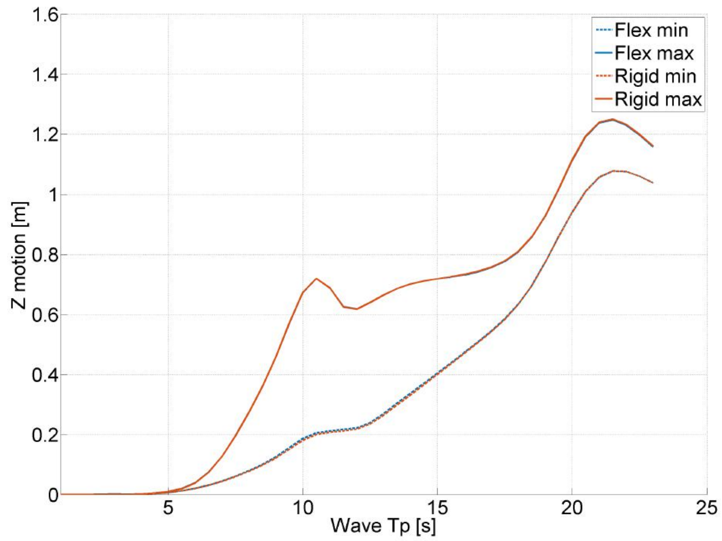

Figure 8.8: Response hook 22 Z motion, flexible and rigid beams

The flexibility of the crane beams has little influence on the response in the Y and Z direction. In general the X response of the flexible model is higher for wave peak periods above 11s. Below this period the rigid beam model gives higher X responses.

It can be concluded that the motions are mostly depicted by the properties of all the wires in the system. The sideways motion is not accounted for by the wires, which is clearly visible in the natural frequencies and the X motion of the hook. Because the rigid beam model gives larger response for the wave peak period below 11s the rigid beams are considered conservative for the period with the most wave energy. Further details of the comparison can be found in Appendix C

8.3 Output

For all five Liftdyn models new calculations have been performed. The following RAOs have been generated:
Survival conditions RAOs

- Vessel motions: $X, Y, Z, \phi, \theta, \psi$

Operational conditions RAOs

- Vessel motions: $X, Y, Z, \phi, \theta, \psi$
- Hook 11 forces: F_X F_Y F_Z
- Hook 21 forces: F_X F_Y F_Z
- Hook 12 forces: F_X F_Y F_Z
- Hook 22 forces: F_X F_Y F_Z

The vessel motions RAOs have been obtained at the center of the tub at deck level, as this point corresponds to the input point in the FEA model.

The output RAOs are stored as separated amplitudes and phase shifts. To account for the phase shift in the time signal calculation the ROAs are converted to complex numbers.

9 Dynamic finite element model

Analyzing the system on its dynamic behavior and rigidity will be performed with the finite element model described in chapter 6. This model however is prepared for static loading and therefore changes have been made on the boundary conditions, calculation procedure and load input methods.

9.1 Modal superposition

In the static analysis the "Static General" solving method is used. This method solves the motion equations for a time step. This method is time-independent, so does not include inertia effects. For the dynamic modeling one is interested in these inertia effects. In general two solution techniques are available, which include these inertia effects: Direct solutions and frequency response solutions. In general the direct solution methods come at great computational effort, whereas the frequency response solutions are efficient but not sufficient for all types of dynamic modeling. Especially problems which include large non-linearities cannot be solve in the frequency domain. If large non-linearities are present in the analysis, the Eigen frequencies change significantly as a result of the loading the system. These large non-linearities can only be calculated by direct integration of the equations to an equilibrium.

In this research the crane, the material and geometry behavior, is considered linear. With this assumption the dynamic response of the crane to a load can be characterized by its Eigen frequencies and mode shapes. The deformation of the crane can be calculated by the linear combination of the modes shapes, modal superposition. In the first step the natural frequencies and mode shapes are calculated, dependent on the number of frequencies used, this step can be computational expensive. Once the natural frequencies are obtain the actual analysis can be performed. Further details of modal superposition can be found in Appendix E.

9.2 Abaqus

In the Abaqus software the modal analysis is performed with the following steps:

1. Extraction of the natural frequencies and mode shapes
2. Calculation of the external load vector at each time instant
3. Integration of the equation of motion for each i^{th} mode
4. Expanding the model solution into displacements
5. Further calculations specified by the user, like calculation of the stresses

In Abaqus the desired number of Eigen frequencies are extracted using a step prior to the modal analysis. The more modes used in the analysis, the more accurate the results are. However using more modes, cost more computation time. For this research the first 40 natural frequencies have been used. This number yielded from a small analysis done, for a range of mode numbers. The first few Eigen modes are visualized in Appendix D.

9.2.1 Loading

The loading of the system has been done in the form of vessel motions and force amplitudes of the hooks. The time signals obtained, are translated into tables with an time interval of 0.25s. The forces have applied on the 4 hook location like the static simulation, Figure 6.8. The force applied is the sum of the static force and the time dependent amplitude. The vessel motion have been applied at the boundary condition.

9.2.2 Boundary conditions

The vessel motions are obtained at the center of the tub at deck level. To apply these motions to the crane, the boundary conditions of the tub have been applied at the same point. By connecting (yellow lines) the tub edge (highlighted red) with this point (Blue-orange point) the boundary conditions are translated to this edge. Hereby is the edge motions slaved to the boundary conditions point.

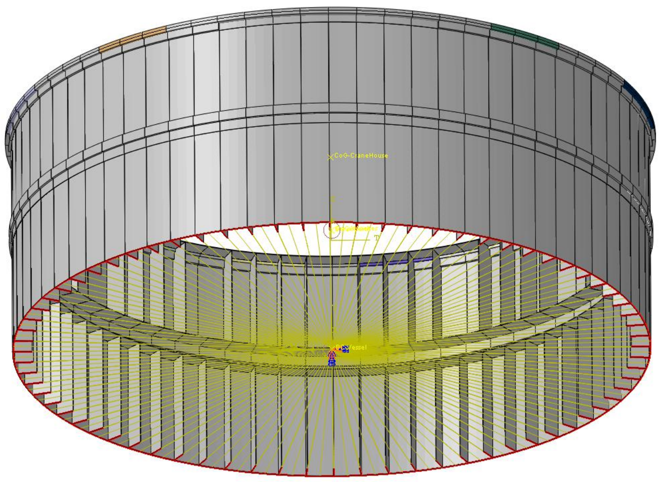

Figure 9.1: Point boundary conditions (Tub bottom view)

9.2.3 Base motions

The motions of vessel act on the boundary condition. Because the boundary condition is fixed in all 6 degrees of freedom, applying these vessel motions in the form of forces is not possible. Therefore the vessel excitations are performed in the form of a base motions. If the prescribed motion cannot be described by a single set of rigid body motions, multiple base motions are created. One of these base motions is handled as the main base motion, called the Primary base. The other base motions are used as secondary bases. The difference in these two bases can be seen in the way they are formulated: Primary Base uses the "modal participation" method, translating the prescribed motion into inertia load

$$F_{pb} = [M]\{\ddot{u}_{pb}\} \tag{9.1}$$

Secondary bases are handled with the "big mass" method, which applies a point force to each degree of freedom (N) in the analysis step.

$$F^N_{sb} = M_+ \ddot{u}^N_{sb} \tag{9.2}$$

The equation of motion for the primary and secondary base motions is defined as follows:

$$[M]\{\ddot{u}\} + [C]\{\dot{u}\} + [K]\{u\} = -F_{pb} + \sum_N F^N_{sb} \tag{9.3}$$

All the six vessel motions are applied to the boundary conditions at the tub in the form of these base motions [3].

9.3 Dynamic Load cases

The dynamic load cases consist of the time signals of the vessel motions and hook force amplitudes. The continuous time signals are transformed into tables which are loaded in the Abaqus models. The amplitudes are stored with an interval of 0.25s. This interval is assumed to be small enough to describe the amplitude waves, because the lowest wave period in the spectrum is 1.5s.

9.3.1 Time signal

The motion and force RAOs are obtain from the updated Liftdyn model, chapter 8. The response in time domain can be calculated from the RAO and a sea state. The sea state is described by a wave spectrum, $S(\omega, \theta_w)$. The formulation of this spectrum can be found in subsection 4.3.4. For both the survival and operational loading conditions wind seas are assumed, described by a JONSWAP spectrum [11].

The RAOs describe the response of the vessel motions and hook forces per regular wave. In order to multiply the wave spectrum with the RAOs, the spectrum must be described as a regular wave: per frequency (ω) and per direction of the waves (θ_w). Equation 9.4 describes the individual wave amplitude for i ($1,2,3,\ldots n$, no. of frequencies) and j ($1,2,3,\ldots m$, No. of directions).

$$A_{i,j} = \sqrt{2 \cdot S_(\omega_i, \theta_{w,j}) \cdot \Delta\omega \cdot \Delta\theta_w} \tag{9.4}$$

Multiplying the wave amplitude and the RAO results in the amplitude of the response per frequency and direction, Equation 9.5.

$$\begin{aligned} u_{i,j} &= A_{i,j} \cdot RAO_u(i,j) \\ F_{i,j} &= A_{i,j} \cdot RAO_F(i,j) \end{aligned} \tag{9.5}$$

Superposing of the regular response for all wave frequencies and direction the response in the time domain is created. The phase angles used in the superposing represent the shift of the individual waves components with respect to each other. These angles are generated randomly and uniform distributed between 0 and 2π. The values are stored to insure that all the time traces are based on the same phase angles.

$$\begin{aligned} &\sum_{i=1}^{n}\sum_{j=1}^{m} u_{i,j} \cdot cos(\omega_i t + \phi_{i,j}) \\ &\sum_{i=1}^{n}\sum_{j=1}^{m} F_{i,j} \cdot cos(\omega_i t + \phi_{i,j}) \end{aligned} \tag{9.6}$$

With Equation 9.6 the time signals are created for the survival and operational dynamic run in Abaqus. For the survival case only the vessel motions time signals were used as input. The operational cases also include the twelve force amplitude time signals. Figure 9.2 and 9.3 show the random wave elevation signal and the heave response of the vessel in the survival configuration for a 20 min time signal.

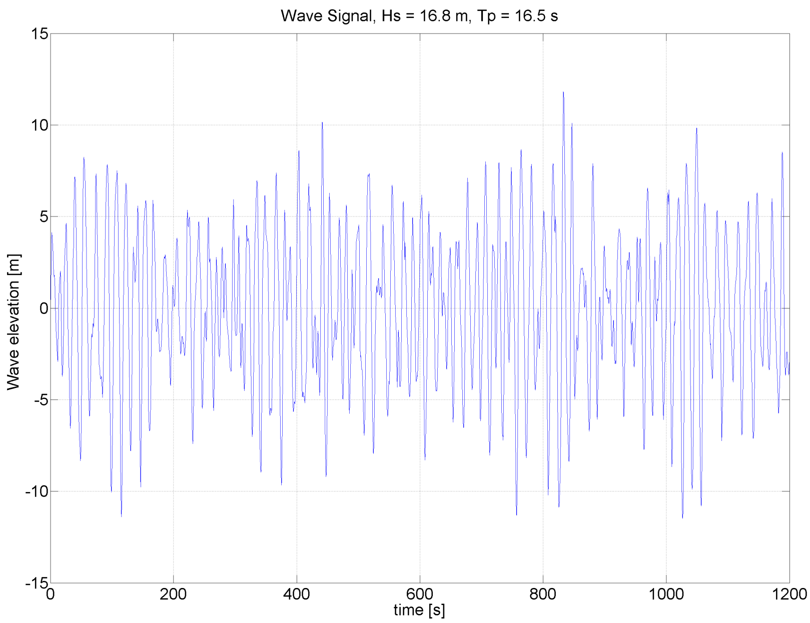

Figure 9.2: Wave elevation time signal (20 min)

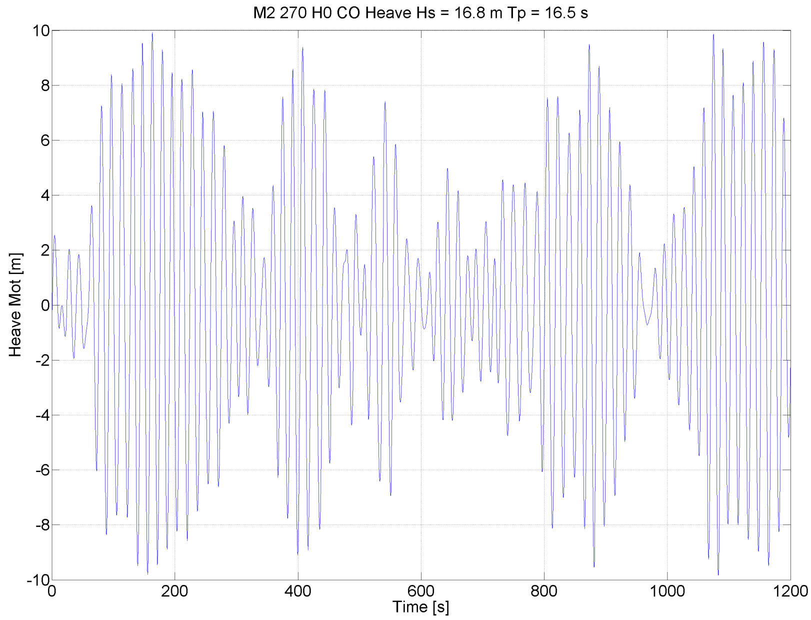

Figure 9.3: Heave response amplitude time signal (20 min M2 270 model)

9.3.2 Survival loading condition

For the survival condition analyses a sea state typical for storm conditions has been used. The parameters used are chosen such that the worst conditions for this sea state will be evaluated. The worst conditions are based on the largest responses from the Liftdyn analyses, chapter 8.

Table 9.1: Survival condition parameters

Parameter	Symbol	Unit	Value
Duration	t	$[s]$	1200, 10800
Significant wave height	H_s	$[m]$	16.8
Wave heading	θ_w	$[deg]$	0
Wave peak period	T_p	$[s]$	16.5
Peak enhancement factor	γ	$[-]$	3.3
Wave spread exponent	n	$[-]$	10

Table 9.2 shows the peak values at the crane origin found in the time signals.

Table 9.2: Survival case time signal peak values

Model	Duration $[s]$	θ_w $[m]$	Surge $[deg]$	Sway $[m]$	Heave $[m]$	Roll $[deg]$	Pitch $[deg]$	Yaw $[deg]$
M2 180	1,200	0	5.09	1.44	9.91	6.34	6.82	1.24
M2 270	1,200	0	5.06	1.44	9.92	6.34	6.72	1.19
M2 270	10,800	0	6.12	2.03	14.30	8.77	6.63	1.38

9.3.3 Operational loading conditions

For the operational loading conditions a calm sea state with Hs = 1m has been used. Again the parameters which coincide with the largest response have been used for the analyses, chapter 8. The combination of largest response have been observed for two wave headings, therefore they have both been analyzed.

Table 9.3: Operational condition parameters

Parameter	Symbol	Unit	Value
Duration	t	$[s]$	10,800
Significant wave height	H_s	$[m]$	1
Wave heading	θ_w	$[deg]$	270 & 315
Wave peak period	T_p	$[s]$	11
Peak enhancement factor	γ	$[-]$	3.3
Wave spread exponent	n	$[-]$	6

Table 9.4 and 9.5 show the peak values at the crane origin and hooks found in the motion and force time signals.

Table 9.4: Operational time signal peak value of the vessel motions

Model	Duration $[s]$	θ_w $[deg]$	Surge $[m]$	Sway $[m]$	Heave $[m]$	Roll $[deg]$	Pitch $[deg]$	Yaw $[deg]$
M3 90	10,800	270	0	0.35	0.29	0.47	0	0
M3 90	10,800	315	0.15	0.13	0.11	0.14	0.11	0.07
M3 180	10,800	270	0.20	0.45	0.31	0.46	0.09	0.22
M3 180	10,800	315	0.13	0.13	0.10	0.13	0.11	0.09
M3 270	10,800	270	0	0.37	0.32	0.54	0	0
M3 270	10,800	315	0.09	0.13	0.12	0.16	0.14	0.07

Table 9.5: Operational time signal, peak values of the hook forces

Model	Duration $[s]$	θ_w $[deg]$	Fx $[kN]$	Fy $[kN]$	Fz $[kN]$	Fx $[kN]$	Fy $[kN]$	Fz $[kN]$
			Hook 11			Hook 12		
M3 90	10,800	270	0	9,665	12,126	0	9,665	12,126
M3 90	10,800	315	1,207	3,213	4,093	1,207	3,000	4,207
M3 180	10,800	270	3,561	9,150	18,327	2,924	9,150	14,421
M3 180	10,800	315	1,502	2,873	6,728	1,315	2,873	4,438
M3 270	10,800	270	1	9,991	13,498	1	9,991	13,496
M3 270	10,800	315	2,267	3,045	3,256	2,267	3,464	6,265
			Hook 21			Hook 22		
M3 90	10,800	270	0	9,658	15,860	0	9,658	15,860
M3 90	10,800	315	1,691	3,211	4,702	1,691	2,997	5,133
M3 180	10,800	270	3,547	9,339	5,369	2,931	9,339	8,845
M3 180	10,800	315	1,497	3,153	1,789	1,315	3,153	3,185
M3 270	10,800	270	1	9,978	14,951	1	9,978	14,951
M3 270	10,800	315	2,018	3,043	5,538	2,018	3,458	3,631

10

Dynamic analysis results

Both the survival, as well as the operational cases have been evaluated with Abaqus. The judgment of the models is based on the same criteria as the static results chapter 7, the Von Mises stress failure criteria and the displacement.
The result are again treated with the "stress envelope" method, only this time the peak value of each time step is taken, instead of each load case.

10.1 Survival loading condition

In the survival loading conditions a time trace of 3hr is used. From the previous load case assessment a wave peak period of 16.5s and a significant wave height of 16.8m induced the worst vessel response. For the survival case a heading of 0deg is used because the vessel can be positioned without any restriction.
The best crane orientation during a storm has not yet been determined, however it seems logic to position the crane over deck, leaving the choice between 180deg and 270deg. All the orientations in between are considered worse, because of the combination of vessel roll and pitch. A 1200s run has been performed for both crane positions. The best crane position will be based on the stress levels in the crane.

10.1.1 Crane position comparison

For the comparison a lower yield scale is used in Figure 10.1 and 10.2, to emphasize the differences in the two crane orientations.

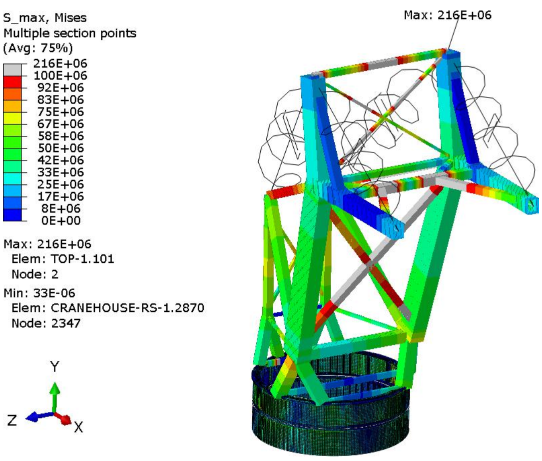

(a) M2 180 (ISO view)

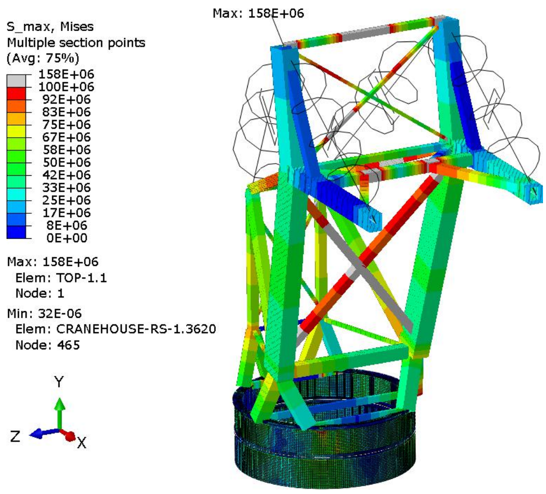

(b) M2 270 (ISO view)

Figure 10.1: M2 crane position Von Mises Stress $[N/m^2]$ comparison

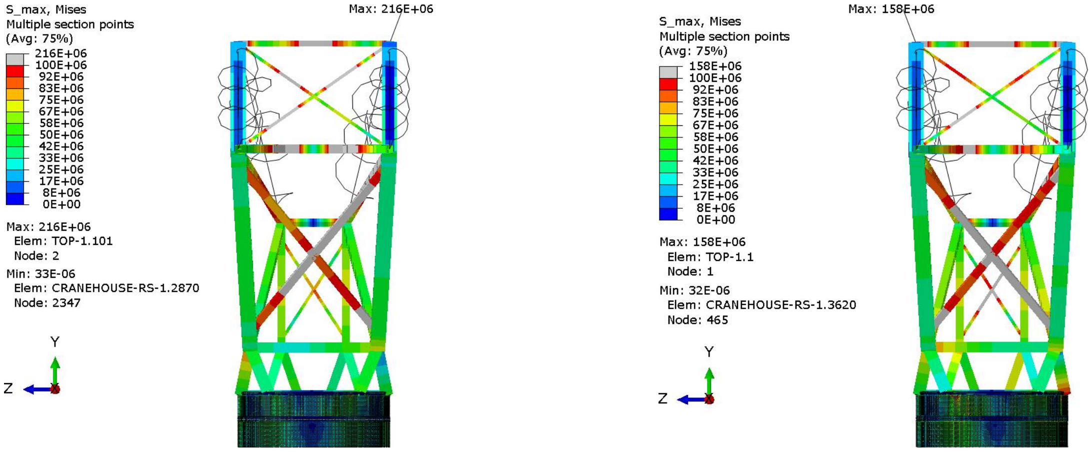

(a) M2 180 (front view) (b) M2 270 (front view)

Figure 10.2: M2 crane position Von Mises Stress $[N/m^2]$ comparison

From the comparison it is seen, that for the crane in the 270deg configuration lower stress levels are observed during a 20 minute MPM run. Therefore it is concluded that the 270deg orientation is beneficial for the structural integrity of the crane.

10.1.2 Full analysis

The 20 minute comparison run showed the beneficial crane orientation to be 270deg. Therefore this configuration is submitted to the full 3hr MPM run. The parts that exceed the allowable stress are depicted in Figure 10.3, 10.4 and 10.5. The stress scale in the figures b is set such that only the parts which exceed the allowable stress, 405N/m^2, are shown.

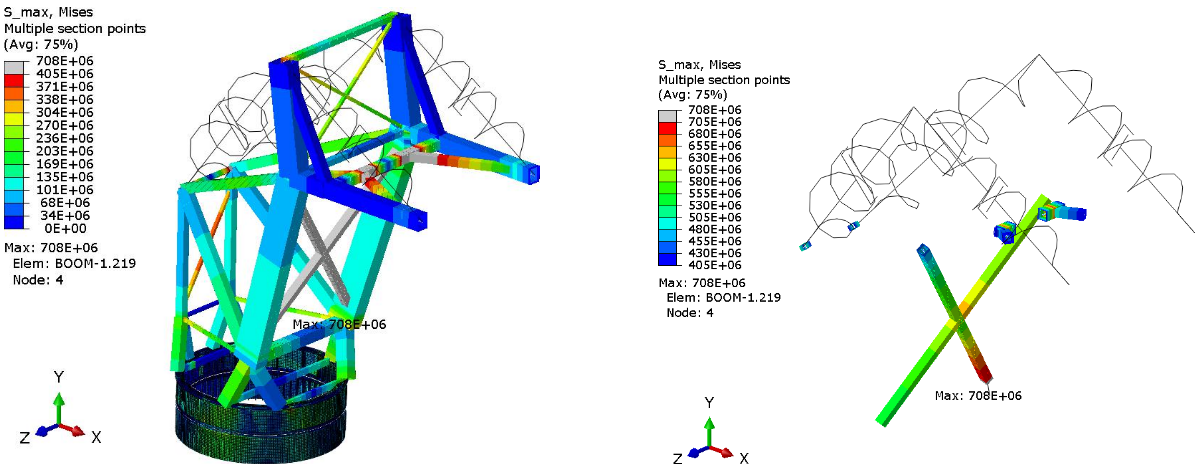

(a) Crane model (ISO view) (b) Failure elements (ISO view)

Figure 10.3: M2 270 Von Mises Stress $[N/m^2]$

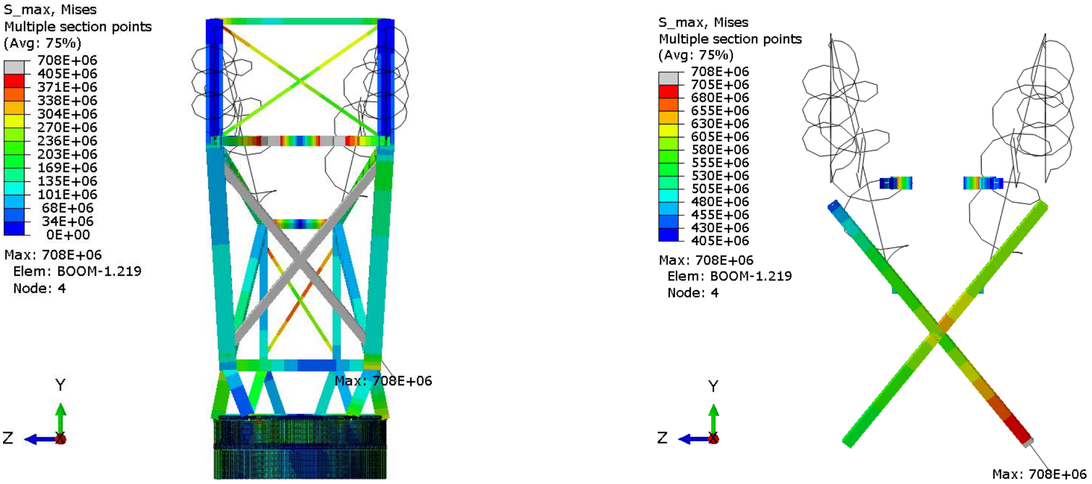

(a) Crane model (front view)

(b) Failure elements (front view)

Figure 10.4: M2 270 Von Mises Stress $[N/m^2]$

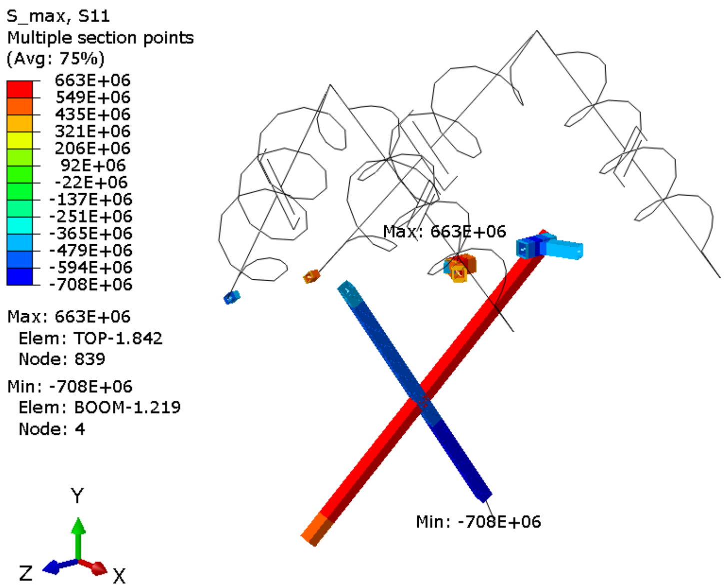

Figure 10.5: M2 270 failure elements axial Stress $[N/m^2]$ (ISO view)

10.1.3 Evaluation

Evaluation of the outcome of the comparison and 3hr storm study lead to the following conclusions:

- **Crane orientation:** From the comparison it can be seen, that for the crane in the 270deg orientation lower stress levels are observed during a 20 minute MPM run. Therefore it was concluded that the 270deg orientation is beneficial for the structural integrity of the crane.
- **Failure parts:** The main parts of the crane all stay intact during the a storm with a peak period of 16.5s and a wave height of 16.5m. The tub and crane house show no exceedance of the allowable stress. However several cross bracing members, mainly in the boom and jib, do exceed the limit by a factor 2. Peak stresses of 700N/mm^2 are observed at the connection between the boom and braces. The peak stresses are mainly induced by the axial forces in the braces.

  The parts indicated as failure elements require strengthening in order to meet the stress criterion. The required adjustment of these parts is considered feasible in reality. Therefore the failure of parts due to the survival loading conditions is not considered a show stopper for this concept study.

10.2 Operational loading conditions

The operational loading conditions are separated in to three crane orientation, 90, 180 and 270. In the Liftdyn study, chapter 8 the worst wave peak period and wave heading were determined. A sea state was formulated with the following parameters:

- Wave peak period: 11s
- Wave heading: 270deg and 315deg
- Significant wave height: 1m
- Duration: 3hr

For the operational conditions the allowable stress is 300N/mm^2. All the crane orientation have been evaluated for the two heading directions over a 3hr time signal. The results of the operational analyses are shown Figure 10.6 to 10.11. Figures b show the crane elements that exceed the allowable stress, note that the stress scale is set from 300 to 450N/mm^2.

M3 90 H270

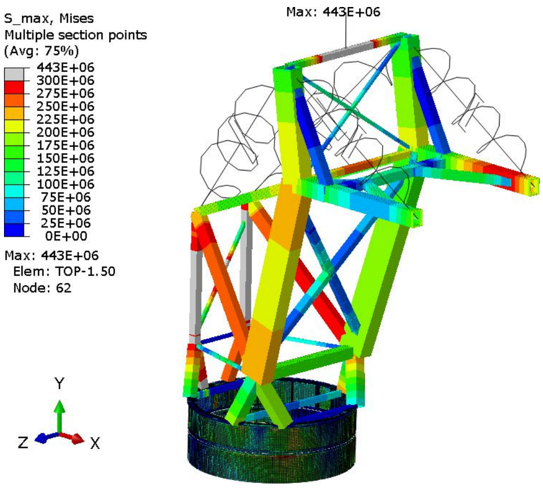

(a) Crane model (ISO view)

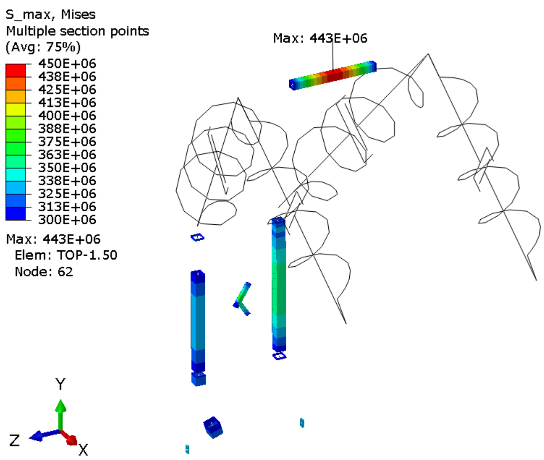

(b) Failure elements (ISO view)

Figure 10.6: M3 90 H270 Von Mises Stress [N/m^2]

M3 90 H315

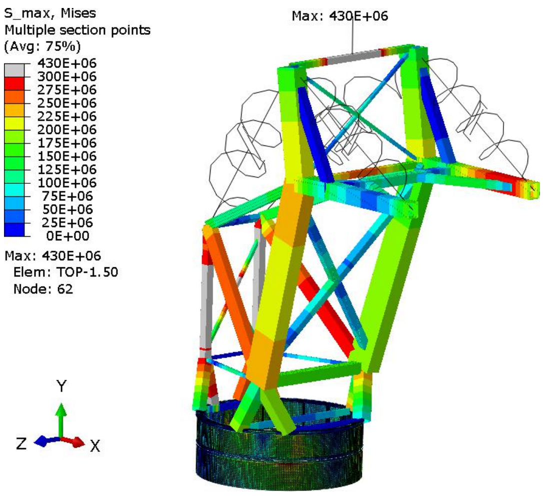

(a) Crane model (ISO view)

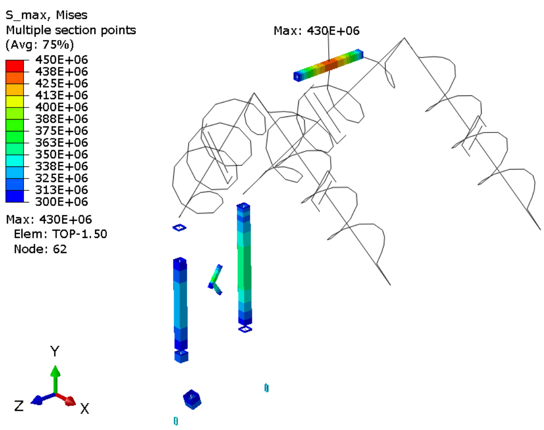

(b) Failure elements (ISO view)

Figure 10.7: M3 90 H315 Von Mises Stress [N/m^2]

M3 180 H270

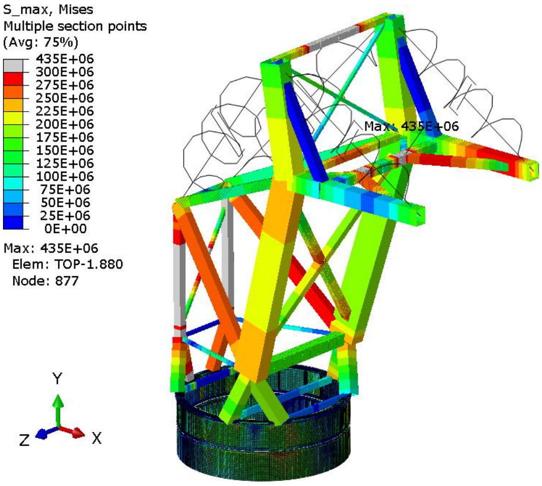

(a) Crane model (ISO view)

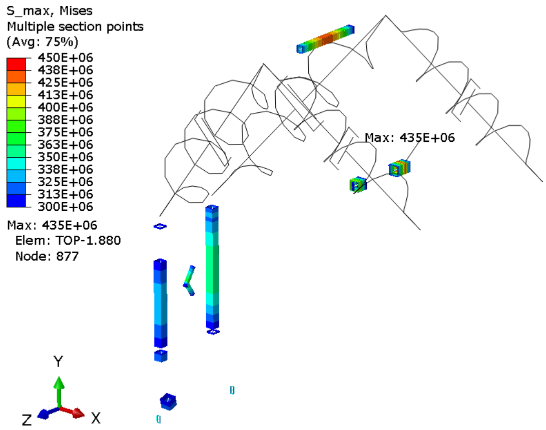

(b) Failure elements (ISO view)

Figure 10.8: M3 180 H270 Von Mises Stress $[N/m^2]$

M3 180 H315

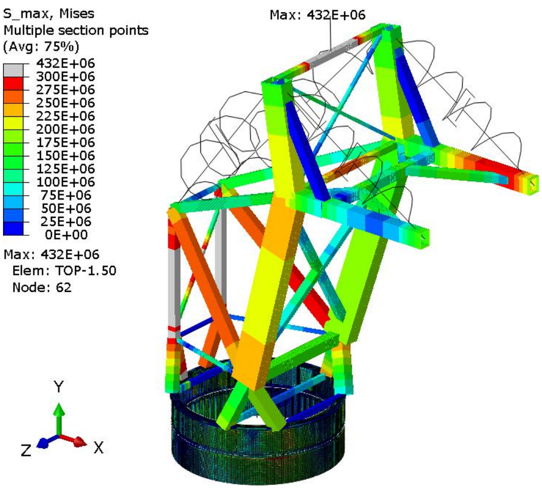

(a) Crane model (ISO view)

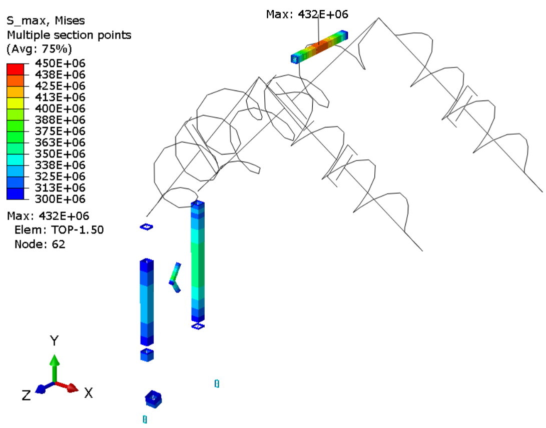

(b) Failure elements (ISO view)

Figure 10.9: M3 180 H315 Von Mises Stress $[N/m^2]$

M3 270 H270

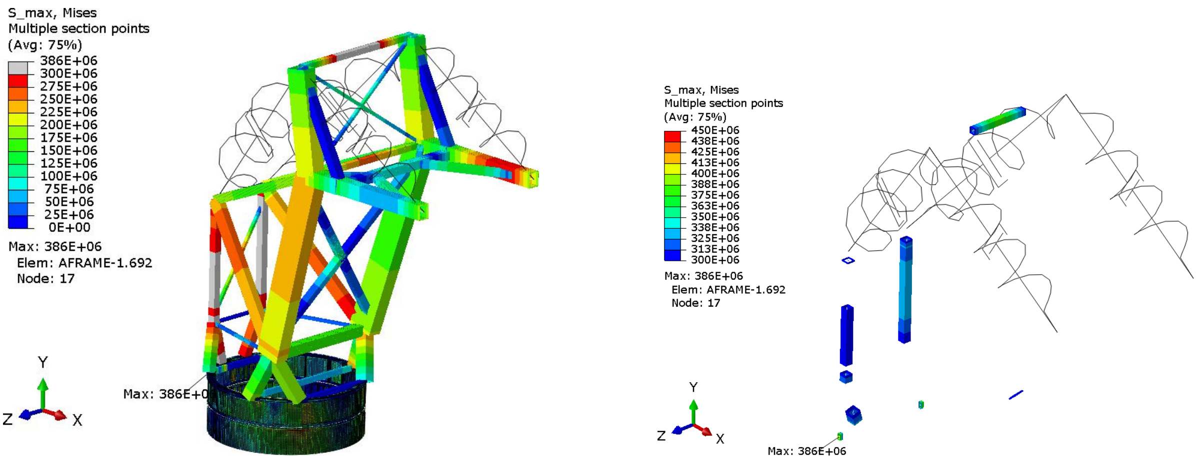

(a) Crane model (ISO view)

(b) Failure elements (ISO view)

Figure 10.10: M3 270 H270 Von Mises Stress $[N/m^2]$

M3 270 H315

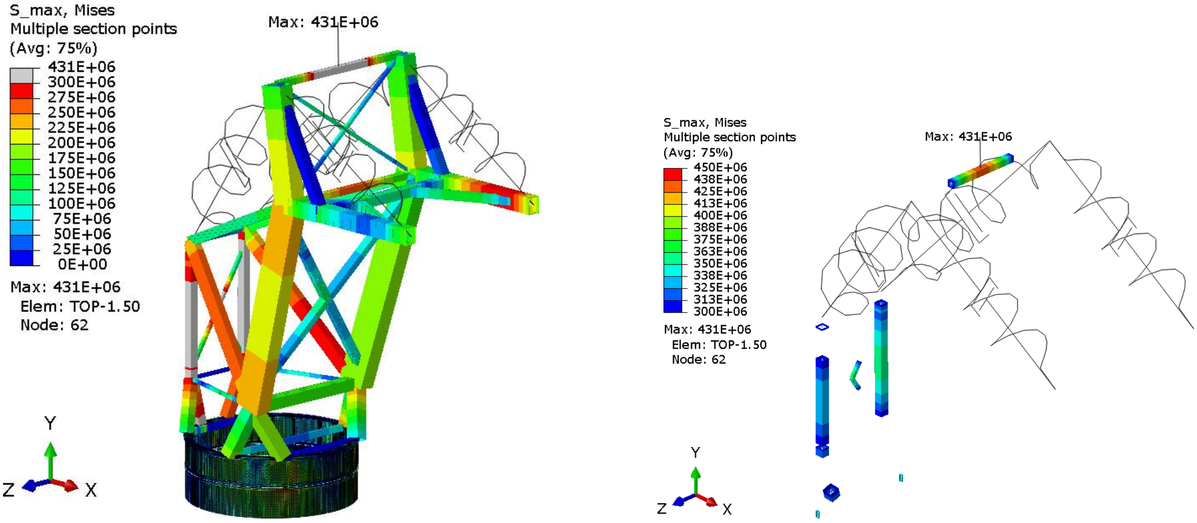

(a) Crane model (ISO view)

(b) Failure elements (ISO view)

Figure 10.11: M3 270 H315 Von Mises Stress $[N/m^2]$

Table 10.1 gives an overview of the peak stresses from the survival and operational analyses.

Table 10.1: Overview peak stresses dynamic runs

Runs	Heading $[deg]$	Peak stress $[N/mm^2]$
Survival		Allowable: 405
M2 180, 20min	0	216
M2 270, 20min	0	158
M2 270, 3hr	0	708
Operational		Allowable: 300
M3 90, 3hr	270	443
M3 90, 3hr	315	430
M3 180, 3hr	270	435
M3 180, 3hr	315	432
M3 270, 3hr	270	386
M3 270, 3hr	315	431

10.2.1 Evaluation

The mild sea state with a Hs of 1m results in large stress amplitudes in the model. It was expected that a DAF of 1.1 in the static case would be sufficient for a significant wave height of 2m. However, the stress criterion is already exceeded with the 1m wave height. Further investigation of the model and the input resulted in the following conclusions:

- **Eigen Frequency:** The input vessel motions and hook forces are derived from a sea state with a wave peak period 11s. This peak period was chosen prior to the dynamic analyses. For a 11s period the hydrodynamic analysis showed the largest vessel motion responses chapter 4. Investigation of the RAOs of the hook forces showed a large peak at 11s. The vessel motions did not show extraordinary responses at the 11s range, therefore the natural frequencies of the system have been evaluated. The crane structure itself did not show resonance behavior for the wave spectrum frequencies Appendix D. Therefore the peak stresses observed are likely to be caused by the movement of the lift object. Due to the hook configuration the object moves as an parallelogram, which influences the sling length used for the Eigen frequency calculated. In the first instance it was assumed that the sling length would reach from the attachment point at the crane to the center of gravity, which resulted in an pendulum frequency outside the wave energy region. However the parallelogram effect shortened the sling length, resulting in an Eigen period of 11.3s, exactly in the wave energy area. This resulted in horizontal motion response of the load of 8m at an Hs of 1m, clearly resonance of the load was occurring. Lifting the load higher, results in a lower Eigen period, shifting to higher wave energy levels.
- **Heading:** The excitation of the topside in the Eigen period is deteriorated if the vessel is excited in the roll motion. With a symmetric semi-submersible the roll excitation is considerably reduced in head or following waves, however the asymmetric hull configuration of the HLV24k also introduce roll excitation, again exciting the topside. The response of the vessel does show lower roll excitation for some heading directions, but the heading is pre-determined by the installation orientation of the load and can therefore not be influenced.

Taken into account the Eigen frequency issue and the heading dependency, one can conclude that this crane configuration introduces several problems when lifting high topside modules, which was considered one of the main benefits of this crane configuration. One possible solution would be to increase the height of the crane, introducing extra construction costs and structural weight. A solution can also be sought in rigging arrangements and constraining methods, however constraining a 24,000t load excited at its Eigen period will be challenging.

The crane has a high lifting capacity but is quite dependent on the sea state, heading and load height, parameters which cannot be influenced. The operability and workability research will provide more insight on the pros and cons of this vessel compared to a traditional semi-submersible crane vessel.

11 Workability analysis

The operational limits of the HLV24k have been studied by performing an operability and workability assessment. To quantify the results, the comparison with a conventional SSCV (Sleipnir) has been made. The parameters used for the comparison are shown in Table 11.1.

The operational limits for a heavy lift vessel mostly relate to the vessel motions, structural integrity of the crane and lift operation experiences. The criteria to assess the operability and workability of the two vessel are shown in Table 11.2. The assessment has been performed for lifting conditions. Pre-lift conditions and set down operations require different criteria and have not been included in this research. The calculations of the responses have been performed for a JONSWAP spectrum.

Table 11.1: Vessel input

Parameter	Unit	HLV24k	Sleipnir
Hook load	$[t]$	6,000	9,400
SWL	$[t]$	24,000	18,800
Object width	$[deg]$	60	30
Object length	$[deg]$	100	110
Object height	$[deg]$	60	60

Table 11.2: Lift criteria

Criterion	Unit	HLV24k	Sleipnir
Heave	$[m]$	1	1
Roll	$[deg]$	0.5	0.5
Pitch	$[deg]$	0.5	0.5
Offlead *	$[deg]$	3	1
Sidelead *	$[deg]$	3	3

* The off- and sidelead are the horizontal forces on the main blocks of the crane. The presented value is the allowable angle at which this force occurs for the SWL at the minimum lifting height. The angle is measured between the vertical and the hoist wires.

11.1 Operability

The operability of a vessel indicated the allowable significant wave height per wave heading and peak period for a lift operation. The allowable wave height is determined by the criteria, Table 11.2. For each criterion the response of the vessel is determined. Dividing the response by the criterion results in the allowable weight height. Because all the criteria have to be met at the same time, the minimum of all the wave heights results in the operability curve of the vessel. The operability of the HLV24k and the Sleipnir have been calculated and visualized in Figure 11.1 and 11.2. The operability limit is plotted as the maximum allowable Hs per wave heading and peak period.

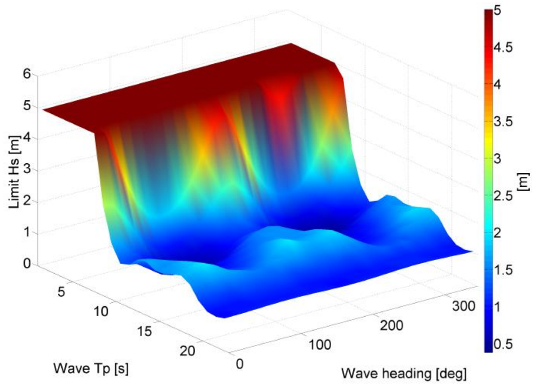

Figure 11.1: HLV24k operability

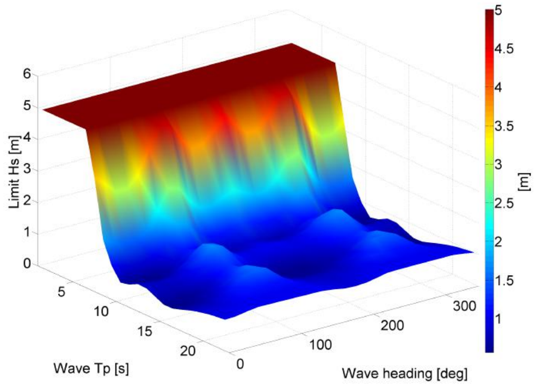

Figure 11.2: Sleipnir operability

The Envelope of the operability for all the wave headings is given in Figure 11.3. The minimum and maximum lines refer to the worst and best possible heading in the operability.

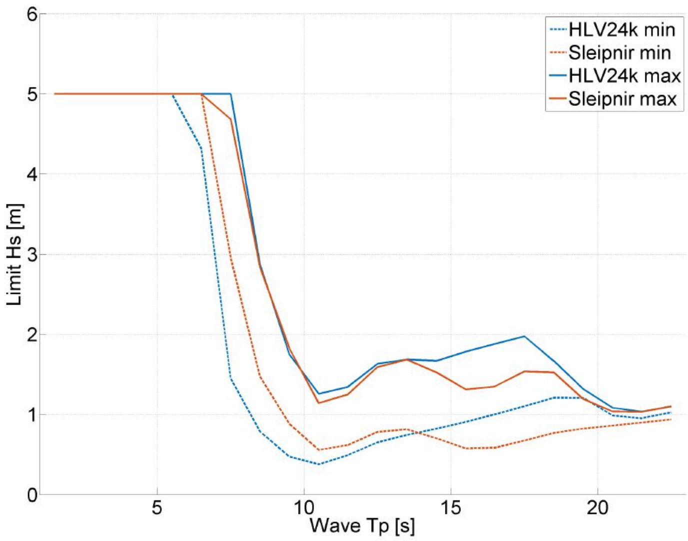

Figure 11.3: Operability envelope of the HLV24k and the Sleipnir

The results per heading direction can be found in F.

11.2 Workability

The operability only indicates the wave height limit for the heading and directions. To quantify the real life situation the wave statics have to be taken into account. If a poor operability is found for a specific wave period, but this wave does rarely occur in real life the workability is hardly influenced.

Per wave heading and peak period the operability wave height is compared with wave data. The number of waves below this wave height are called the workable waves. The workability is calculated as tge percentage of the workable waves over the total number of waves. Summing the percentages of all the wave heading and peak period combinations results in an overall workability. Again the distinction between the worst and best heading for the vessels has been made.

The wave data are the average wave data over the main operational areas in the world. Work seasons of the areas has been taken into account. This set of wave data is referred to as the scatter data and are depicted in

Appendix G.

The workability percentages for all wave height and peak period combinations are visualized in Figure 11.4.

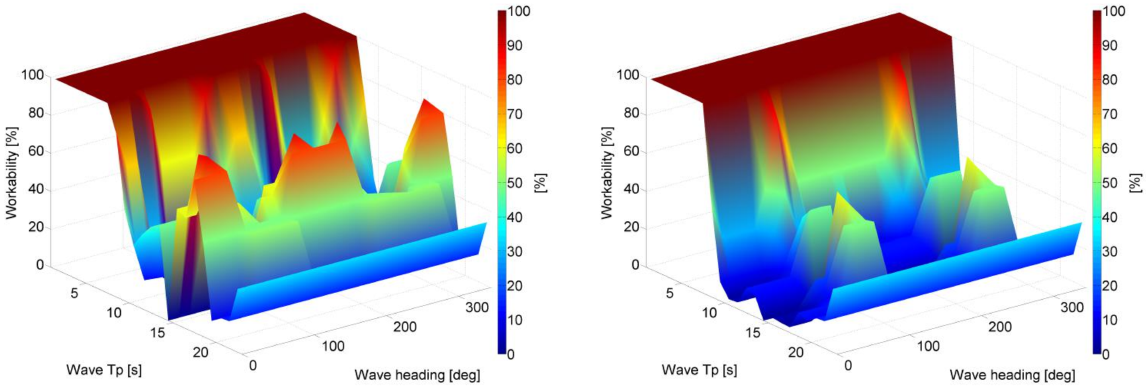

(a) HLV24k

(b) Sleipnir

Figure 11.4: Workability graph[%]

The overall workability of both vessels can be found in Table 11.3.

Table 11.3: Workability percentage

	Heading	HLV24k	Sleipnir
Workability:	Worst	41%	55%
	best	74%	75%

11.3 Evaluation

The operability envelope shows clearly the influence of the resonance of the lift object on the HLV24k. At a wave period around 11s the HLV24k shows a low operability compared to the Sleipnir.
In general the Sleipnir has a higher operability profile for the worst wave heading, whereas the best wave heading indicate similar limits for both vessels. This is emphasized in the workability percentages, where the workability for the best heading is similar. However in real operations the heading of the vessel is mainly dictated by the orientation of the offshore structure. The HLV24ks heading dependent performance is therefore hard to influence. Furthermore the sea state and lift height of the object have a large influence on the workability of the HLV24k.
A more accurate operability and workability profile of the vessel can be obtained by including transit conditions, operational profile, weather and season data and all the stages in a lift operation. Although analyses performed are not complete, the do give an indication of the HLV24k's performance.

IV
Evaluation

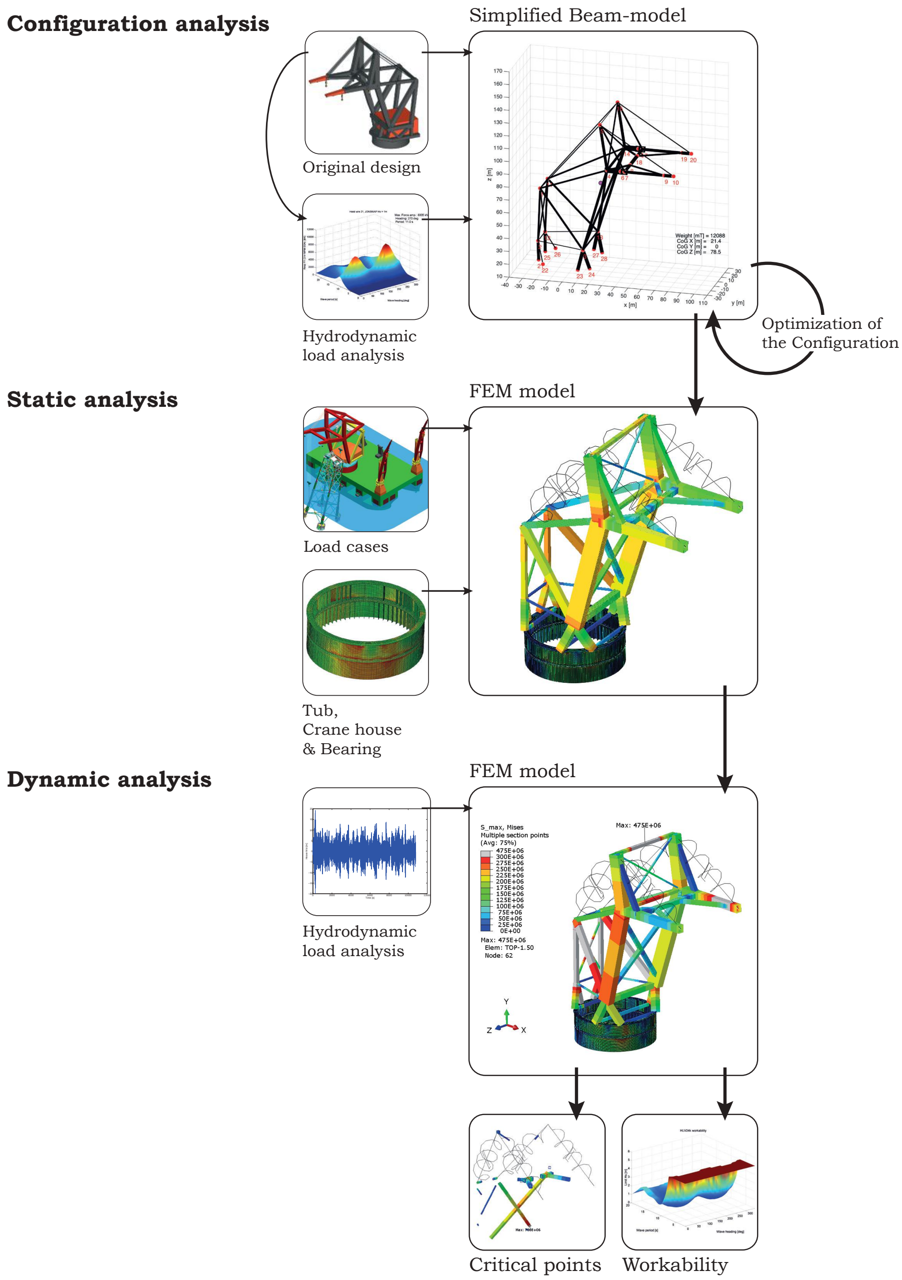

12 Discussion

The interpretation and limitations of the research will be discussed. The validity of the methods and models is questioned. The results will be explanation and their importance will be evaluated.

12.1 Discussion on Methodology

In this thesis several models and methodologies are used to come to the required results. The use of model is inherent to simplifications, which lead to sensitivities in the models. These sensitivities will be discussed per model in the following sections.

12.1.1 Configuration analysis

Beam model

The beam models used for the initial configuration optimization are an useful tool to give an indication of the behavior of the structure. Because several simplifications are used its outcome cannot reflect the reality. The major influence on these outcomes is the mesh used on the beam. For simplicities sake the mesh is chosen very coarse, resulting in inaccurate deflections. In this case the main parameter of interest are the governing forces and moments in the beam, which are not dependent on the mesh. However force and moments induced by large deformations are not included in the model.
The boundary conditions at the eight legs representing the connection at the crane house are fixed in all six DoF. This assumption states that the tub, bearing and crane house are infinite stiff, whereas in practice this is not the case.

WAMIT analysis

The diffraction analysis performed is done with on a panel model which simplifies the hull geometry by assuming curve panel with flat ones. This simplification introduces error in the outcome of the analysis.

Liftdyn analysis

The crane responses are calculated with Heerema in-house software package Liftdyn. In this software the crane boom and other crane parts are model with infinite rigid elements connected via joints and connectors. These rigid elements do not account for any beam deflection which do occur in reality.

Geometry optimization

The optimization of the coordinate is performed with the fmincon solver. The fmincon solver finds the local minimum, instead of the global minimum sought-after. To approach this global minimum a multistart function is applied in MATLAB. In theory the change of finding the global minimum is only 100% if infinity MultiStart points are used, whereas in this optimization the number is limited due to computational effort. Therefore it could be that a optimization has not found the global minimum.

During the optimization the beam ratio is fixed. The assumption was made that over the whole structure a beam has a square profile. This ratio could however influence the outcome of the results, one could imagine that a beam does not require the same area moment of inertia in both cross-section directions. Therefore the highest bending resistance is assigned to both direct, resulting in a conservative beam profile.

12.1.2 Static analysis

Finite Element Method model

The mesh size in a finite element model is a balance between the accuracy of the model and the computational costs. By means of a convergence study the mesh size has been determined to be sufficient enough for this model, however a finer mesh size will show a small deviation in the results.
The cranes slewing capability is made allowed by the bearing between the tub and the crane house. A bearing has hardly any resistance in the tangential directions, the main one being the friction. This is modeled by placing connectors between the tub edge and crane edge. These connectors allow for tangential movement without friction, introducing the first error. A second error is introduced when the crane in rotated with a large displacement. Because the connectors are only allowed to move in the initial tangential direction, large rotation result in an change in the perimeter of the crane house and tub. This results in a overestimate of the hoop stress.

Static load cases

Nine load cases were created to evaluate the most likely loading during the HLV24k lifetime. There will always be load cases which are different in configuration and load from the cases examined. This could lead to loading which is not evaluated in the finite element analyses.

12.1.3 Dynamic analysis

Finite Element Method model

Besides the sensitivities described in subsection 12.1.2, the dynamic analysis uses a time domain input. Modal analysis is used to solve that time domain operational load cases at low computational effort. The behavior of a system is typically only described by a few Eigen modes, mostly lower frequency ones. The number of Eigen frequencies used in the analysis is limited by to the minimum time step used. Excluding high frequencies is inevitable in order to get a finite analysis. By excluding some frequencies the possibility exists that particular motions are not properly taken into account, leading to an error in the results.

Liftdyn beam modelling

For the dynamic analysis the vessel responses are calculated with an updated Liftdyn model. Each infinite rigid beam is replaced with four rigid beams connected with a joint, locking axial and torsional movement. The bending and transverse movement of the beams is modeled with a springs. Compared to the model used in the configuration optimization the beams are modeled more accurate. However the axial and torsional are still not included, as well as the effect of cross bracing between the beams. Due to limitations in the Liftdyn software the beams of the crane parts could not be modeled as separate bodies.

Workability

Based on the scatter data the workability is calculated. The scatter data are an average of the main work areas and the seasons. All the entries in the data set are considered to be omni directional, where in reality directionality dependents on the area and season.
The HLV24k and Sleipnir have been compared for the workability. Both the vessels lifting their maximum capacity introduces a skewed comparison. The maximum lift capacity of the vessel is not the same. If the HLV24k was lifting the same load as the Sleipnir, the workability is likely to be different.

12.2 Discussion on Results

The results obtained in this research are discussed per part. The influences, of the sensitivities in the methodology, on the results are touched upon.

12.2.1 Configuration analysis

The spacing in the top of the A-frame has not been formulated in the constraints. In hindsight this constraint should have been taken into account, because the unbuildable configuration 17 yielded from the optimization. Construction of configuration 17 is not feasible because there is no space for the placement of sheaves and the connection with the luffer beams. Therefore configuration 17 is eliminated from the optimization.

The Crane weight calculated in the optimization is not complete. The weight is only used for the comparison study, as equipment weight is not taken into account, as well as the weight of the tub, bearing and crane house, which contribute significant to the total.

The tub, bearing and crane house are considered to be infinitely stiff, due to the boundary conditions set at the bottom nodes of the eight A-frame-legs. In reality radial and transverse deformation of the crane house are likely to occur, which influence these connection by introducing shear stresses and bending moments in the A-frame-legs.

The beam model represents the physical behavior of the crane structure. Because of the use of beam elements the local effects of the load will not be visible in the results. The beam profiles and plate thicknesses are based on the highest load found in each beam, which could well be a local effect. The cross-sections are considered to be homogeneous over the element, which in reality would not be the case. Because the local effects are not taken into account the weight is an conservative number. On the other hand, rectangular (non-square) can be more efficient/effective compared to the applied square beams.

The optimization has been performed with the loading calculated with original crane configuration. The accelerations obtained in Liftdyn are largely dependent on their coordinates with respect to the vessels rotation points. A higher point will have a larger excitation and acceleration than a lower point for the same vessel motions. Because of the optimization the coordinates of the acceleration points change, which will result in changing loading conditions. The iteration step of updating the hydrodynamic calculation to the new geometry has not been made. However the majority of the optimized configuration has an overall height reduction, resulting in conservative calculations.

12.2.2 Static analysis

The judgment of the results of the finite element analyses are all based on the use of S450 steel. The allowable stress is calculated with the yield strength of the material. In this research a yield strength of $450 N/mm^2$ has been assumed for all the shell and beam elements. Especially for the shell elements this is overestimation of the allowable stress. The yield strength of a steel material depends on the steel grade and the plate thickness. The value used in the research is only valid for small thicknesses, the thicker the material gets, the lower is the yield strength. The shell elements in the bottom structure of the crane go as thick as 500mm, resulting in a lower allowable stress. This effect can be obviated by the use of higher steel grades. This overestimation is the case in all the FEA used in the research.

12.2.3 Dynamic analysis

In the updated Liftdyn model the beam flexibility for shear and bending has been taken into account. Axial and torsional behavior has been fixed. The torsion in the crane boom, as visible in the second Eigen mode of the crane, will have influence on the stresses obtained. Especially the combination of vessel roll, pitch and yaw motion are likely to excite the crane in a torsion motion. The results of such a torsional motion is neglected in the hook loading, which yields to lower stress levels in the crane. The results obtained in the model analysis of the survival 3hr run are valid for a typical survival storm. The sea state is based on 50 years statistic of the North Sea. Because the load case is based on the statistic, there will always be a wave which will exceed the highest wave height used in this research. There is a change that this vessel will encounter an extremer sea state during its lifetime. The structural integrity for such a case is not analyzed.

Workability

The workability calculated for the two vessel is done for the sake of comparison. The combination of the assumption in scatter data and the generalization in operational dependent choices result in errors in the workability of the vessel. The workability percentage is in practice dependent on a range of parameters defined by operational choices:

- Area of operation: The area in which the operation is performed is mainly based on the season and the weather forecast. In general the operations shift to regions of the world, which are in the spring or summer season. To include this parameter in the research one would have to research a lifetime operations profile and base the workability on the area of operation, resulting in an increase of the workability.
- Heading: In the workability the worst and best heading are considered. However the heading is mostly depicted by the operation. For instance the placement of a topside on a jacket can only be done at a predefined orientation. This sets the vessel direction, not being able to choose the heading.
- Lift object: The workability in this thesis is based on the biggest lift possible, which in reality will not or rarely occur. A variety of lifts will be performed over the whole capacity range of the crane, influencing the vessel and crane behavior. It can be stated that the biggest lift is a conservative measure for the workability.

13

Conclusions & recommendations

From the conducted thesis research, one is able to draw conclusions with regards to the feasibility of the single crane configuration. Besides the feasibility, the effectiveness of the concept compared to a dual crane semi-submersible can be quantified. The structural analyses have provide more information on the critical factors of the crane design and outline the possible weight reductions by optimization. The final step of the research has to provide more insight on the operability and workability of the concept. Furthermore some recommendations are stated for improvement of the results and a direction for further research.

13.1 Conclusions

Configuration optimization

The first step was to evaluate the configuration of the crane. A optimization study has given more inside on the optimal design for the operational profile of the crane.

- **CoG:** The center of gravity of the crane is lowered compared to the original design, which is beneficial for the motion behavior characteristics of the vessel. Although the vessel weight is relatively large compared to that of the crane, it does influences the vessel stability and behavior.
- **A-frame-legs:** In the original design the eight A-frame legs were attached at an angle to the crane house edge. The new configuration sets this angle to be in-line with the crane house shell. By loading the beam in axial direction shear and bending are reduced, optimizing the material usage and profiles strength, resulting in a weight reduction. Besides the legs, the crane house benefits from a lower bending moment as the cylinder wall thickness, stiffener size and cross beam size reductions lead to a weight saving.

Static analysis

A finite element analysis has been performed on the optimized crane configuration. Nine governing static load cases have been assessed individually. The assessments lead to the following conclusions regarding the static analysis.

- **Crane weight:** The crane weight has decreased in comparison with the original design, resulting in lower production costs. The main weight reductions are seen in the two jibs and the crane house structure, whereas increases are found at the tub structure and wires. The elements that exceed the allowable stress have to be strengthened. If done with the current steel grade used, these parts will increase in weight. To reduce this effect high strength steel can be used on the failure parts. Furthermore, application of high strength steel in the top elements of the crane will be beneficial for the crane weight and CoG location.
- **Structural Strength:** The results of the load cases have been evaluated and the crane showed sufficient structural strength during all the cases. However there are several parts which do exceed the allowable stress, but these appear to be local stresses and therefore not critical for the feasibility of the design.
  The displacement of crane parts are within limits set by HMC experience. Besides, the operational hoist-in of the luffing wires reduces the displacement.

- **Beam profiles:** Several beam elements have been updated after a first run of static calculations. The initial square beam profiles were taken from the MATLAB optimization study. Loading conditions during the static research showed direction dependent strength requirements, resulting in several beam profiles being adjusted to a non-square rectangular shape.

Based on the results of the static analysis it can be concluded that the new optimized configuration looks promising for the operational profile. However is must be noted that the assumed square beam profiles do not suit the loading conditions and were therefore adjusted for several beams.

Dynamic analysis

The static loading includes a dynamic amplification factor (DAF), to cover for the variation in loading due to inertia effects and vessel motions. The dynamic analysis will provide insight on these effects and the choice of the DAF.

- **Crane position:** Analyses between the two survival crane models showed lower stress levels for the 270deg orientation. Therefore it was concluded that the 270deg orientation is beneficial for the structural integrity of the crane during survival conditions.
- **Failure parts:** The main parts of the crane all stay intact during the a storm condition set. The tub shows no allowable stress exceedance, neither the main structural beams. However the cross bracing in the boom and the diagonal bracing of the jib do exceed this limit, inducing plastic deformation. Because relatively few parts exceed the allowable stress, redesigning and strengthening these parts could obviate the vulnerable areas.

Six operational loading conditions are evaluated with finite element analyses. Despite incorporation of a dynamic amplification factor in the design, the stress criteria are already exceeded at 1m significant wave height. Further investigation of the model and the input resulted in the following conclusions.

- **Eigen Frequency:** The vessel motions and hook forces are derived from a governing sea state. Further research indicated large hook force responses for the analyzed wave peak period, indicating resonance of the topside motions. Evaluation of the natural frequencies and mode shapes of the system showed load motion excitation by the vessel motions, resulting in large horizontal force responses on the crane. The rectangular hook configuration and the required lift height are the main causes of this resonance.
- **Heading:** The excitation of the topside in the Eigen period is deteriorated by the vessel's roll motion. The asymmetric hull configuration of the HLV24k introduces roll excitation for all headings, again exciting the topside. Although the vessel response does show lower roll excitation for some heading directions, the heading can often not be chosen as it is highly dependable on the project particulars.

Taken into account the Eigen frequency limitation and the heading dependency, one can conclude that the crane configuration introduces several issues at lifting high topside modules, which was considered one of the main benefits. A possible remedy would be to increase the height of the crane, leading to extra construction costs and structural mass. A solution can also be sought in rigging arrangements and constraining methods, however damping a 24,000t lift object excited at its Eigen frequency will be challenging.

13.2 Recommendations

Based on the performed research, the discussion and recommendations the recommendation can be made. The recommendations are specified per research part.

Configuration analysis

- Optimization of the geometry requires further investigation of the approach and the solver techniques used. Furthermore, the optimization goal and constraints could be evaluated and formulated more specific.
- Future optimizations would benefit from the implementation of more detailed and adjustable beam profiles, including longitudinal variations.
- Include the tub, bearing and crane house in the model, providing a more accurate simulation of the reality.
- Implementation of iterations of the hydrodynamic inputs, which are dependent on the obtained configurations.

Static analysis

- Research on the use of high grade steel, on the failure elements and the parts located high in the crane.
- Assessment of a more detailed model of the eight points connecting the A-frame legs with the crane house.
- More insight in the tub, bearing and crane house has to be obtained. Analysis of a more detailed model is suggested including the deformation of the vessel at the tub interface. Also the integration of the tub in the column below deck level has to be taken into account, as a round and rectangular structure have to be connected. Adding the non-structural crane elements like winches, floors and engines, including their support frames is recommended.
- For structural research of future concepts it is advised to include a more redefined model, including the truss structures and detailed connection points between the parts, providing more insight on local effects in the critical parts of this design.
- Lifting with jibs in an upright position can be one of the benefits of this crane, as this configuration increase the lifting height for two hooks significantly. Structural analysis on this configuration should be performed.
- If decided to continue with the HLV24k the feasibility of the adjustable luffer beams should be investigated, as this expands versatility of the crane.

Dynamic analysis

- Fatigue assessment including the transit conditions of the crane, where the number of cycles is governing and not the stress levels.
- The crane's structural integrity during lift-off and set-down operations has to be researched.
- The effect of wind loading on the vessel, crane and lift object should be taken in account.
- The jibs upright configuration changes the pendulum length of the outer hoist. A few Liftdyn analyses will provide quick answers on the possibilities of reducing the lift object resonance and is therefore suggested before continuing to the detail design phase of the HLV24k.
- For new conceptual studies it is recommended to start with a basic Eigen frequency research of the system. Especially paying attention to the influences of hook and rigging arrangements.
- The operability and workability of the crane require additional research, including transit conditions, operation profile and weather and season data. In this way the possibilities of increasing the imposed motion behavior limit values can be further evaluated.
- An interesting research topic for Heerema would be the possibilities of (active) damping or restraining solutions for a lift object. Both concept vessels as the current fleet could benefit from damping and restraining mechanisms, as workability is likely to increase.

A

Codes and Standards

For the Offshore industry several codes and standards are developed, mainly in the seventies, on the design and operations of lifting appliances. Every part of the world refers to another standard for operations in their region. The two most commonly used ones are DNV 2.22 Lifting appliances [8] and Lloyd's Register: Code for lifting appliances in a marine environment [18].

Heerema applies mainly the DNV code on all of their crane designs. For this reason, this codes will be applied on the design of the HLV24k crane design. The following sections will give a summary of the essentials applicable on the crane design. In the brackets is the reference to the actual codes.

A.1 DNV 2.22

A.1.1 General (CH.1.1)

A.1.1.1 Crane design definitions (C200)

Table A.1: Definitions

Definition	Description
Offshore crane	Lifting appliances on board vessels intended for cargo handling outside the vessel while at sea
Winch luffing crane	A crane where the boom is controlled by wire ropes through a winch
Heavy lift crane	Crane with safe working load above 250t or 2,500 kN

A.1.2 Materials (Ch.2.1)

A.1.2.1 Steel categories (A 200)

Table A.2: Categorisation for structural members

Category	Description
Special	Highly stressed areas where no redundancy for total collapse exist.
Primary	Structures carrying main load
Secondary	Structures other than primary and special members.

A.1.2.1.1 Specified steel parameters

Table A.3: Categorisation for Rolled structural steel specified yield strength

Category	Specified yield stress $[N/mm^2]$
Normal strength steels	$\sigma_y = 265$
High strength steels	$265 < \sigma_y \leq 420$
Extra high strength steels	$420 < \sigma_y \leq 750$

A.1.2.1.2 Forged rings for slewing bearings

Table A.4: Bolts Slewing ring steel requirements

Strength class (ISO 898)	Ulitimate strength $[N/mm^2]$	Yield strength $[N/mm^2]$	Elongation [%]
8.8	800-1,000	640	14
10.9	1,000-1,200	900	12

A.1.2.2 Steel wire ropes

Steel wire ropes and wire locks for cranes shall generally be manufactured and tested in compliance with the requirements stipulated in the following, as well as EN 13414-1 "Steel wire rope slings – Safety" and EN 13411-3 "Terminations for steel wire ropes", respectively.

A.1.3 Loading (Ch.2.2.A)

All the loads to be considered in structural analysis are divided in the following categories:

- Static loads
- Dynamic loads
  - Operational loads
  - Vessel motion loads
- Climatic loads
- Miscellaneous loads
- Mechanism loads
- Load chart

NOTE: Vertical and Horizontal refer to the coordinate system of the vessel

A.1.3.1 Static loads (A200)

Static loads refer to the following loads:

Table A.5: Static loads definition

Load	Symbol	Description
Dead weight	(SG)	All the loads due to the dead weight of all the crane components
Working load	(WL)	Static weight of the load suspended on the hook, including rigging.
Safe Working load	(SWL)	Static weight of the load lifted. Working load excluding the rigging.
Pre-stessing	(PL)	Loads on structural items due to pre-stressing of bolts & wire ropes.

Except for pre-stressing, all the static loads act in the direction of the gravity. Horizontal and vertical components due to heel and trim are to be considered in the static loads. The maximum semi-submersibles heel and trim angles during operation with no wind and waves acting are to be used, with a minimum of:

- Heel: 3deg
- Trim: 3deg

A.1.3.2 Operational loads

Vertical (sec.2.A300 and sec.6.B200)

Vertical loads (SV) due to operational motions consist of the working load multiplied by the Dynamic Amplification Factor, which covers both the inertia forces and shock.

$$SV = WL \cdot \psi \tag{A.1}$$

$$\psi = 1 + V_R \sqrt{\frac{C}{W \cdot g}} \tag{A.2}$$

$$V_R = 0.5 \cdot V_L + \sqrt{V_{in}^2 + V_t^2} \tag{A.3}$$

$$V_L = \min \begin{cases} \text{Available hoisting speed} \\ 0.6 \cdot H_S \end{cases} \tag{A.4}$$

$$V_{in} = \begin{cases} 0.6 \cdot H_S, & 0 \leq H_S \leq 3(m) \\ 1.8 + 0.3(H_S - 3), & H_S > 3(m) \end{cases} \tag{A.5}$$

with:

SV	Vertical dynamic loads
ψ	Dynamic Amplification Factor
C	Geometric stiffness coefficient referred to hook position
G	Gravitational acceleration = $9.81 m/s^2$
V_R	Relative velocity $[m/s]$ between load and hook at the time of pick-up.
V_L	Maximum steady hoisting speed $[m/s]$ for the rated capacity to be lifted.
V_{in}	Downward velocity $[m/s]$ of the load at the time of lift off
V_t	velocity $[m/s]$ from motion of the crane jib tip if the crane is located on a floating unit.

Horizontal (sec.2.A400 and sec.6.b300)

The horizontal dynamics loads (SH) due to operational motions are:

- Inertia forces (F_I):

Maximum possible acceleration/deceleration of slewing-, traveling-, traversing- and luffing motions

- centrifugal forces (F_C):

Lateral force due to the slewing action of the crane at the jib sheave:

$$F_{C,lat} = \left(\frac{WL}{100}\right) \cdot (2.5 + (0.1 \cdot r \cdot n) + H_S) \tag{A.6}$$

$$F_{C,rad} = \max \begin{cases} \left(\frac{WL}{1000}\right) \cdot n^2 \cdot r \\ \psi \cdot WL \frac{2.5 + 1.5 \cdot H_S}{H_W + L_v} \end{cases} \tag{A.7}$$

with:

$F_{C,lat}$	Lateral force (side lead)
$F_{C,rad}$	Radial force (off lead)
r	Load radius (distance revolving axis to load center)
n	Revolutions per minute (RPM)
H_S	Significant wave height
H_W	Distance between the jib sheave and the c.o.g of the load
L_v	Vertical distance from heel point to jib sheave

The Dynamic Amplification Factor for design purposes shall not be taken less than:

$$\psi = \begin{cases} \geq 1.3, & 10kN \leq WL \leq 2500kN \\ \geq 1.1, & WL > 5000kN \end{cases}$$

Linear interpolation shall be used for intermediate values of W between 2 500 kN and 5 000 kN.

A.1.3.3 Vessel motion loads (A500)

Vessel motion loads (SM) Inertia forces due to ship motion shall be calculated in accordance with the Rules for Classification of Ships, Pt.3 Ch.l Sec.4 B "Ship Motions and Accelerations".The forces shall be combined to 10^{-8} probability level to correspond with safety factors as specified for Load Case III. See also Appendix C.

A.1.3.4 Climatic loads (A600)

The possible climatic load effects are:

- Wind loading (SW)

$$F_W = A \cdot q \cdot C \cdot sin\alpha \tag{A.8}$$

$$q = q_{10} \cdot (0.9 + 0.01H) \tag{A.9}$$

with:

F_W	Wind force $[N]$
A	Exposed area in $[m^2]$
q	Air velocity pressure
C	Average pressure coefficient for the exposed surface
α	Wind direction angle to the ex-posed surface
ρ	Mass density of the air: $1.225 kg/m^3$
v	Wind velocity in $[m/sec]$
q_{10}	The velocity pressure 10m above ground $[N/m^2]$
H	Considered height $[m]$

Table A.6: Average pressure coefficient per member type

Type of member	C-Value
Flat-sided	2.0
Tube $\varnothing < 0.3m$	1.2
Tube $\varnothing \geq 0.3m$	1.2
Machinery	1.2
Containers loads	1.2
Other load shapes	1.0

Offshore minimum values:

Table A.7: Air velocity pressure minima

Location	Condition	q_{10} $[N/m^2]$
Open sea	operation	360
Open sea	transit	1,200

- Snow/Ice loading (SI)

Snow and ice loads may be neglected in the design calculations except for cranes working under exceptional conditions, or for cranes of special designs being particularly sensitive to such effects.

- Temperature (ST)

Temperature induced loading: loads due to temperature variations shall be considered only in special cases, such as when members are not free to expand. In such cases the maximum temperature fluctuation for outdoor cranes shall normally not be taken less than 65°C. For indoor cranes possible special sources of heat shall be considered. (Note that the maximum and minimum temperatures shall always be taken into account when selecting the materials)

A.1.4 Load cases (Ch.2.2.B)

For the purpose of making the nominal safety dependent upon the probability of occurrence of the loading, three general cases of loading are defined:

- Case 1: Working without wind (B200)

Representation of operating in harbor conditions

$$SG + SV + SH \tag{A.10}$$
$$= SG + \psi \cdot WL + SH \tag{A.11}$$

- Case 2: Working with wind (B300)

Representation of operating in offshore conditions

$$SG + SV + SH + SW \tag{A.12}$$
$$= SG + \psi \cdot WL + SH + SW \tag{A.13}$$

- Case 3: Crane subjected to exceptional loads (B400)

Representation of Transit and survival conditions is generally coverd by the following equation:

$$SG + SM + SW \tag{A.14}$$

However a special case is considered for the loading of the crane in transit with the boom being secured in a boom rest or cradle.

- Case 3.1: Crane without jib support in transit condition (App C.) This case considers the loading of the crane in the transport condition without the boom supported in a cradle. This condition can be critical with respect to excessive yielding and fatigue damage. This case will cover the extra check for this special securing method in transit mode.

The following assumption are made:

- Slewing motion is prohibited by applying a locking mechanism.
- The boom/jib is secured by tension in the crane's hoisting wire and tension in the crane's luffing wires.
- Load calculations is independent of the crane position.
- Crane's location on-board the vessel is accounted for.

Case 3.1 considers the same equation except for the vessel motion loading:

$$SG + SM^* + SW \tag{A.15}$$

Vessel motions loads SM^*:

The inertia forces caused by the vessel accelerations are described in the following four load combinations:

- Vertical force
- Vertical and transverse force
- Vertical and longitudinal force
- Vertical, transverse and longitudinal force

These four combinations have to be checked for both vessel acceleration directions (positive and negative) and for initial heel/trim. The number of load combinations will therefore be 16.

Combined vessel accelerations shall be calculated for extreme values (probability level 10^{-8}). Shock loads in the crane shall be avoided, upward vertical acceleration never exceeds 1.0 g. The forces resulting of these accelerations are calculated in Equation A.16, A.17, A.19 and A.21. According to Ship Rules Pt. 3 Ch.1 Sec.4 C501 the forces are based on the extreme response but are modified to a probability level of 10^{-4}.

$$P_V = (g \pm 0.5 \cdot a_V) \cdot m \tag{A.16}$$

$$P_V = g \cdot M \tag{A.17}$$
$$P_T = \pm(0.67 \cdot a_T) \cdot m \tag{A.18}$$

$$P_V = (g \pm 0.5 \cdot a_V) \cdot m \tag{A.19}$$
$$P_L = \pm(0.67 \cdot a_L) \cdot m \tag{A.20}$$

$$P_V = (g \pm 0.5 \cdot a_V) \cdot m \tag{A.21}$$
$$P_T = \pm(0.27 \cdot a_T) \cdot m \tag{A.22}$$
$$P_L = \pm(0.67 \cdot a_L) \cdot m \tag{A.23}$$

with:

g	Gravitational constant
m	Total mass of the unit $[t]$
a_V	Combined vertical acceleration $[m/s^2]$
a_T	Combined transverse acceleration $[m/s^2]$
a_L	Combined longitudinal acceleration $[m/s^2]$

NOTE: Combined acceleration is the result of all the vessel motions without gravity.

Based on consideration of the static system of the crane in transport condition, the acting forces and the stresses in transit are similar or less to those of Case 1 and 2. Therefore it may be concluded that the transit condition is not critical with respect to buckling.

- Cases overview:

Table A.8 gives an overview of the loads used per case.

Table A.8: Load cases overview

	Case 1	Case 2	Case 3
SG	X	X	X
SV	X	X	
SH	X	X	
SW		X	X
SM			X

A.1.5 Strength calculations (Ch.2.2.C)

The safety of the structures and components are evaluated for the following failure mechanisms:

- Excessive yielding
- Buckling
- Fatigue fracture

A.1.5.1 Yielding

Verification of the safety may be based on the Working Stress Design (WSD) or the Load and Resistance Factor Design (LRFD) method. The safety factors in Table A.9 have been used.

Table A.9: excessive yielding criteria

Method	Parameter	Case 1	Case 2	Case 3
WSD	S_f	1.50	1.33	1.10
	γ_f	1.30	1.16	0.96
LRFD	γ_m Elastic	1.15	1.15	1.15
	γ_m plastic	1.30	1.30	1.30

A.1.5.1.1 WSD method

The safety factors are applied on the yield stress of the material

$$\sigma_y / S_f \tag{A.24}$$

with:

σ_y	Yield stress
S_f	Safety factor

A.1.5.1.2 LRFD method

The safety factors are applied on the loading of the material

$$S_f = \gamma_f \cdot \gamma_m \tag{A.25}$$

with:

S_f	Safety factor
γ_f	Load factor
γ_m	Material factor

A.1.5.2 Buckling

The guiding principle is that the safety against buckling shall be the same as the required safety against the yield limit load being exceeded.

The safety factors given in Table A.10 are based on the assumption that the critical stresses are determined by recognized methods, taking possible effects of geometrical imperfections and initial stresses into account.

Table A.10: Buckling criteria

Buckling	Case 1	Case 2	Case 3
Elastic	1.86	1.66	1.38
Elastic-plastic	1.69	1.51	1.25

A.1.5.3 Fatigue

For fatigue calculations normally the latest edition of F.E.M. standard (Federation Europeenne de la Manutention), DNV-RP-C203 or equivalent national standards for cranes may be referred to. Group A5(whip) and A3(main).
Fatigue calculation have to be considered for loading cases 1 and 3.
The calculated maximum stress amplitude shall not exceed the permissible stress for fatigue, which is critical stress amplitude divided by a safety factor of 1.33, Equation A.26

$$\sigma_{max} < \sigma_{all} = \sigma_{cr} \cdot 3/4 \tag{A.26}$$

with:

σ_{max}	Maximum calculated stress amplitude $[N/mm^2]$
σ_{all}	Allowed stress amplitude $[N/mm^2]$
σ_{cr}	Critical stress amplitude $[N/mm^2]$

The fatigue check procedure is as follows:

1. Select a hot spot.
2. Select applicable S-N curve.
3. Calculate the possible stress concentration factor $[SCF]$.
4. Calculate the stress range for the transit condition $[\Delta\sigma_0]$.
5. Calculate the fatigue damage for the transit condition $[D_{tr}]$.
6. Calculate the allowed fatigue stress in working condition $[\sigma_{allowed}]$.
7. Apply the k-factor to the allowed stress amplitude $[\sigma_{allowed} \cdot k]$.
8. Check fatigue for working condition.

- Fatigue CASE 3.1:

A fatigue check as caused by the vessel motions only:
The fatigue check is based on stress ranges by applying the altering (positive and negative) of the accelerations. Conservatively for each hot spot the maximum stress range from the four load combinations may be selected: $\Delta\sigma_0$

The $\Delta\sigma_0$ value is the stress range (for a particular hot spot) that has a probability of 10^{-4} of being exceeded and therefore represents the maximum stress range within $n_0 = 10^4$ cycles.

$$n_y = \frac{L_d}{T_m} \tag{A.27}$$

with:

n_y	loading cycles for a period of years [-]
L_d	specified period, design life [s]
T_m	Mean wave period for number of years [s]

After determining the applicable SN-curve, an estimate fatigue damage for the number of years can be calculated with the following formula:

$$D_{tr} = \frac{n_0}{\overline{a}} \cdot \frac{(SCF \cdot \Delta\sigma_0)^m}{(\ln n_0)^m} \cdot \Gamma(1+m) \cdot \frac{n_y}{n_0} \tag{A.28}$$

with:

D_{tr}	Accumulated fatigue damage over the specified period [-]
n_0	Number of loading years [-]
$\overline{a}$	Parameter in SN-curve [-]
SCF	Stress concentration factor [-]
$\Delta\sigma_0$	Stress range [N/mm^2]
m	Parameter in SN-curve [-]
Γ	Gamma function [-]

To perform the fatigue calculation for working conditions in such a way the transit conditions is accounted for, the following factoring is applied to the working conditions stress level.

$$k = \left[1 - D_{tr} \cdot \left(\frac{4}{3}\right)^m\right]^{\frac{1}{m}} \tag{A.29}$$

with:

k	Multiplication factor for the allowed stress amplitude, accounting for transit conditions

Calculation of natural-frequencies and Eigen modes is normally not covered. The natural period of the boom/jib is quite different when the boom/jib rests in a cradle compared to when it is supported by hoisting and luffing wires. If, for instance, the ship movement has the same period as a natural period for the jib, quite a dynamic amplification of the displacements in the jib may occur. Additional securing systems for the jib may be required if the in-service experience of the crane shows that large vibrations may occur under transport condition.

A.1.6 Design and strength of particular components (Ch.2.2.D)

A.1.6.1 Jib buckling stability

The buckling stability of a jib may be solved by determining the slenderness ratio and the permissible stress as a function of these ratios. The effective buckling length used for the calculations depends on its support and type of structure. For a luffing wire support jib the effective length may be taken as:

$$L_{eff} = L \cdot \left(2 - \frac{B}{A}\right) \tag{A.30}$$

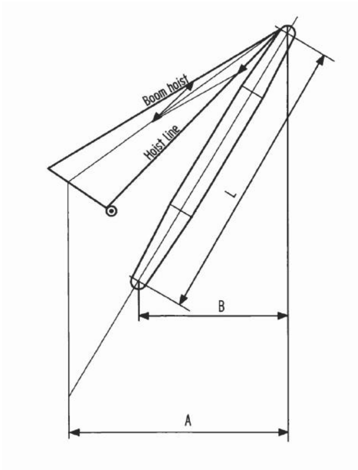

Figure A.1: Effective length of a jib

For latticed jib structures the following correction factor shall be applied to the effective length:

$$k_{L_{eff}} = \begin{cases} \sqrt{1 + \frac{300}{(L_{eff}/i)^2}}, & \frac{L_{eff}}{i} > 40 \\ 1.1, & \frac{L_{eff}}{i} \leq 40 \end{cases} \tag{A.31}$$

with:

i	Radius of gyration $[mm]$
$k_{L_{eff}}$	Latticed jib structure correction factor [-]

B

Hull study

A hull study has been performed by Heerema Marine Contractors, in order to obtain the most sufficient hull for workability and the deck layout [13]. In total 25 different hull versions were analyzed. The hull shapes differ in several parameter of which the main are: length, width, number of colums, size and position of the columns and pontoons. All the hull simulations were performed for the 27m draft. Figure B.1 and B.2 give an overview of the final hull I01a.

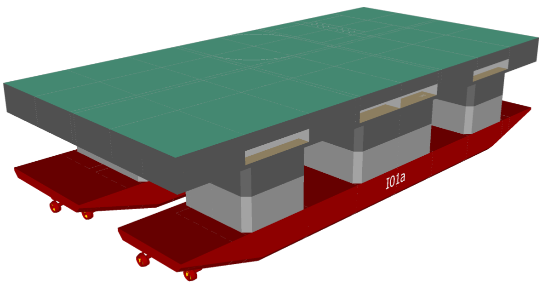

(a) With deckbox

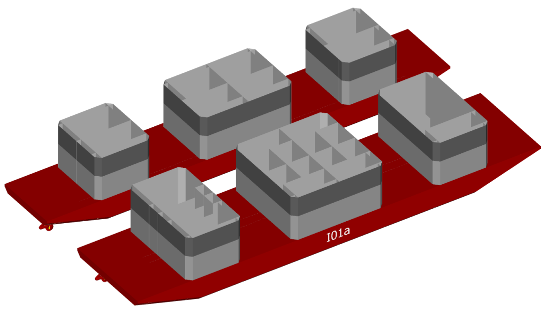

(b) Without deckbox

Figure B.1: Hull I01a (ISO view)

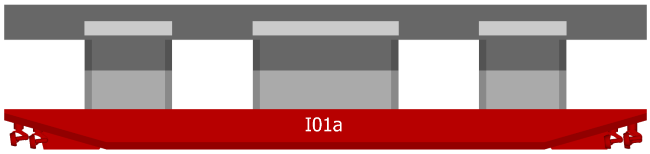

(a) Hull I01a (Port side view)

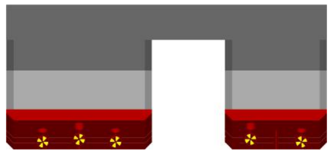

(b) Hull I01a (Aft view)

Figure B.2: Side and front view hull I01a

B.1 Hull analysis

The analysis for the hull design was performed with the following cycle:

- 3D model creation in MultiSurf
- Calculation of the carene table
- Light unit weight estimation
- Configuration of the ballast tanks' plan
- Calculation of hydrostatic Loading Conditions
- WAMIT diffraction analysis
- Motion reponse analysis in Liftdyn
- Comparison of motion behavior value and targets.

Loading conditions have been analyzed on a very basic level. For the purpose of sizing the hull and selecting the most promising design the hull was submitted to the initial stability and floating condition criteria. The most promising design models are in the second stage judged on the last four criteria:

1. Initial Stability
2. Floating conditions
3. Transit draft to be less than 12m
4. Motions at 27 m draft, 0t load
5. Maximum load in crane at 27m draft
6. Minimum draft at target crane load of 24,000t

From the second stage was concluded that hull model I01a shows the best characteristic of all the hull analyzed. Therefore this hull will be used for further development of the HLV24k concept, including this thesis. The following results illustrates the performance of the hull:

- Minimum transit draft: 11.96m
- Similar motion behavior as the Sleipnir vessel
- Max. lifting capacity at 27m draft: 24,000t

B.2 I01a hull

The hull research determined the most promising to be hull I01a. Table B.1 gives an overview of the hull dimensions.

Table B.1: Main vessel dimensions

Structural part	Length $[m]$	Width $[m]$	Height $[m]$
Hull	220	110	49.5
Port side pontoon	220	50	13.75
Starboard pontoon	220	35	13.75
Column SB 1	30	35	23.75
Column SB 2	50	35	23.75
Column SB 3	30	35	23.75
Column PS 1	30	50	23.75
Column PS 2	50	50	23.75
Column PS 3	30	50	23.75

Figure B.3 provides the main dimensions in the three orthogonal projections.

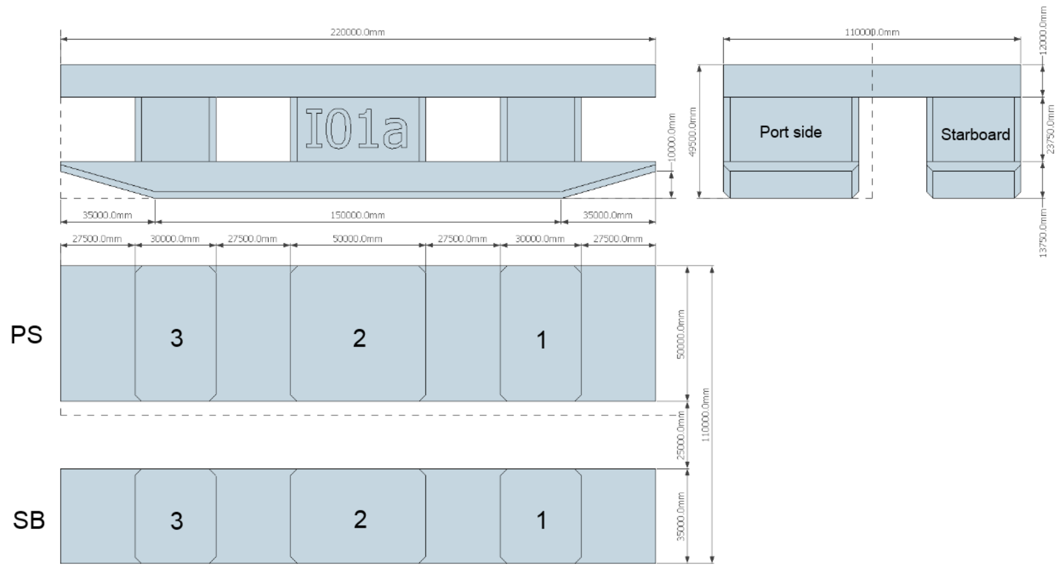

Figure B.3: Main dimensions of hull I01a

B.2.1 Light unit weight

The light unit weight is build up from the structural weight of the hull and the vessel equipment. The crane is not included in this weight. A high level estimation of the LUW was performed by HMC. The vessel is divided in groups and each group is assigned a specific weight per volume. The coefficients were derived from the design of the new Heerema semi-submersible, the Sleipnir.
In the LUW is include:

- Pontoons
- Columns
- Deckbox
- Superstructures
- Owners reserve
- Load support frame
- Vessel equipment: all propulsion related equipment

The centre of gravity of these components have been taken equal to the center of volume.

Table B.2: Operational Vessel weight

Parameter	Weight		CoG	
		X_s	Y_s	Z_s
	$[t]$	$[m]$	$[m]$	$[m]$
Light Unit Weight	132,928	112.31	1.44	29.4
Personal	150	180	-25	54.5
Stores	2,000	154.17	-25	43.5
General deck cargo	2,000	110	0	54.5
ROV	100	110	0	52.5
Snow & ice	500	115	-10	52.5
Service tanks	500	60	20	43.5
Load support	1,500	110	55	49.5
MGO	10,000	110	-37.5	33.18
Fresh water	2,000	110	-37.5	36.36
LNG	10,000	110	21.25	18.75
Original crane configuration	27,889	0	9.47	47.35
Hooks	4 x 350	–	–	–

B.3 WAMIT model

The WAMIT program contains software to perform a diffraction analysis of a shape in a fluid [25]. A diffraction analysis is used to determine the wave forces and the added mass and damping coefficients on a submerged body.

To obtain these forces and coefficients the software solves the linearized velocity potential using 3D source distribution on the submerged surface of the shape. The surface of the shape is divided into a number of panel elements. The distribution of the source singularities on the panels results in the velocity potential, describing the fluid flow around the submerged shape. The pressure distribution, calculated from the velocity potential, determines the added mass and damping coefficients, as well as the wave forces on the hull.

WAMIT is a computer progam which uses linear and second-order potential theory for the analysis of submerged bodies, subjected to waves. A submerged or partly-submerged body is divided into several panels. For each of these submerged panels areas the velocity potential and fluid pressure is solve, using the boundary integral equation method. Next to these calculations a diffraction analysis has been performed, taking into account the effect of incident waves on the body and the radiation for each body mode motion. The solutions of the diffraction analysis are used to obtain the hydrodynamic properties of the bodies, including added-mass, damping coefficients, excitation forces, RAOs, fluid pressure and mean drift forces WAMIT manual[25].

In order to determine the vessel responses in the three load cases, the diffraction analysis is performed for the three drafts: 12, 19 and 27m.

B.3.1 Configuration

The sea conditions used in WAMIT are depicted in Table B.3. The wave frequencies used correspond to those of a fully developed sea for a range of wind speeds, as shown in Figure B.4.

Table B.3: Wave parameters

Parameter	Unit	Range	Step size
Frequency	$[rad/s]$	0.03 - 1.59	0.01
Frequency	$[Hz]$	0.005 - 0.25	0.0015
Heading	$[deg]$	0 - 345	15

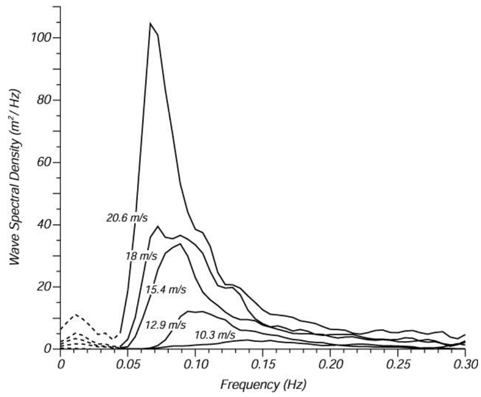

Figure B.4: Fully developed sea spectrum [11]

B.3.2 Input

The diffraction analysis has been performed for the three load cases categories. Table B.4 states the load case specific parameter which are used as input for WAMIT. To be able to perform a diffraction calculation the submerged hull has to be modeled in a panel model. The creation of the panel models has been done with the software package MultiSurf [4]. The panel models used in the analyses are depicted in Figure B.5.

The hydrodynamic calculations require the weight distribution of the vessel. The distribution of the weight is different for all loading conditions, due to project equipment on board, crane position, vessel ballasting etc. The wave induced forces calculated are dominated by the shape and draft of the vessel. The shape and draft are not dependent on the weight distribution, therefore the change in weight distribution is neglected. For each draft one weight distribution case is used.

Table B.4: Hull I01a load case specific parameters

Parameter	Unit	Transit	Survival	Operational
Total weight	$[t]$	198,049	281,607	358,003
Ballast*	$[t]$	8,507	92,064	168,461
Load	$[t]$	0	0	24,000
LCG	$[m]$	110.41	110.03	110.04
TCG	$[m]$	2.27	2.27	2.27
VCG	$[m]$	38.83	29.36	25.21
T	$[m]$	12.02	19.01	27.00
AWL	$[m^2]$	18,699	9,275	9,275
LCB	$[m]$	110	110	110
LCF	$[m]$	110	110	110
TCB	$[m]$	2.27	2.27	2.27
VCB	$[m]$	6.48	9	12
KMT	$[m]$	130.17	51.8	45.65
KML	$[m]$	399.9	97.72	81.77
Ψ	$[deg]$	270	270	90
R_{XX}	$[m]$	41.4	42.1	43.2
R_{YY}	$[m]$	54.8	49.7	53.5
R_{ZZ}	$[m]$	55.7	51.9	58.1
$T_{0,\phi}$	$[s]$	11.4	23.5	26.0
$T_{0,\theta}$	$[s]$	6.9	14.4	17.3

* The ballast water is spread such that an even keel is maintained

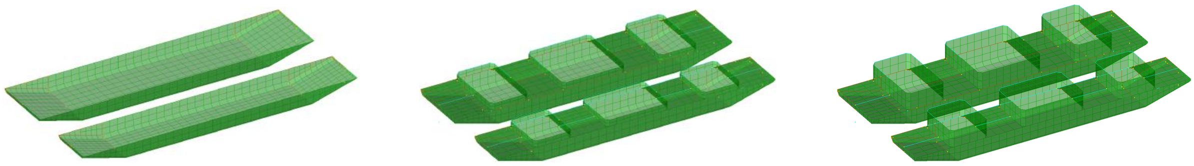

(a) T = 12m (b) T = 19m (c) T = 27m

Figure B.5: Hull I01a Multisurf panel model

C
Liftdyn comparison

Liftdyn analyses are normally performed with models with rigid boom elements. flexibility of the beams is not included because the response of the crane are constantly calibrated with response measured at the real vessel. The deflections of the beams are compensated by the tweaking the stiffness, damping and pre-tension of the luffing en hoist wires.

The response of a concept vessel can off-course not be validated with an real life model, especially when the crane configuration is complete different from the existing cranes. For that reason the optimized configuration of the crane was modeled such that beam flexibility is included in the model. To make a judgment of the modeling procedures a comparison has been made. For this comparison a new Liftdyn model of the optimized configuration was constructed with rigid beams. An comparison has been made between the stiffness of the crane models and the motions of one of the hooks. For sake of the comparison only the beams elements are different in the two models. All the other parameters are kept the same. The two models are visualized in Figure C.1.

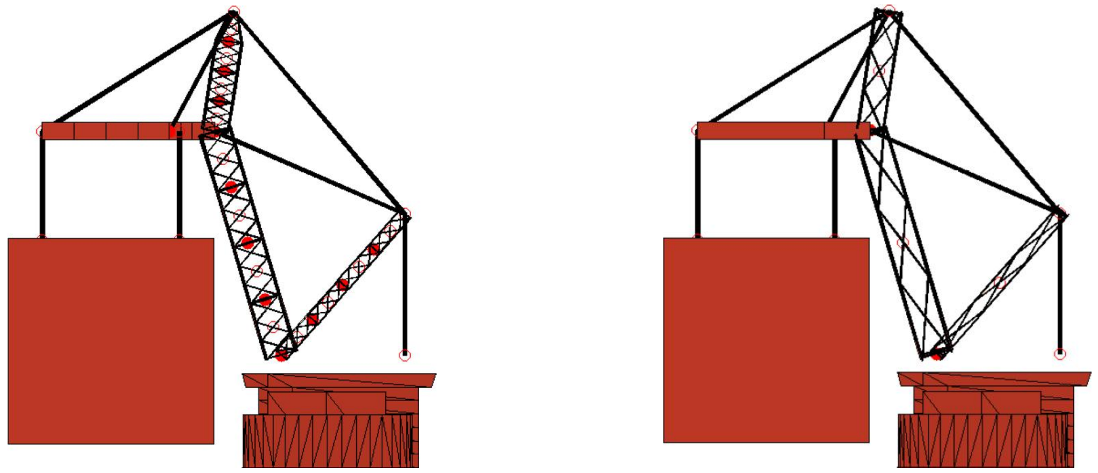

(a) Crane close up flexible beams

(b) Crane close up rigid beams

Figure C.1: Comparison models, M3 90

The hollow red dot indicate the CoG of a rigid body, the solid red dot represents a spring matrix. In-line connectors are visualized by the solid black lines. The black truss- and orange box are the rigid body elements.

C.1 Eigen frequencies

Modeling of the crane with or without beam bending should have an influence on the stiffness of the crane. The stiffness is directly related with the Eigen periods of the system. Table C.1 shows the Eigen period of the corresponding mode shape. The number of the shapes corresponds with the modes of the rigid model. Due to the modeling with springs of the flexible model, it has 85 mode shape, compared to the 18 of the rigid model.

Table C.1: Add caption

Shape	Part	Motion	Eigen period Flexible [s]	Rigid [s]	Δt [s]
1	Vessel	**Yaw (RZ)**	**2499.65**	**2483.13**	**16.52**
2		Sway (Y)	479.45	479.45	0.00
3		Surge (X)	429.92	429.97	-0.05
4		Roll (RX)	44.51	44.47	0.04
5		Pitch (RY)	28.49	28.42	0.07
6		Heave (Z)	20.65	20.65	0.00
7	Object	RZ	11.97	11.87	0.10
8		Y (-)	10.77	10.77	0.00
9		Y (+)	10.73	10.73	0.00
10		X	10.33	10.13	0.20
11		RX	2.04	2.03	0.01
12		**RY**	**3.03**	**1.04**	**1.99**
13		Z	0.83	0.75	0.08
14	Boom	Y & RX	0.79	0.51	0.28
15	Top	RX	0.21	0.14	0.07
16	Jibs	Z & RX	0.18	0.09	0.09
17	Top & Jib	Y & RX	0.17	0.08	0.09
18	A-frame	RX	0.12	0.06	0.06

C.2 Hook motion

Furthermore the response of the outer hook 22 (the top block on the jib element) is compared. The motions response in X, Y and Z direction are compared for a JONSWAP spectrum with Hs = 1m. Figure C.2 to C.9 show the responses per wave heading.

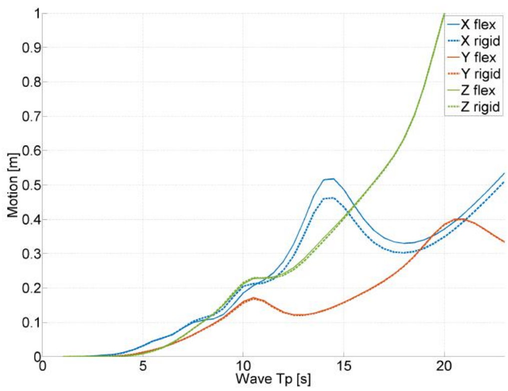

Figure C.2: Motion responses Hook 22 0deg

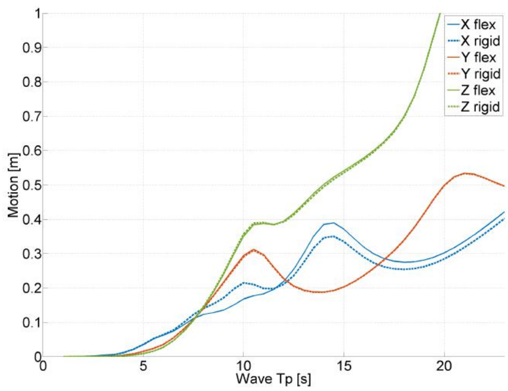

Figure C.3: Motion responses Hook 22 45deg

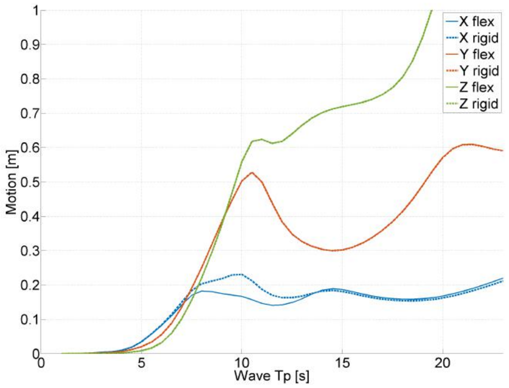

Figure C.4: Motion responses Hook 22 90deg

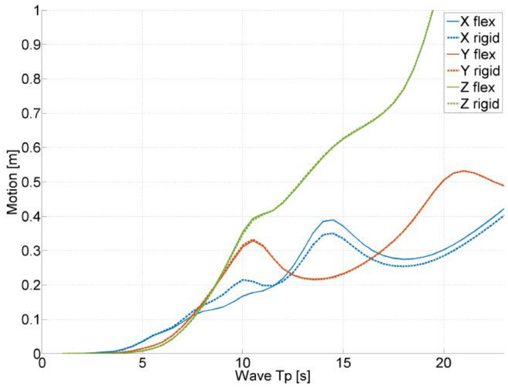

Figure C.5: Motion responses Hook 22 135deg

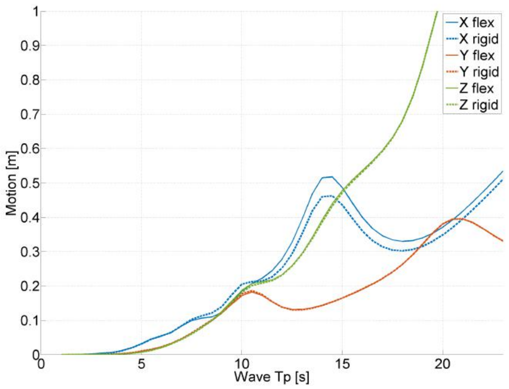

Figure C.6: Motion responses Hook 22 180deg

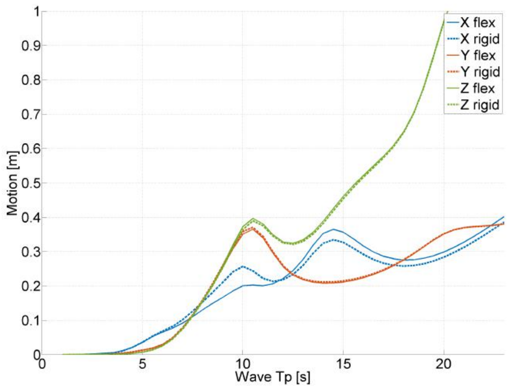

Figure C.7: Motion responses Hook 22 215deg

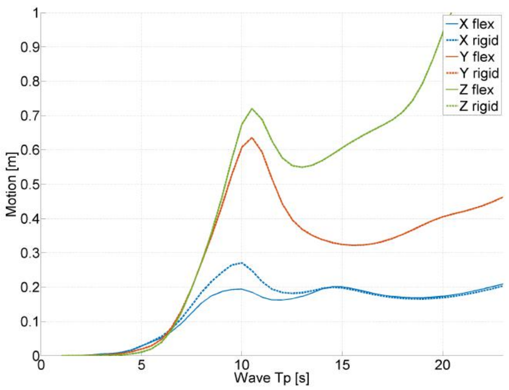

Figure C.8: Motion responses Hook 22 270deg

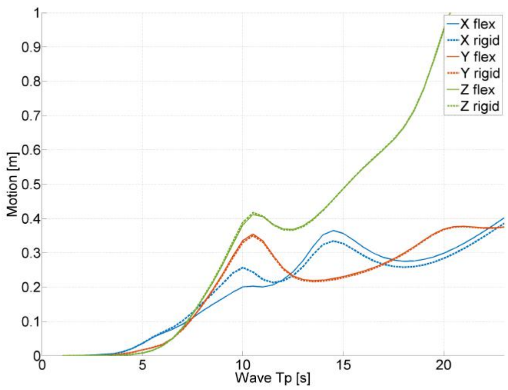

Figure C.9: Motion responses Hook 22 315deg

C.3 evaluation

From the Eigen frequencies comparison, two modes are of significant difference. First of all the Yaw motion of the vessel. The yaw motion is restricted by an arbitrary spring, because this motion does not have a restoring force in real life. The only possible solution for the change in yaw natural period is the X motion of the load, weakening the system. The second deviation is found at the pitch motion of the lift object. Here the flexibility of the two jibs caused the Eigen period of the RY motion to be higher. Also the sideways bending of the crane is visual in the mode shape. This motion is restricted in the fixed model, hence the differences.

The response of hook 22 motion in X, Y and Z direction is evaluated for the eight main wave headings. The flexibility of the crane beams has almost no influence on the response in the vertical and Y (offlead) direction. However the X (sidelead) direction shows differences between the two models. The bending of the crane in the sideways direction is the main cause of the deviation. In the rigid model the sideways bending of the crane is fixed, whereas the flexible beams allow bending in that direction. In general the X response of the flexible model is higher for wave peak periods above 11s. Below this period the rigid model gives higher X responses.

It can be concluded that the motions are mostly depicted by the properties of all the wires in the system. The sideways motion is not accounted for by the wires, which is clearly visible in the natural frequencies and the X motion of the hook. Because the rigid beam model gives larger response for the wave peak period below 11s the rigid beams are considered conservative for the period with the most wave energy.

D

Modal Analysis

To get a first indication of the structural rigidity of the crane concept an modal analysis has been performed. The natural frequencies provided a quick insight on the stiffness of the crane. Resonance is expected when a natural frequency of the crane fits in the vessel motion frequencies.

D.1 Crane

The analysis of the crane has been performed with the analytical beam model in MATLAB, the Liftdyn model and the finite element model. Performing the analysis in with three different models allows for a comparison between them. The first Eigen mode of system has the lowest frequency. The Frequencies of the crane are at the upper boundary of the wave spectrum, therefore only the first five modes are checked. Figure D.1 to D.5 show the first five modes of the Abaqus and Liftdyn model.

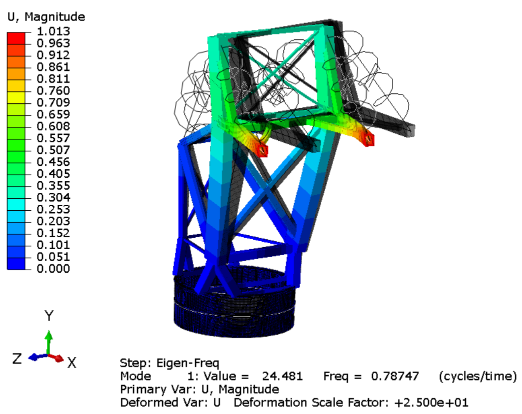

(a) Abaqus Eigen mode 1

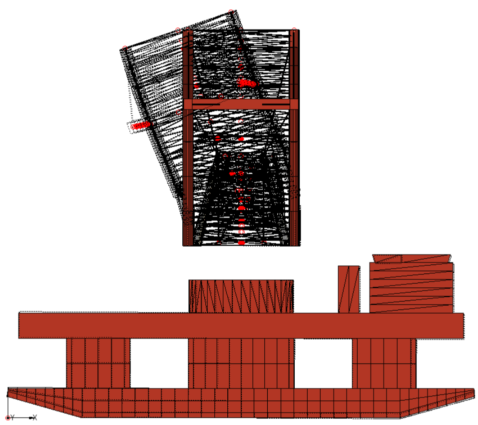

(b) Liftdyn Eigen mode 9

Figure D.1: Matching Eigen mode 1 Abaqus and Liftdyn model

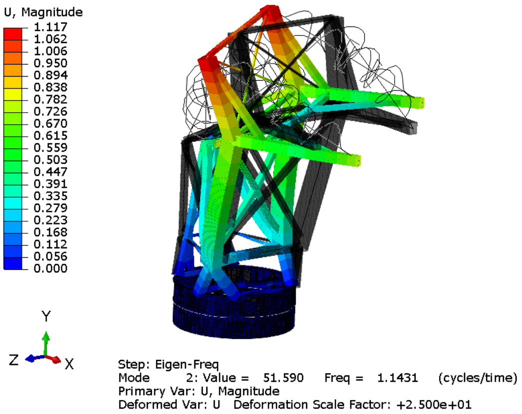

(a) Abaqus Eigen mode 2

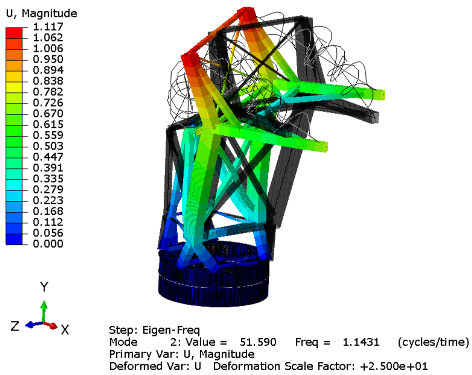

(b) Liftdyn Eigen mode not available

Figure D.2: Matching Eigen mode 2 Abaqus and Liftdyn model

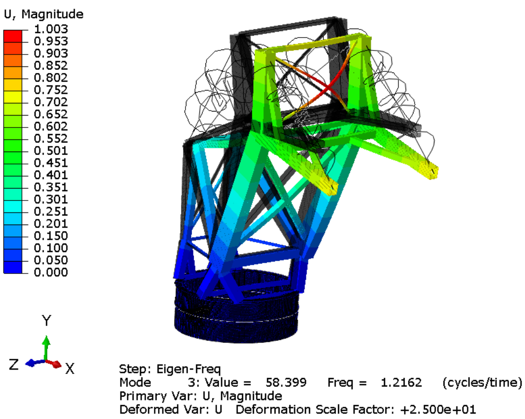

(a) Abaqus Eigen mode 3

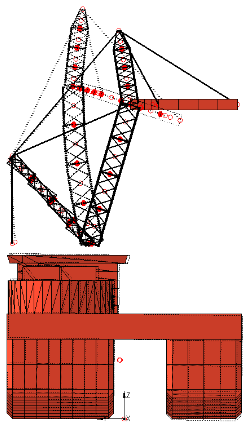

(b) Liftdyn Eigen mode 12

Figure D.3: Matching Eigen mode 3 Abaqus and Liftdyn model

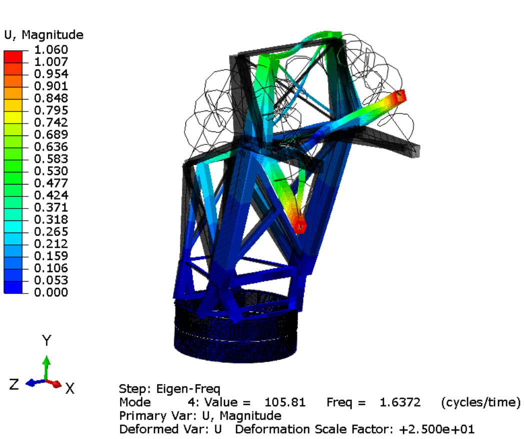

(a) Abaqus Eigen mode 4

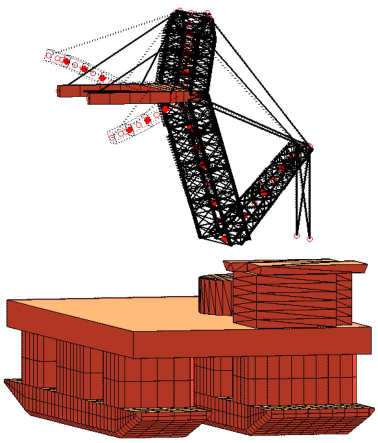

(b) Liftdyn Eigen mode 15

Figure D.4: Matching Eigen mode 4 Abaqus and Liftdyn model

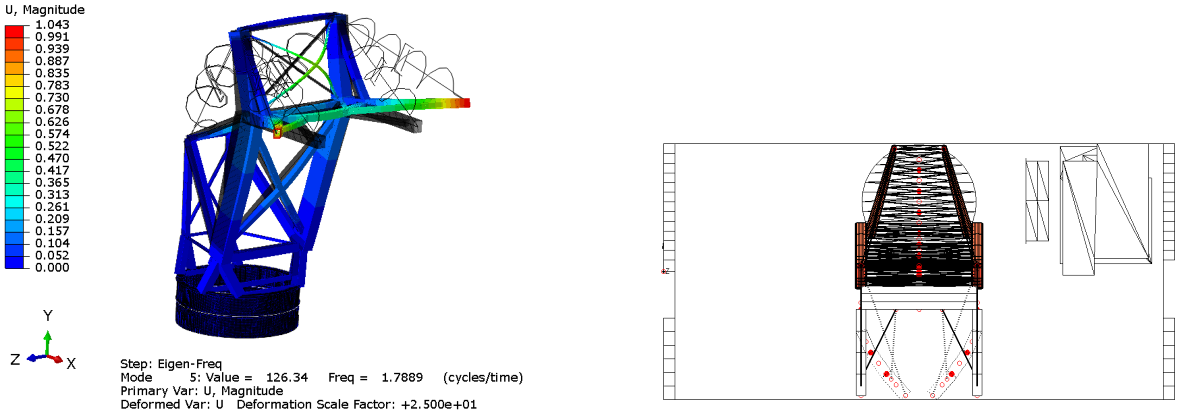

(a) Abaqus Eigen mode 5

(b) Liftdyn Eigen mode 20

Figure D.5: Matching Eigen mode 5 Abaqus and Liftdyn model

D.1.1 Evaluation

An overview of the five first Eigen periods is shown in Figure D.6

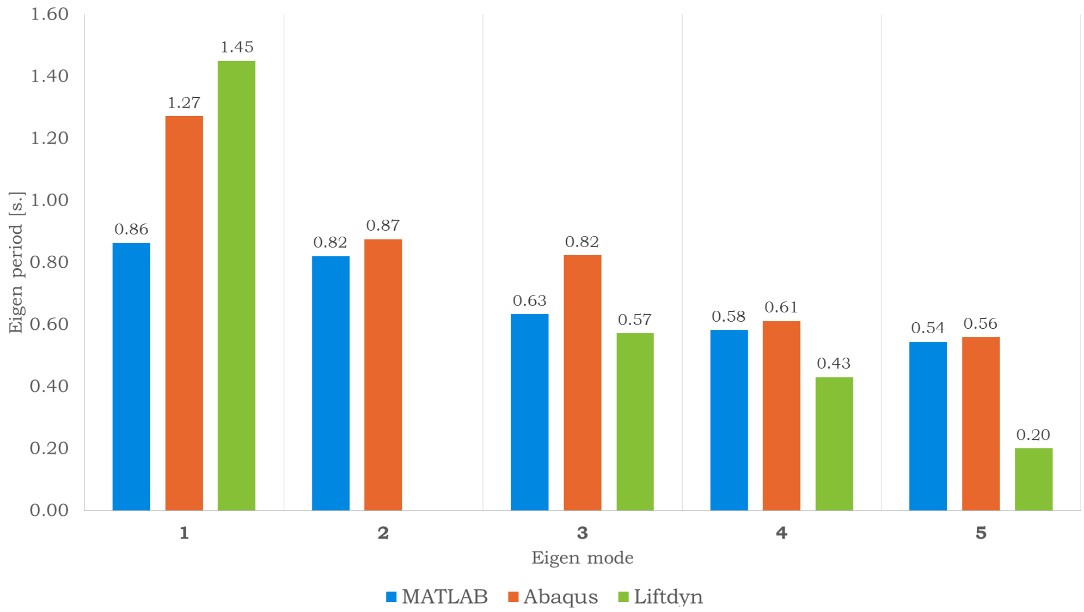

Figure D.6: Eigen period comparison

All three models show similar results for the first five modes. Mode 2 and 5 both include torsion of the crane. In the Liftdyn model the torsional springs are not modeled, hence the absence of mode 2 and the lower natural period in mode 5. All the results show sufficient stiffness of the crane, non of them interfere with the vessel excitation frequencies. Resonance behavior is not likely to occur for this crane configuration, therefore not indicated as a show stopper.

D.2 Individual beams

A modal analysis of the crane parts is performed to check is the beams themselves are likely to resonate on their own. The first Eigen mode of a beam has the lowest frequency. Because the Frequencies of the beams are at the upper boundary of the excitation frequency of the vessel, only the first Eigen mode is checked.

D.2.1 Equation of Motion

The displacement method is used in order to obtain the equation of motion Equation of Motion (E.o.M). The following assumptions are made:

- The material is linear elastic
- Shear deformation is negligible
- Rotary inertia is negligible
- Only small deflections are considered
- The beam does not vibrate in axial direction

Constitutive equation:

$$V = H \cdot tan(\theta) \tag{D.1}$$

Kinematic relation:

$$tan(\theta) = \frac{\partial w}{\partial x} \tag{D.2}$$

Under the assumption that no axial vibration occurs, the horizontal component H is constant. Therefore the H must be equal to the external horizontal force: For small angle's the following is true:

$$H = T \cdot tan(\theta) \approx T \tag{D.3}$$

Resulting force (Newton's second law):

$$F = m \cdot a = \rho \cdot A \cdot \frac{\partial^2 w(x,t)}{\partial x^2} \tag{D.4}$$

Balance of moments:

$$V = \frac{\partial M}{\partial x} \tag{D.5}$$

Moment (Euler-Bernoulli):

$$M = -EI \cdot \frac{\partial^2 w(x,t)}{\partial x^2} \tag{D.6}$$

Balance in vertical forces:

$$\rho A \frac{\partial^2 w(x,t)}{\partial t^2} = -V(x) + V(x + \Delta x) - H \cdot tan\theta \tag{D.7}$$

$$= \frac{\partial}{\partial x} \cdot V - H \frac{\partial w(x,t)}{\partial x} \tag{D.8}$$

$$= \frac{\partial}{\partial x} \cdot \frac{\partial M}{\partial x} - T \frac{\partial^2 w(x,t)}{\partial^2 x} \tag{D.9}$$

Equation of Motion for free vibration of an uniform beam:

$$EI \frac{\partial^4 w(x,t)}{\partial x^4} + T \frac{\partial^2 w(x,t)}{\partial x^2} + \rho A \frac{\partial^2 w(x,t)}{\partial t^2} = 0 \tag{D.10}$$

Harmonic displacement equation:

$$w(x,t) = W(x) \cdot exp(i\omega t) \tag{D.11}$$

The spatial solution is obtained by substituting the harmonic displacement equation Equation D.11 into the E.o.M. Equation D.10:

$$EI \frac{d^4 W(x)}{dx^4} \cdot exp(i\omega t) + T \frac{d^2 W(x)}{dx^2} \cdot exp(i\omega t) + \rho A \omega^2 \cdot W(x) \cdot exp(i\omega t) = 0 \tag{D.12}$$

Equation D.12 rewritten results in:

$$EI\frac{d^4W(x)}{dx^4}+T\frac{d^2W(x)}{dx^2}-\rho A\omega^2\frac{d^2W(x)}{dt^2}=0 \tag{D.13}$$

By assuming the solution W(x) to be:

$$W(x)=C\cdot exp(\beta x) \tag{D.14}$$

Substitute Equation D.14 in Equation D.13 to obtain:

$$\beta^4+\frac{T}{EI}\cdot\beta^2-\frac{\rho A\omega^2}{EI}=0 \tag{D.15}$$

The roots [β] of Equation D.15 are:

$$\beta_1=\sqrt{\left(\frac{T}{2EI}+\sqrt{\left(\frac{T}{2EI}\right)^2+\frac{\rho A\omega^2}{EI}}\right)} \tag{D.16}$$

$$\beta_2=\sqrt{\left(\frac{T}{2EI}-\sqrt{\left(\frac{T}{2EI}\right)^2+\frac{\rho A\omega^2}{EI}}\right)} \tag{D.17}$$

$$\tag{D.18}$$

The solution can be expressed as:

$$W(x)=C_1cosh(\beta_1x)+C_2sinh(\beta_1x)+C_3cos(\beta_2x)+C_4sin(\beta_2x)=0 \tag{D.19}$$

A pinned - pinned beam is considered, because not all connection types are known. The pin-pin beam is a conservative assumption. The boundary conditions at $x=0$:

$$W(0)=0 \quad \text{zero displacement} \tag{D.20}$$

$$\left.\frac{d^2W}{dx^2}\right|_{x=o}=0 \quad \text{zero bending moment} \tag{D.21}$$

The boundary conditions at $x=l$:

$$W(l)=0 \quad \text{zero displacement} \tag{D.22}$$

$$\left.\frac{d^2W}{dx^2}\right|_{x=l}=0 \quad \text{zero bending moment} \tag{D.23}$$

Implementing the boundary conditions results in the following relations:

$$C_1+C_3=0 \tag{D.24}$$

$$C_1-C_3=0 \tag{D.25}$$

$$C_1cosh(\beta_1l)+C_2sinh(\beta_1l)+C_3cos(\beta_2l)+C_4sin(\beta_2l)=0 \tag{D.26}$$

$$C_1\beta_1^2cosh(\beta_1l)+C_2\beta_1^2sinh(\beta_1l)+C_3\beta_2^2cos(\beta_2l)+C_4\beta_2^2sin(\beta_2l)=0 \tag{D.27}$$

The non-trivial solution will be obtain by solving the determinant is zero.
The matrix of the homogeneous equations:

$$C_n=\begin{bmatrix} 1 & 0 & 1 & 0 \\ 1 & 0 & -1 & 0 \\ cosh(\beta_1l) & sinh(\beta_1l) & cos(\beta_2l) & sin(\beta_2l) \\ \beta_1^2cosh(\beta_1l) & \beta_1^2sinh(\beta_1l) & \beta_2^2cos(\beta_2l)0 & \beta_2^2sin(\beta_2l)\end{bmatrix} \tag{D.28}$$

$$\text{Frequency equation}: det(C_n)=-2\beta_1^2sinh(\beta_1l)\cdot sin(\beta_2l)-2\beta_2^2sinh(\beta_1l)\cdot sin(\beta_2l) \tag{D.29}$$

$$\text{Frequency equation}=0 \qquad \text{for} \qquad sinh(\beta_1l)\cdot sin(\beta_2l)=0 \tag{D.30}$$

Since $sinh(\beta_1 l) > 0$ for $\beta_1 l \neq 0$, the roots of Equation D.19 are:

$$\beta_2 l = n\pi \qquad \text{for} \qquad n = 1,2,3,\cdots \tag{D.31}$$

Natural frequency equations:

$$f_n = \frac{n^2\pi}{2l^2}\sqrt{\frac{EI}{\rho A}}\sqrt{1+\frac{Tl^2}{n^2\pi^2 EI}} \tag{D.32}$$

Table D.1 gives an overview of the natural frequencies and period of the crane part for the first mode $n = 1$.

Table D.1: Modal analysis results crane parts for the first mode

Part	Section	Length $[m]$	Force $[kN]$	Natural period $[s]$
Boom	MAIN	68.25	-2.7E+05	0.22
	Diag	38.39	-2.1E+04	0.30
A-frame	AF-BACK-CROSS-OUT	40.00	-4.3E+01	0.54
	AF-BACK-IN	17.24	-3.4E+02	0.03
	AF-BACK-LEG	62.38	2.4E+05	0.34
	AF-BACK-OUT	16.15	3.4E+02	0.03
	AF-BASE	34.21	-1.3E+01	0.19
	AF-BASE-FROINT	50.00	1.3E+05	0.23
	AF-DIAG	45.16	1.2E+04	0.63
	AF-FRONT-CROSS-IN	30.00	-2.1E+04	0.12
	AF-FRONT-CROSS-OUT	48.00	-3.3E+04	0.29
	AF-FRONT-IN	19.15	-2.6E+05	0.04
	AF-FRONT-LEG	72.35	-2.0E+05	0.34
	AF-FRONT-OUT	16.39	-2.4E+05	0.03
	AF-TOP	50.00	-3.5E+04	0.42
Jib	MAIN	37.03	-8.0E+04	0.10
	DIAG	33.54	-9.9E+03	0.17
Luffer	LUFFER	57.54	-2.3E+04	0.43
Top	BACK-LEG	46.27	-1.9E+05	0.12
	DIAG-HOR	20.07	-9.6E+03	0.08
	DIAG-VER	34.07	-3.1E+03	0.36
	FRONT	50.00	-2.4E+03	0.22
	FRONT-LEG	39.36	3.4E+04	0.24
	MAIN	13.34	-8.3E+04	0.01
	MIDDLE	50.00	5.6E+03	0.54
	Top	50.00	1.4E+03	1.54

observations:
1. If $T = 0$ the natural frequency will be same as that of a simply supported beam
2. If $EI = 0$ the natural frequency reduces to that of a taut string. Only valid for $T \geq 0$
3. If $P > 0$ the natural frequency increases as the tensile force stiffens the beam.
4. If $P < 0$ the natural frequency decreases as the tensile force stiffens the beam.

D.2.2 evaluation

Resonance of the individual beams is not expected because all the first natural periods are outside the expected wave periods for a typical JONSWAP spectrum. Therefore the resonance behavior of the individual beams is not indicated as a show stopper.

E

Modal superposition

In general two solution techniques are available, which include these inertia effects: Direct solutions and frequency response solutions. In general the direct solution methods come at great computational costs, whereas the frequency response solutions are cheaper but not sufficient for all types of dynamic modeling. Especially problems which include large non-linearities cannot be solve in the frequency domain. If large non-linearities are present in the analysis, the Eigen frequencies change significantly as a result of the loading the system.

The deformation of a structure can be calculated by the linear combination of the modes shapes. The linear behavior of the structure can be now be solved with the modal superposition technique. The modal superposition technique is a method to the reduce the complex system of equation into an system of only a few calculations.

E.1 Theory

The basic principle of the modal superposition is explained for an arbitrary example of a mass oscillating on a spring and dashpot [3] [22].

Determine the equation of motion of the system:

$$[M]\{\ddot{u}\} + [C]\{\dot{u}\} + [K]\{u\} = F \tag{E.1}$$

The system can be based on the eigenvectors by rewriting the displacement vector as linear combination of the eigenvectors.

$$\{u\} = [\phi]\{Z\}, \qquad \{\dot{u}\} = [\phi]\{\dot{Z}\}, \qquad \{\ddot{u}\} = [\phi]\{\ddot{Z}\} \tag{E.2}$$

$\{Z\}$ is the vector with modal displacement
$[\phi]$ transformation matrix, eigenvector columns

Substituting the displacement vectors in the equation of motion gives:

$$[M][\phi]\{\ddot{Z}\} + [C][\phi]\{\dot{Z}\} + [K][\phi]\{Z\} = F \tag{E.3}$$

It is important to design the crane in such a way that the frequencies at which it may be loaded are not close to the natural frequencies. The natural frequencies are obtained by considering the dynamic response of the unloaded structure. In the modal superposition analysis the first step is to calculate these natural frequencies and mode shape (eigenvectors). Ignoring the damping the natural frequencies can be calculated by:

$$[M]\{\ddot{u}\} + [K]\{u\} = 0 \tag{E.4}$$

Assuming the harmonic displacement the eigenvector problem can be written as:

$$\left([K] - \omega_i^2[M]\right)\{\phi_i\} = 0 \tag{E.5}$$

ω_i is the i^{th} natural frequency
$\{\phi_i\}$ is the i^{th} eigenvector, mode shape

Solving this equation results in N eigenvalue, where N is the number of degrees of freedom in the system. For the modes $i = 1 \ldots N$, the i^{th} natural frequency corresponds to the i^{th} eigenvector. The eigenvector is also referred to as the mode shape, it is the deformed shape (not deformation) of the structure during vibration in the i^{th} mode.

The obtain eigenvectors are normalized to the mass matrix:

$$\{\phi_i\}^T[M]\{\phi_j\} = 1 \text{ if } i = j \tag{E.6}$$
$$= 0 \text{ if } i \neq j \tag{E.7}$$

$$\{\phi_i\}^T[K]\{\phi_j\} = \omega_j^2 \text{ if } i = j \tag{E.8}$$
$$= 0 \text{ if } i \neq j \tag{E.9}$$

Multiplying Equation E.3 with $[\phi]^T$ results in:

$$[\phi]^T[M][\phi]\{\ddot{Z}\} + [\phi]^T[C][\phi]\{\dot{Z}\} + [\phi]^T[K][\phi]\{Z\} = [\phi]^T F \tag{E.10}$$

With the help of the eigenvector properties and the mass normalization the equation becomes:

$$\{\ddot{Z}\} + [C_\phi]\{\dot{Z}\} + [\omega^2]\{Z\} = [\phi]^T F \tag{E.11}$$

$[C_\phi]$ is the modal damping matrix. However the damping matrix $[C]$ is often not defined, instead the damping of each mode as a fraction of the critical damping is used: $[C_i]$.
$[\phi]^T F$ is the generalized force. The vector contains the force scale in the direction of the eigenvector. The product of this vector with a force $(\{\phi_i\}^T \cdot F)$ determines if the i^{th} mode will be loaded.
$[\omega^2]$ (matrix) contains all the natural frequencies of the modes at the diagonal positions. The vector $\{Z\}$ contains the modal co-ordinates, for each eigenvector the scale factor at a given time instant is available. The linear combination of all the eigenvectors multiplied with the scale factor will give the total deformation of the crane at that time instant.

Now the damping matrix and the natural frequency matrix are both diagonal, the equation of motion of each mode is independent. This results in the following equation of motion:

$$\ddot{Z} + C_i\dot{Z} + \omega^2 Z = \{\phi_i\}^T F \tag{E.12}$$

The modal superposition method solves for each mode the amplitude. Each mode is multiplied with the corresponding scale factor. Superposing these scaled mode shapes gives the total deformation of the system. These displacements can than be used to calculate the occurring stresses at each time increment.

E.2 Verification dynamic Abaqus analyses

At first the "implicit dynamics" step has been applied for the dynamic analysis. This type of solution technique is the most general used and also most expensive method available. This method is can be applied to a broad range of applications, including problems which include highly non-linear material and geometry behavior, contact surfaces and moderate energy dissipation, viscous damping and plasticity of materials.

Although the results were as expected, the computational cost per analysis was too high. Therefore an alternative method was used, modal superpositions chapter 9. To determine if the model superposition principle was applicable for the dynamic research, a simple beam model has been made, analyzed and compared to the results of the implicit dynamic runs.

Figure E.1: Validation beam, initial condition

This beam has been subjected to a displacement-time signal ($u_y(t)$) at the left end node. A point force was applied at the right end node (F_u)

Figure E.2: Validation beam, loading condition

The validation of the model superposition method has been done by comparing the results to "implicit dynamics" method. The assumption was made that "implicit dynamics" analysis accurately describes the behavior of the beam.

For the dynamic verification analysis 3 time traces are used; 10, 60 and 600s. For this verification both the displacement and the Von Mises stress levels are compared.

E.2.1 Displacement

10s

The green line represents the displacement-time signal

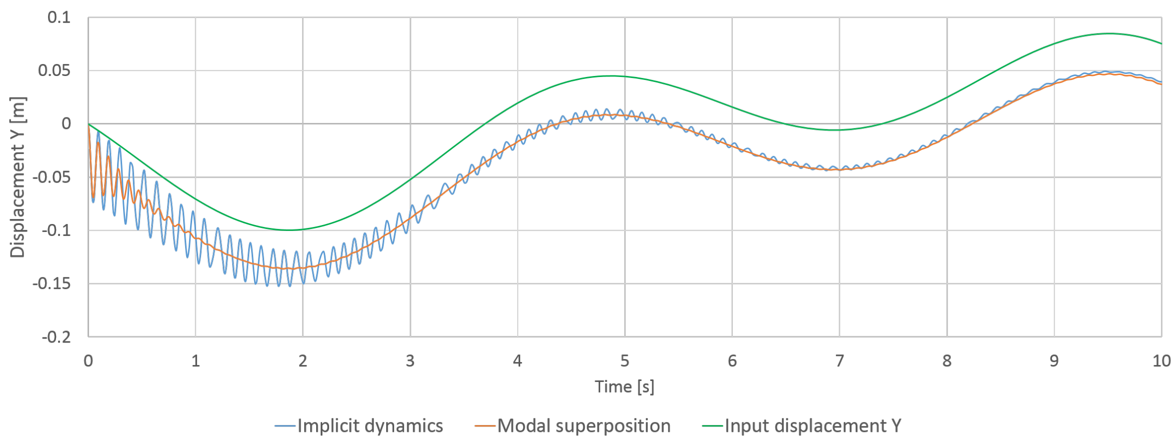

Figure E.3: Beam tip displacement 10s

60s

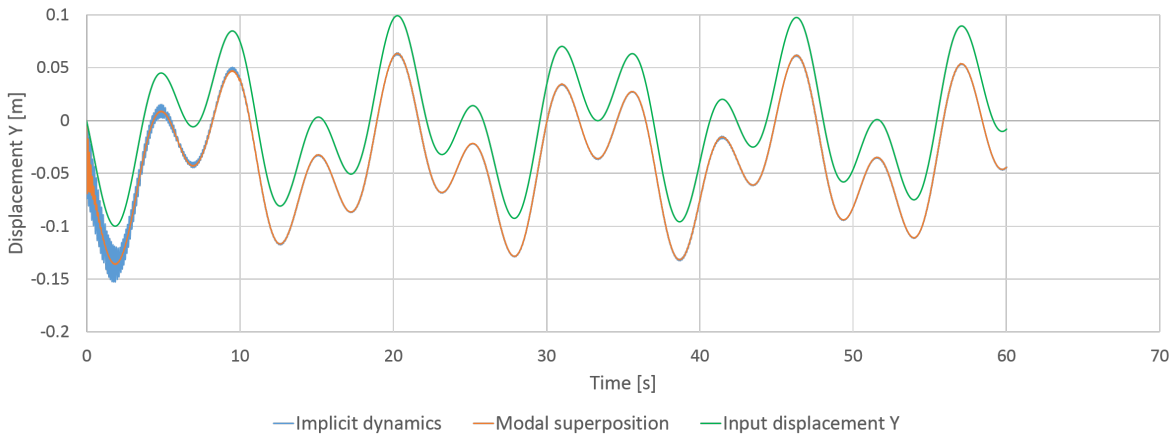

Figure E.4: Beam tip displacement 60s

600s

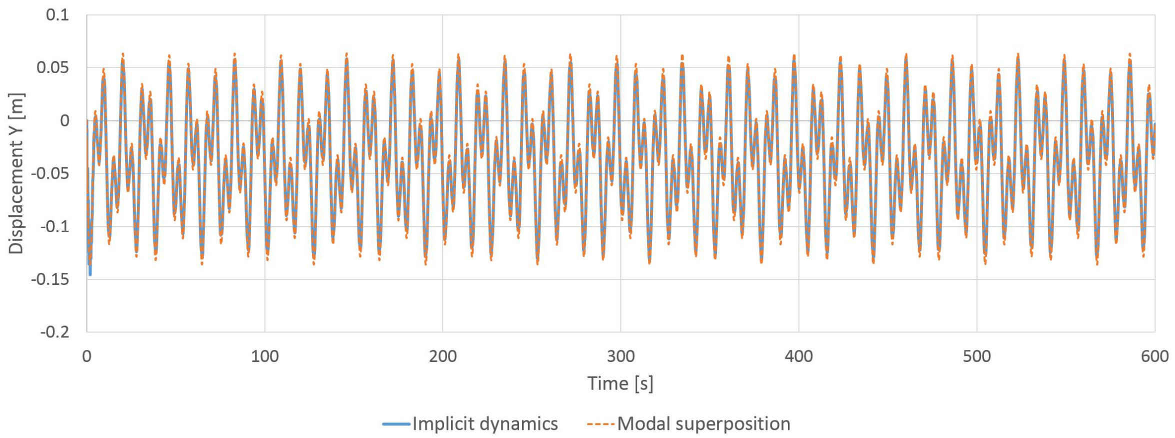

Figure E.5: Beam tip displacement 600s

In the first few seconds the implicit model shows high frequency displacement due the impulse of the point load at the first time step. After ten seconds this impulse is damped out and the implicit and modal technique show similar displacement behavior.

E.2.2 Stress

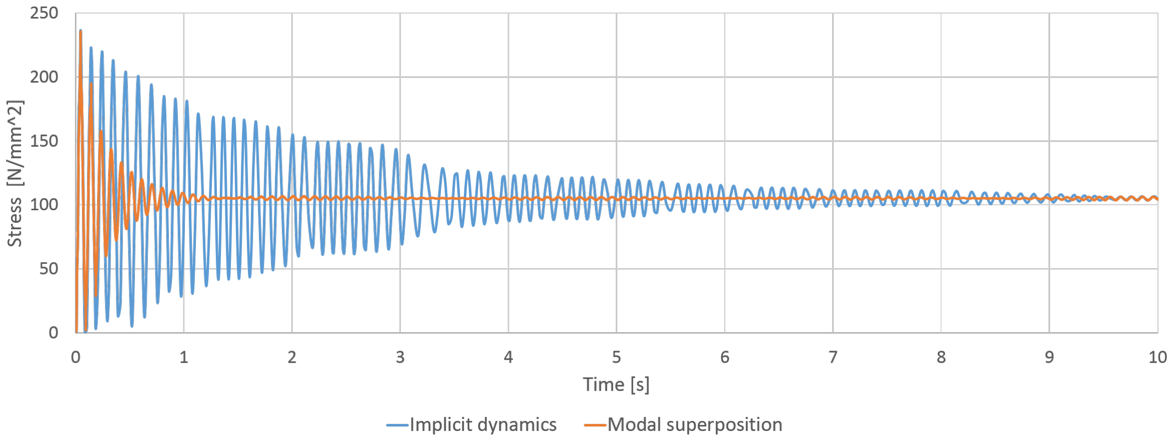

Figure E.6: Beam fixed stress 10s

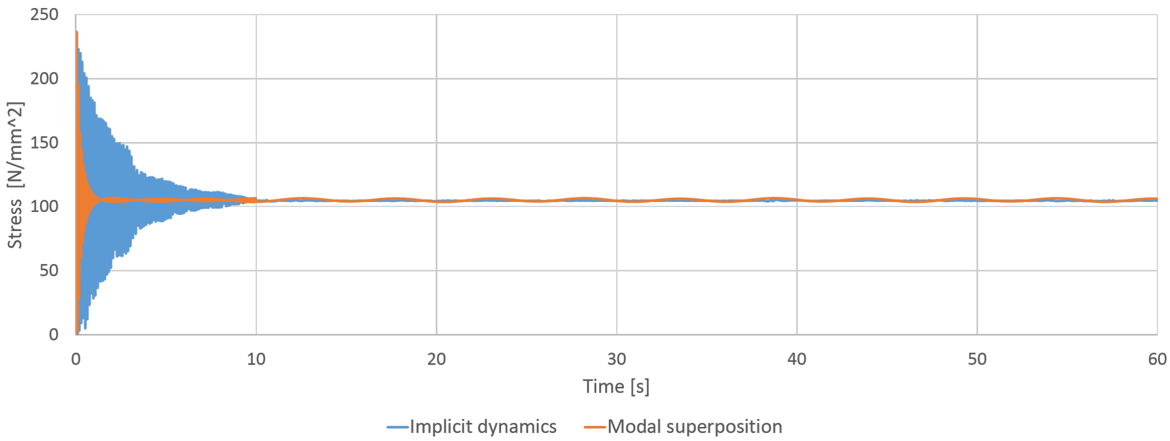

Figure E.7: Beam fixed stress 60s

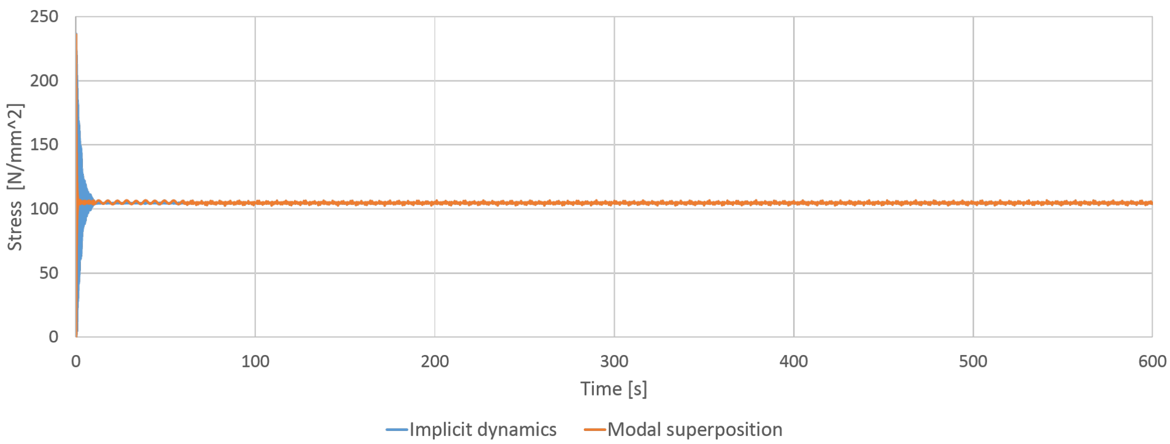

Figure E.8: Beam fixed stress 600s

The impulse of the point load is again visible in the first few second for the implicit solution method. The stress peak damp outs and the modal analysis and implicit analysis show similar stress levels. After 10 second the difference in stress level is only 0.6%. Therefore is concluded that the modal analysis technique shows sufficient accurate results compared to the more accurate implicit method.

E.2.3 HLV24k verification check

Next to the beam model the crane model is also compared for the two types solving methods. As input model the M2 Survival 180 H0 has been used. The crane has been analyzed for a 1,200s time signal of the six vessel motions. The Von Mises stress at the left heelpoint and the top main beam have both been compared for the two techniques. The results of which can be see in the graphs below.

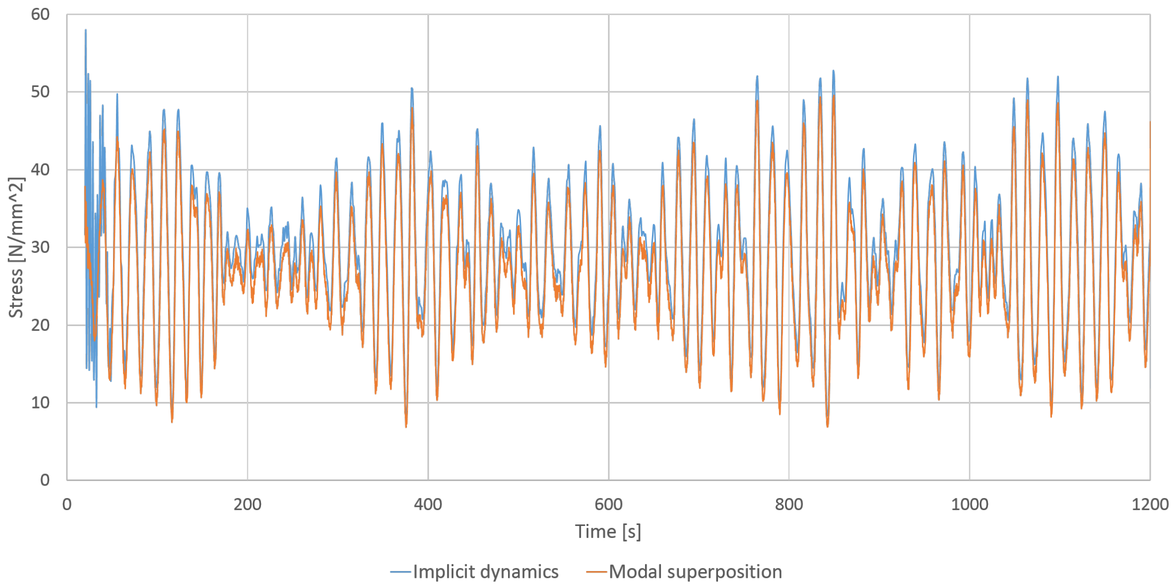

Figure E.9: HLV24k boom heelpoint 1 Stress 1200s

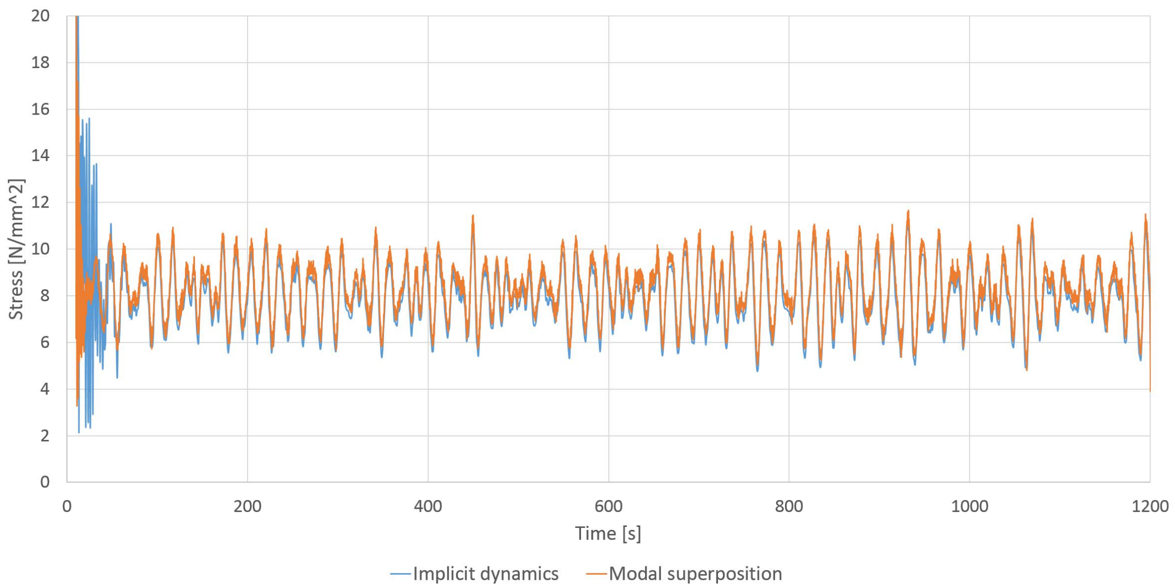

Figure E.10: HLV24k top main beam Stress 1200s

For both points the two solution techniques show similar stress levels. It is concluded that the modal analysis technique yields sufficient accurate results for the type of dynamic analyses that have been performed in Abaqus.

F

Operability graphs

Figure F.1 to F.8 show the operability comparison between the HLV24k and the Sleipnir. The results are give per 45deg wave heading angle.

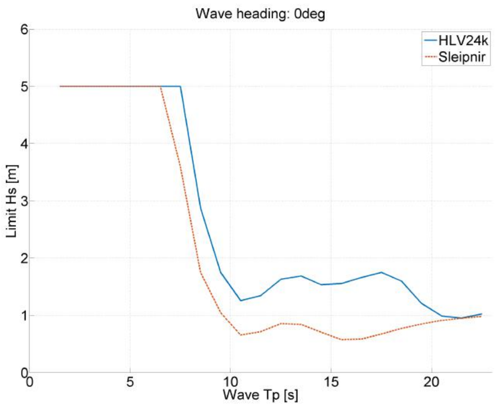

Figure F.1: HLV24k & Sleipnir operability heading 0

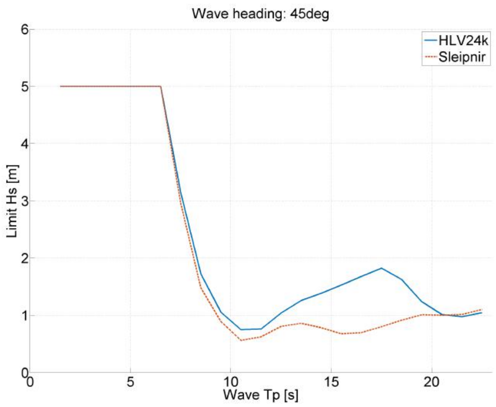

Figure F.2: HLV24k & Sleipnir operability heading 45

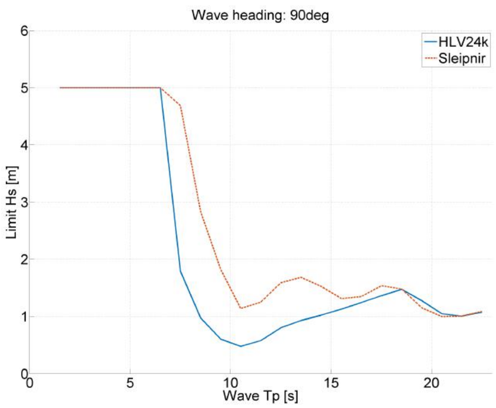

Figure F.3: HLV24k & Sleipnir operability heading 90

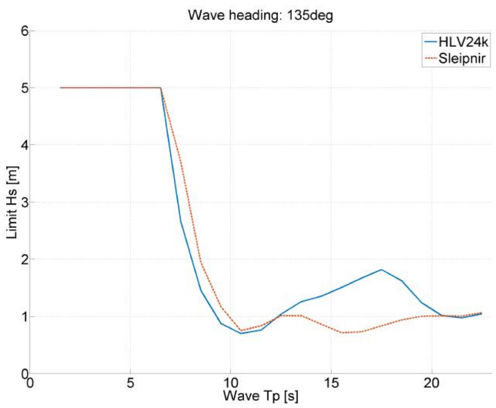

Figure F.4: HLV24k & Sleipnir operability heading 135

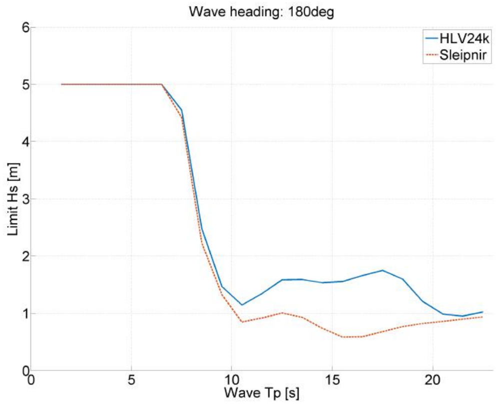

Figure F.5: HLV24k & Sleipnir operability heading 180

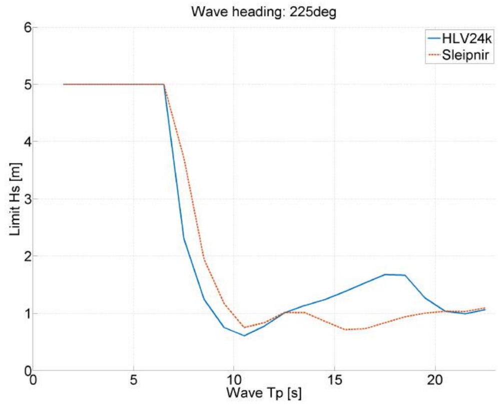

Figure F.6: HLV24k & Sleipnir operability heading 225

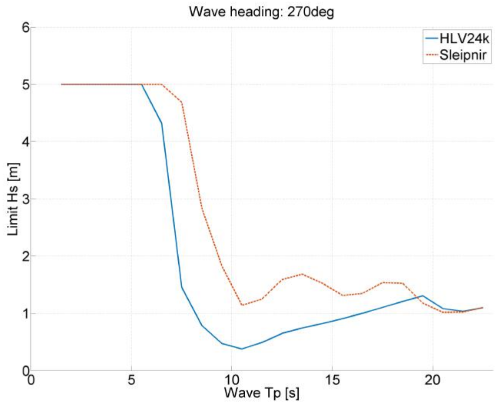

Figure F.7: HLV24k & Sleipnir operability heading 270

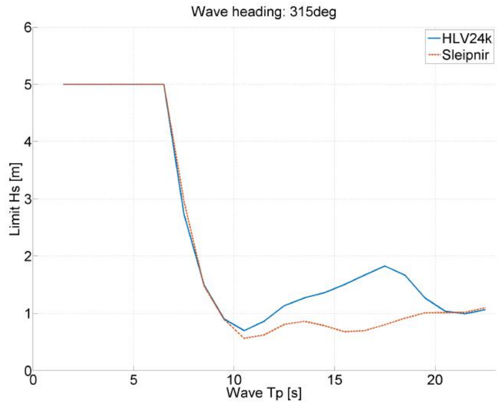

Figure F.8: HLV24k & Sleipnir operability heading 315

G
Scatter data

Table G.1: Operational wave scatter diagram, workability comparison

Hs range		Tp [s]																								Total
[m]	[m]	0.5	1.5	2.5	3.5	4.5	5.5	6.5	7.5	8.5	9.5	10.5	11.5	12.5	13.5	14.5	15.5	16.5	17.5	18.5	19.5	20.5	21.5	22.5	23.5	
15.75	16.25	0	0	0	0	0	0	0	0	0	0	0	0	0	0	0	0	0	0	0	0	0	0	0	0	0
15.25	15.75	0	0	0	0	0	0	0	0	0	0	0	0	0	0	0	0	0	0	0	0	0	0	0	0	0
14.75	15.25	0	0	0	0	0	0	0	0	0	0	0	0	0	0	0	0	0	0	0	0	0	0	0	0	0
14.25	14.75	0	0	0	0	0	0	0	0	0	0	0	0	0	0	0	0	0	0	0	0	0	0	0	0	0
13.75	14.25	0	0	0	0	0	0	0	0	0	0	0	0	0	0	0	0	0	0	0	0	0	0	0	0	0
13.25	13.75	0	0	0	0	0	0	0	0	0	0	0	0	0	0	0	0	0	0	0	0	0	0	0	0	0
12.75	13.25	0	0	0	0	0	0	0	0	0	0	0	0	0	0	0	0	0	0	0	0	0	0	0	0	0
12.25	12.75	0	0	0	0	0	0	0	0	0	0	0	0	0	0	0	0	0	0	0	0	0	0	0	0	0
11.75	12.25	0	0	0	0	0	0	0	0	0	0	0	0	0	0	0	0	0	0	0	0	0	0	0	0	0
11.25	11.75	0	0	0	0	0	0	0	0	0	0	0	0	0	0	0	0	0	0	0	0	0	0	0	0	0
10.75	11.25	0	0	0	0	0	0	0	0	0	0	0	0	0	0	0	1	0	0	0	0	0	0	0	0	1
10.25	10.75	0	0	0	0	0	0	0	0	0	0	0	0	0	0	0	1	0	0	0	0	0	0	0	0	1
9.75	10.25	0	0	0	0	0	0	0	0	0	0	0	0	0	1	1	1	0	0	0	0	0	0	0	0	3
9.25	9.75	0	0	0	0	0	0	0	0	0	0	0	0	1	2	2	1	1	0	0	0	0	0	0	0	7
8.75	9.25	0	0	0	0	0	0	0	0	0	0	0	1	2	3	3	1	0	1	0	0	0	0	0	0	11
8.25	8.75	0	0	0	0	0	0	0	0	0	0	0	1	7	7	4	2	1	0	0	0	0	0	0	0	22
7.75	8.25	0	0	0	0	0	0	0	0	0	0	0	3	9	9	4	2	1	0	0	0	0	0	0	0	28
7.25	7.75	0	0	0	0	0	0	0	0	0	0	1	10	22	11	6	4	1	0	0	0	0	0	0	0	55
6.75	7.25	0	0	0	0	0	0	0	0	0	0	4	23	38	13	7	5	2	1	0	0	0	0	0	0	93
6.25	6.75	0	0	0	0	0	0	0	0	0	1	16	59	45	16	11	6	2	1	1	0	0	0	0	0	158
5.75	6.25	0	0	0	0	0	0	0	0	0	4	31	85	34	13	12	8	2	0	0	0	0	0	0	0	189
5.25	5.75	0	0	0	0	0	0	0	0	1	20	115	120	43	21	19	10	3	1	0	0	0	0	0	0	353
4.75	5.25	0	0	0	0	0	0	0	0	10	80	235	107	53	29	20	11	4	2	1	0	0	0	0	0	552
4.25	4.75	0	0	0	0	0	0	0	2	53	308	265	112	64	37	23	15	5	3	1	0	0	0	0	0	888
3.75	4.25	0	0	0	0	0	0	0	19	258	611	236	133	95	50	32	17	7	4	1	0	0	0	0	0	1463
3.25	3.75	0	0	0	0	0	0	2	95	791	451	216	138	105	58	37	25	9	5	2	0	0	0	0	0	1934
2.75	3.25	0	0	0	0	0	0	34	947	1564	592	381	265	212	141	93	67	25	7	8	5	1	1	0	0	4343
2.25	2.75	0	0	0	0	0	16	653	3245	1485	812	598	473	403	310	237	82	94	60	40	14	4	2	0	0	8528
1.75	2.25	0	0	0	0	1	258	3449	2810	1555	1008	655	625	627	567	0	492	369	137	103	34	9	3	1	0	12703
1.25	1.75	0	0	0	0	241	3627	4083	2733	1756	1043	809	896	1033	911	0	833	559	158	116	43	17	6	1	0	18865
0.75	1.25	0	0	0	67	2194	1745	907	768	487	395	337	365	311	222	0	267	135	40	29	8	4	2	1	0	8284
0.25	0.75	0	0	130	987	759	317	252	231	158	135	111	110	96	51	0	68	37	11	9	3	1	0	0	0	3466
0	0.25	0	15	143	6	19	13	9	9	10	10	8	9	9	4	0	3	1	1	1	0	0	0	0	0	270
Total		0	15	273	1060	3214	5976	9389	10859	8128	5470	4018	3535	3209	2476	511	1922	1258	432	312	107	36	14	3	0	62217

Bibliography

[1] A. Kaveh. *Computational Structural Analysis and Finite Element Methods*. Springer, Switzerland, 2014. ISBN 978-3-319-02963-4.

[2] A. Khennane. *Introduction to Finite Element Analysis Using MATLAB and Abaqus*. CRC Press LFC, Boca Raton, 2013. ISBN 978-1-4665-8021-3.

[3] Abaqus. *Abaqus 6.13.2*. Dassault Systemes, 2013.

[4] AeroHydro Inc. *MultiSurf 8.5 - User Manual*. AeroHydro Inc., July 2013.

[5] A.J.M. Ferreira. *MATLAB Codes for Finite Element Analysis*. Springer, Porto, 2009. ISBN 978-1-4020-9199-5.

[6] D. Horn. Design of Monopole Bases. Design Report, C-Concepts, Inc., 204.

[7] DNV. *Recommended Practice C205 - Environmental Conditions and Environmental Loads*. Det Norske Veritas AS, October 2010.

[8] DNV. *Standard for Certification No. 2.22 - Lifting Appliances*. Det Norske Veritas AS, October 2011.

[9] H. Goldstein, C. Poole & J. Safko. *Classical Mechanics*. Addison-Wesley, Massachusetts, 3rd edition, 1980. ISBN 978-0201657029.

[10] Heerema Marine Contractors, Geert Meskers. *LiftDYN Theory Manual*. Heerema Marine Contractors, 2015.

[11] Holthuijsen, Leo H. *Waves in oceanic and coastal waters*. Cambridge University Press, Cambridge, 2007. ISBN 978-1-4020-9199-5.

[12] HMC internal. Dev80800 hlv24k project baseline. Technical report, Heerema Marine Contractors, 2015.

[13] HMC internal. Dev80800 hlv24k hull sizing and motions study. Technical report, Heerema Marine Contractors, 2015.

[14] HMC internal. *Single Crane Lift Systems - SC-201*. Heerema Marine Contractors, June 2015.

[15] HMC internal. *Dual Crane Lift Systems - SC-211*. Heerema Marine Contractors, June 2015.

[16] J.M.J. Journee and W.W. Massie. *Offshore Hydromechanics*. Delft University of Technology, Delft, 2001.

[17] K.Ellerman, E. Kreuzer, and M. Markiewicz. Nonlinear Dynamics of Floating Cranes. *Nonlinear Dynamics*, 2002.

[18] LR. *Code for Lifting Appliances in a Marine Environment*. Lloyds Register Group Limited, August 2013.

[19] MathWorks Inc. *MATLAB R2013b Documentation*. MathWorks Inc., 2015.

[20] M.K. Bak and M.R. Hansen. Analysis of Offshore Knuckle Boom Crane. *Modeling, Identification and Control*, 2013.

[21] R.C. Hibbeler. *Mechanics of materials*. Pearson Prentice Hall, Upper Saddle River, NJ, 2005. ISBN .

[22] R.D. Cook, D.S. Malkus, M.E. Plesha and T.J. Witt. *Concepts and Applications of Finite Element Analysis*. John Wiley & Sons, Cambridge, 4th edition, 2002. ISBN ISBN 978-0-471-35605-9.

[23] S.S. Rao. *Mechanical vibrations*. Pearson Education, Inc., Upper Saddle River, 5th edition, 2011. ISBN 978-0-13-212819-3.

[24] W. Yang, Z. Zhang and F. Shen. Modeling of system dynamics of a slewing flexible beam with moving payload pendulum. *Elsevier*, October 2006.

[25] Wamit Inc. *WAMIT User Manual, Version 7.1.* Massachusetts Institute of Technology, 2015.

[26] W.C. Young and R.G. Budynas. *Roarks Formulas for Stress and Strain.* McGraw-Hill Companies, Inc., New York, 7th edition, 2002. ISBN 0-07-072542-X.

[27] William Dwight Whitney. Proa. The Century Dictionary and Cyclopedia: An encyclopedic Lexicon of the English Language, 2016. http://etc.usf.edu.

[28] Y.W. Kwon and H.C. Bang. *The finite element method using MATLAB.* CRC Press LFC, Florida, 2nd edition, 2000. ISBN 0-8493-0096-7.